NASA CONTRACTOR REPORT

NASA CR-915

EXPERIMENTAL INVESTIGATIONS OF SIMULATED METEOROID DAMAGE TO VARIOUS SPACECRAFT STRUCTURES

by A. R. McMillan

Prepared by
GENERAL MOTORS CORPORATION
Santa Barbara, Calif.
for Manned Spacecraft Center

NATIONAL AERONAUTICS AND SPACE ADMINISTRATION • WASHINGTON, D. C. • JANUARY 1968

NASA CR-915

EXPERIMENTAL INVESTIGATIONS OF SIMULATED METEOROID DAMAGE TO VARIOUS SPACECRAFT STRUCTURES

By A. R. McMillan

Issued by Originator as Report No. TR66-67

Prepared under Contract No. NAS 9-3081 by
GENERAL MOTORS CORPORATION
Santa Barbara, Calif.

for Manned Spacecraft Center

NATIONAL AERONAUTICS AND SPACE ADMINISTRATION

For sale by the Clearinghouse for Federal Scientific and Technical Information
Springfield, Virginia 22151 – CFSTI price $3.00

ABSTRACT

A theoretical and experimental program has been performed to evaluate high-velocity impact damage to structures composed of two thin metallic sheets spaced some distance apart. The results of this study are applicable to the impact of meteoroids against space vehicles.

Impact against the first sheet or shield was analyzed with a hydrodynamic treatment. This treatment, combined with experiments, shows that the damage mechanisms to be considered for the second sheet are gross deformation, tensile failure, and spallation. Gross deformation and tensile failure were treated with a blast-loaded thin-shell analysis, and spallation with a two-dimensional elastic-plastic treatment.

Multisheet (more than two simple sheets) structures were also analyzed and found to provide less protection within the same total structural thickness and weight than two-sheet structures. Honeycombs between the two sheets were found to be detrimental to the impact resistance of two-sheet structures.

An analysis was also performed to assess the area-time of exposure for a 0.99 probability of no failure. This analysis is presented.

CONTENTS

ILLUSTRATIONS

LIST OF TABLES

INTRODUCTION

For extended-time space missions, e.g., the Apollo mission, the space vehicle must afford some resistance to meteoroid impact damage to provide for a reasonable probability of mission success. This report evlauates the resistance to meteoroid impact damage of structures consisting of two sheets spaced some distance apart.

Meteoroids have velocities between 11 and 72 kilometers per second relative to earth, but exact knowledge of meteoroid density, flux, and composition is lacking.[1] A meteoroid environment was established in 1965 by NASA.[2] This environment is as follows:

a. The isotropic flux-mass relationship for sporadic meteoroids is given by

$$\log_{10} N = -1.34 \log_{10} m - 10.423 \qquad (1)$$

where N is the number of impacts per square foot per day above mass m in grams.

b. The density is 0.5 gm/cm^3 for all particle sizes.

c. The average geocentric velocity is 30 km/sec for all particle sizes.

d. The anisotropic flux during a meteoroid shower is given by

$$\log_{10} N = -1.34 \log_{10} m - 2.38 \log_{10} V - 6.465 + \log_{10} F \qquad (2)$$

where V is the geocentric velocity of the meteoroid stream (km/sec) and F is the ratio of the accumulative meteoroid stream flux to the sporadic meteoroid flux.

e. The ejecta mass flux relationship in the vicinity of the moon can be expressed as

$$N_{ejecta} = 10^{3.83} \left(N_{sporadic} + N_{stream}\right) \qquad (3)$$

and the ejecta has an average velocity of 200 meters per second (maximum velocity of 2.4 km/sec) and a density of 2.5 grams per cubic centimeter.

Recent analysis of photographic meteor data by Dohnanyi,[3] and Clough and Lieblein,[4] along with Pegasus data,[5] suggests that the NASA model environment may be pessimistic in its predictions of small-particle flux. References 3 and 4 also suggest that the average meteor velocity is approximately 20 kilometers per second. Dohnanyi states that velocity and mass distributions are independent to a first approximation; thus Dohnanyi expects the average velocity of all meteoroids to be approximately 20 kilometers per second.

The analysis of a structure to be used for a mission such as Apollo must consider impacts of low-density particles at velocities up to 72 kilometers per second, with an average impact velocity in the range between 20 and 30 kilometers per second. In addition, the possibility of more dense fragments impacting at low velocities must be considered. This report describes a combined analytical-experimental program directed toward an understanding of these problems as related to structures consisting of two metallic sheets spaced some distance apart. Because existing experimental facilities such as the one used in this program have a velocity limitation of approximately 10 kilometers per second, it is necessary to have a theoretical basis of understanding to logically predict the reaction of structures impacted at very high velocities.

The approach described and utilized herein treats the impact of the first sheet, the shock transmission in the second sheet, and the gross deformation of the second sheet.

THEORY

Upon striking a thin sheet a particle or projectile may undergo a variety of processes, depending upon impact conditions such as the particle velocity, the particle material and composition, the angle of impact, and the material strength, and thickness of the thin sheet. (A thin sheet as used herein will be defined as a sheet whose thickness is equal to or less than the diameter of the projectile or particle.) The particle may be stopped by the sheet, may pass through the sheet essentially undamaged, or may pass through the sheet fractured, molten, or vaporized. The last two cases are the cases of interest for meteoroid impacts, as the velocities are sufficiently high to cause melting or vaporization.[6]

If the thin-sheet shield is penetrated, the debris from the projectile and the shield then travel across the space between the sheets and strike the second sheet. Upon striking the second sheet a shock wave is generated within the sheet and this shock traverses the sheet. Depending upon the intensity and the structure of this shock an internal fracture or spall may form, resulting in some cases in complete detachment of some material from the rear surface of the sheet.

In addition, the second sheet will be given an impulsive load by the impact of the particle-shield debris. This load is applied over a very short period of time (a few microseconds) and results in the second sheet moving with some velocity. The sheet can then fail from this load, by tensile failure or shear failure.

The above phenomena will be treated in detail in this study.

PROJECTILE-SHIELD INTERACTION

The impact of a high-velocity particle upon a thin sheet has been considered by several authors. The situation resulting from such an impact is shown in Figure 1 along with a sketch denoting the nomenclature used in this report. As can be seen

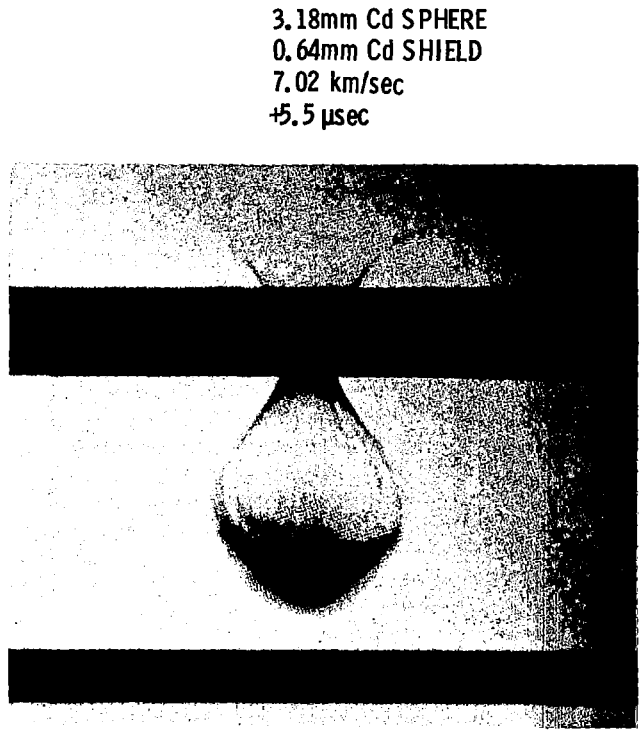

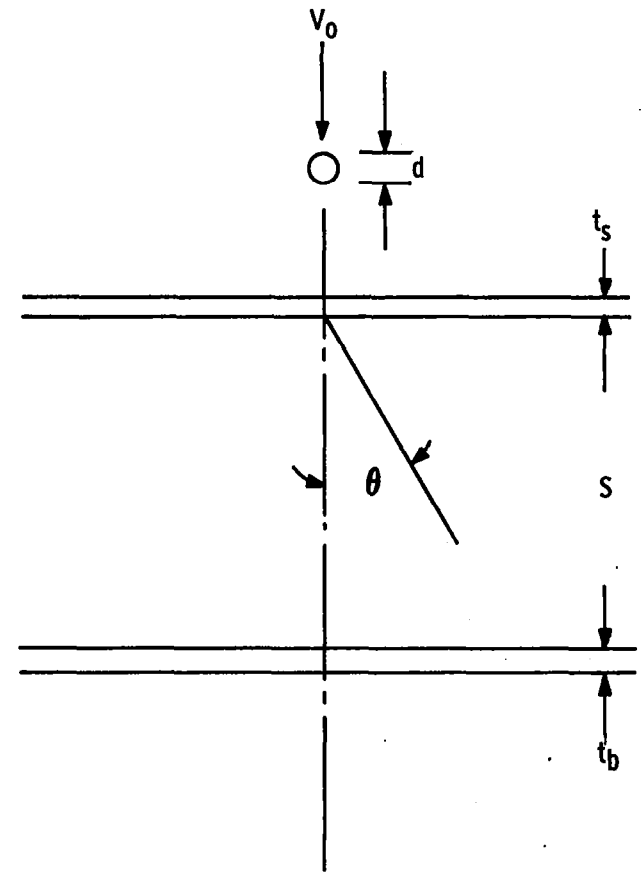

Figure 1 X-Ray of a Thin-Sheet Impact

in the flash X-ray, the projectile-shield debris is widely spread both in spray angle, θ, and along the direction of travel for this impact.

Maiden and McMillan[6] and Sandorff[7] considered a right circular cylinder striking a thin sheet and the one-dimensional shock structure which results along the projectile-shield centerline. It was found that the rarefaction waves from the outside of the cylinder overtake the shock front 0.72 diameter from the interface in the projectile.[6] The shock will reflect from the rear surface of the shield as a rarefaction wave and, depending upon the thin sheet thickness, may overtake the shock front in the projectile. Both treatments concluded that relief from high pressures resulted in the destruction of the impacting particle.

Maiden and McMillan[6] established an optimum shield thickness based upon the centerline shock strength being sufficient, when relieved, to melt or vaporize the impacting projectile. This criterion of optimum shield thickness assures minimal penetration of the second sheet. Also, this criterion calls for decreasing shield thickness with increasing impact velocity.

Sandorff[7] established a criterion for an optimum shield thickness on the basis that the rarefaction from the rear surface of the shield would not overtake the shock in the projectile within the projectile length. This criterion requires increasing shield thickness with increasing velocity.

Both of these criteria are based on a somewhat artificial basis in that they require only that the debris that passes through the shield be in some particular form, and say nothing of the debris distribution. Sandorff requires that the projectile be shocked to the maximum pressure possible; Maiden and McMillan require only that the projectile be shocked sufficiently to melt or vaporize it. Other than to minimize penetration, neither of these criteria explicitly accounts for the reaction of the second sheet.

An accurate evaluation of the effectiveness of a shield should account for spallation and gross-deformation failure of the second sheet. It is clear that, to be effective, the shield must at least either break the impacting particle into small

pieces or cause melting of the projectile to insure that no significant penetration will take place. It is not clear what effect a shield thicker than this will have upon the reaction of the second sheet.

An accurate description of the state of the debris that passes through the shield requires a complete assessment of the pressure-time history of the projectile and shield. This is conveniently possible only through finite difference computations utilizing a high-speed computer. High-speed impacts upon thin sheets have been considered in this manner by Bjork,[8] Riney and Heyda,[9] and Walsh and Johnson.[10] Bjork and Riney and Heyda utilized [illegible]-in-cell (or PIC) computational schemes while Walsh and Johnson have used an Eulerian scheme. These authors have presented results in terms of centerline densities, velocities, and momentum versus spray-angle profiles. The results show that, as the sheet thickness is increased, the debris is spread more and the momentum per unit solid-angle is decreased.

These treatments are hydrodynamic in nature and make no provision for the strength of the shield material. For the thin-sheet case this treatment is sufficiently accurate for the material of interest (i.e., that debris that passes through the shield at high velocity) which has been subjected to pressures many times greater than the strength of the materials. For impacts in the range of meteoroid velocities the debris is expected to be molten or vaporized.[6] The strength of the shield does influence the size of the hole formed. The shock in the shield outside the projectile-shield interface is attenuated very rapidly because of the close proximity of the shield's free surfaces, and very little material is ejected with significant velocity from this area. Thus the hydrodynamic treatments can provide a good description of the high-velocity, hot debris that strikes the second sheet, and the small amount of discrete, low-velocity shield debris can be, in general, ignored.

It was necessary for this study to have a description of the debris that passed through the shield in terms of momentum distribution and density-velocity profiles. To accomplish this a two-dimensional hydrodynamic code, CAMEO developed by J. Tillotson,* was utilized. This is an Eulerian code similar to that used by Walsh and Johnson.[10]

* Presently associated with General Atomics Division of General Dynamics Corporation, San Diego, California.

In this system a set of grids or cells is fixed in space and the material being treated flows through the cells continuously. The problems treated are normal impacts of axisymmetric particles, thus cylindrical coordinates are appropriate. The cells are of rectangular cross section and of a toroidal shape, with the cell volume becoming greater with increasing distance from the axis of symmetry. A description of this code is found in Reference 10.

There are some limitations in this treatment. Because the material moves in a continuous manner it is not possible to follow the position of the particle-shield interface. Because of th[illegible] like-upon-like material impacts can be treated. Second, there is a tendency to "smear" or diffuse material and average densities, velocities, and internal energies. The termination of the calculations was arbitrarily set as the time at which the momentum that had passed through the shield reached the maximum and the kinetic energy of the debris was a maximum. At such time the debris was essentially "set" with very low pressures and with the momentum distribution changing no further with time.

A total of twenty-six CAMEO calculations were made; the conditions of these impacts are summarized in Table I. Sixteen of the problems were computed for data purposes and ten for the purpose of checking the program or to check the computer predictions with experiment.

The CAMEO results scale directly, i.e., equal scale changes of linear dimensions and time produce the same result.[10] It was found, however, that if the problem were initially stated with small masses, computer round-off error would result in relatively large mass, momentum, and energy errors. To prevent this type of error the problems were computed with scaled-up projectiles and shields. Thus the aluminum cylinders and spheres used for computation had masses of about 45 grams; the aluminum rods 205 grams; and the cadmium spheres 146 grams. With masses of these sizes the energy error was of the order of one percent.

Table I
IMPACT CONDITIONS FOR CAMEO CALCULATIONS

Problem Number	Projectile	Shield t_s/d	Velocity (km/sec)	Purpose
1–6	Al Cylinder	0.30	7.2	Test Cases
7	Al Cylinder	0.228	7.6	Data
8	Al Cylinder	0.228	30	Data
9	Al Cylinder	0.228	22.5	Data
10	Al Cylinder	0.228	15	Data
11	Al Cylinder	0.111	30	Data
12	Al Cylinder	0.333	30	Data
13	Al Cylinder	0.500	30	Data
14	Al Cylinder	1.00	30	Data
15–16	Al Sphere	0.264	7.2	Test Case
17	Al Sphere	0.20	30	Data
18	Al Rod	0.50	5	Test Case
19	Cadmium Sphere	0.20	6	Data
20	Al Rod	0.76	5	Test Case
21	Al Cylinder	0.228	50	Data
22	Cadmium Sphere	0.100	6	Data
23	Cadmium Sphere	0.300	6	Data
24	Cadmium Sphere	0.500	6	Data
25	Al Cylinder, $\rho_o = 0.483$ cm/cm^3	—	30	Data
26	Al Cylinder	0.228	30	Data

The first six test cases were used to minimize the error described above and to determine the effect of cell size upon the computations. It was found that the smallest cell sizes or the finest zoning reduced the magnitude of error. Coarse zoning tends to lose detail but the gross features tend to the same values. Figure 2 presents the total axial and radial momenta of the debris as a function of time for problems CAMEO 5 and 6. CAMEO 6 was a factor-of-three finer in zoning than was CAMEO 5; i.e., the projectile in problem 6 consisted of nine

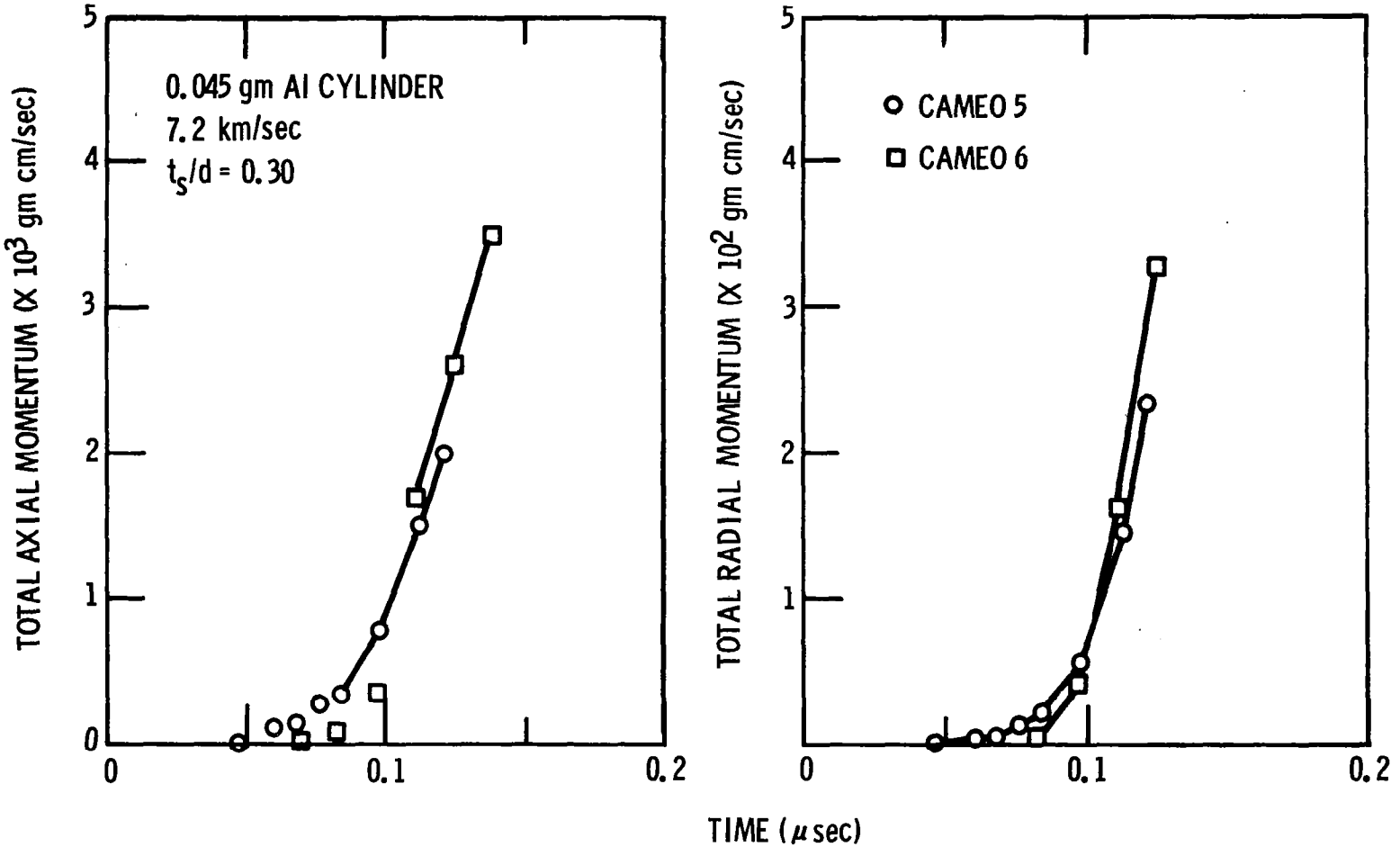

Figure 2 Computed Debris Momenta vs Time

times as many cells as CAMEO 5, and the shield was nine cells thick in CAMEO 6 and three cells thick in CAMEO 5. As can be seen the momenta initially are not the same but approach the same values very rapidly, with perhaps a time lag.

The total kinetic energy, as presented in Figure 3, also rapidly approaches the same values, with again a time lag. From these tests the conclusion was drawn that, although the coarse zoning lacked fine-time precision, the overall gross effects were essentially not affected.

On the basis of these test cases, it was decided to perform the early-time calculations with as fine zoning as possible. This decision conflicted with the restricted number of zones due to limitations imposed by the size of the available computer memory core and auxilliary memory system could not be used with existing facilities. There were two solutions to this problem: to rezone at some stage in the computation (e.g., convert n^2 zones into n zones), or to increase the size of the zones with increasing distance from the impact area.

It was determined that, since the debris would be in a highly expanded form in the cases of interest and would be undergoing little interaction, and also that rezoning would present difficulties in maintaining both conservation of momentum and energy, it would be best to increase zone sizes with increasing distance from the impact point. A typical zoning procedure of this type is presented in Figure 4. As can be observed, the zones are all of the same size in the area surrounding and including the impact point and, in addition, are of square cross-sectional area. At greater distances from the impact area, the zone sizes increase and become rectangular in cross-section. The zoning procedure utilized in Figure 4 was used for CAMEO 7 through 10. Similar schemes were utilized for all other CAMEO data computations.

Several of the CAMEO computations were compared with experiment to provide checks upon the accuracy of the computational results. The outputs from CAMEO 4 and 19 are presented in Figures 5 and 6, along with experimental results of total axial momentum as a function of the tangent of the spray half-angle. The experimental points were obtained by means of a double ballistic pendulum,

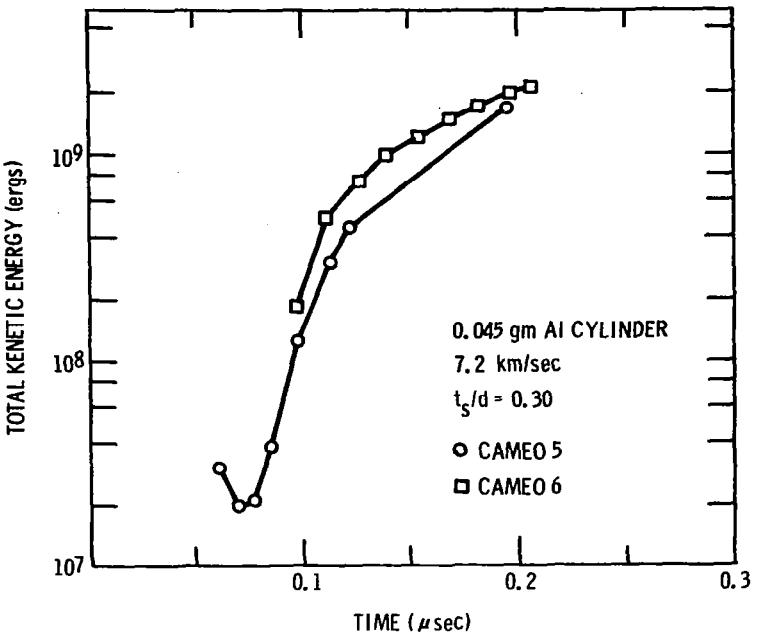

Figure 3 Computed Debris Energies vs Time

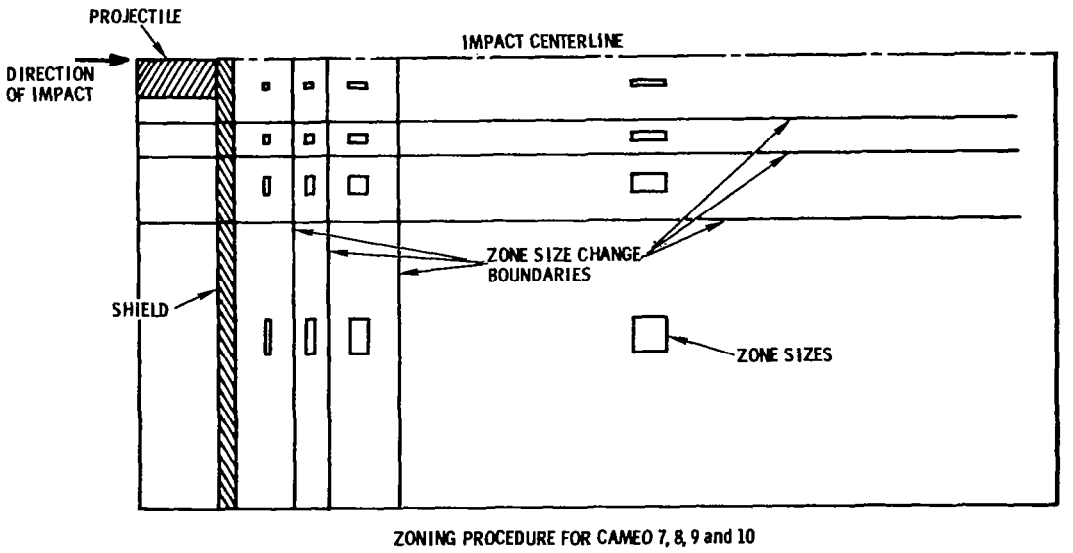

Figure 4 CAMEO Zoning Procedure

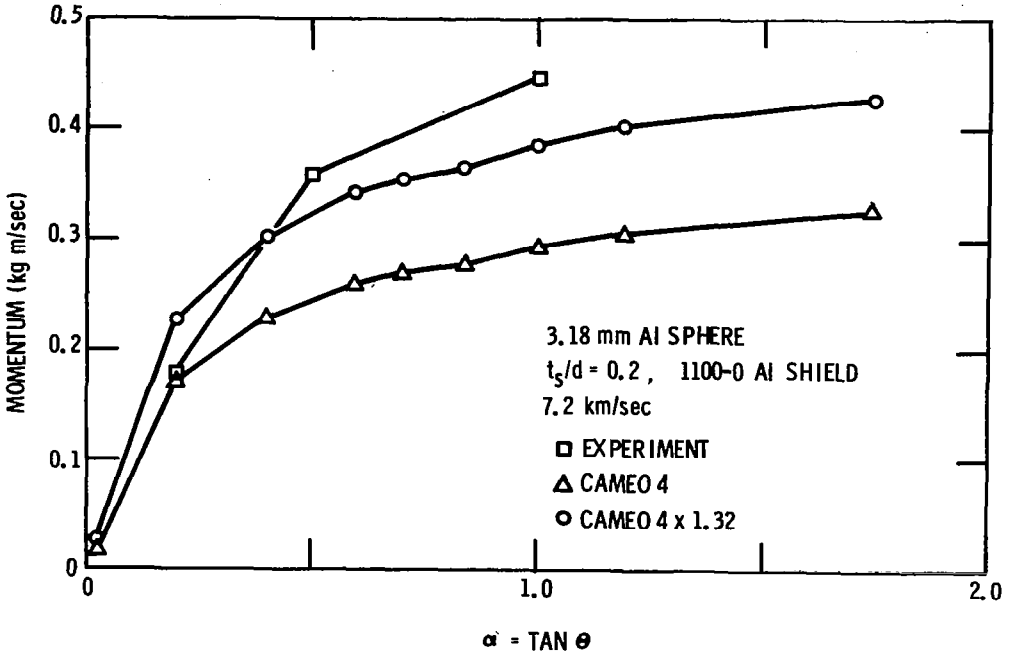

Figure 5 Momentum vs Spray Half-Angle (Aluminum Impact)

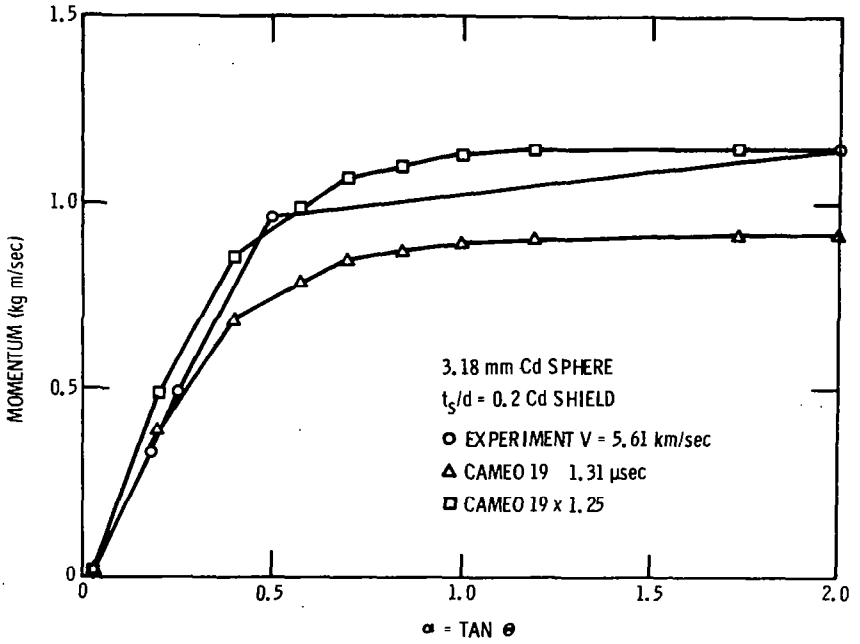

Figure 6 Momentum vs Spray Half-Angle (Cadmium Impact)

shown in Figure 7. The shield is mounted upon the pendulum support structure and the second sheet is mounted in two sections on the two pendulums. The debris from the projectile and shield strikes the second sheet and imparts its momentum to the two pendulums. The motions of the pendulums are monitored with small neon lights mounted upon the pendulums; the lights flash at a known constant frequency and expose the film in a stationary open-shutter camera. The record obtained thus gives a direct measure of the distance the pendulum travels versus time. A typical camera trace for a dual-pendulum test is shown in Figure 8, along with a segmented second sheet.

It is important to note that the momentum measured utilizing the ballistic pendulum is the momentum felt by the sheet that is struck by the debris, and it is not the momentum of the debris. The CAMEO output is the momentum of the debris, and the total axial momentum is about the same as the momentum of the original impacting particle. The debris may rebound upon striking the second sheet, resulting in an increase in the momentum felt by the second sheet. If the debris were completely vaporized and underwent perfectly elastic collisions with the second sheet, it would have twice the axial momentum of the debris. Experiments performed up to eight kilometers per second give momentum increases of up to about 1.5 times the impacting particle momentum.

Thus the comparisons made in Figures 5 and 6 required correction for the momentum multiplication effect. In Figure 5 the CAMEO output is presented (as triangles) together with the output multiplied by the measured multiplication factor from experiment (as circles). The agreement is fairly good, with two experimental points within 15% of the computed points and the point at the smallest angle within 25%. The smallest angle experimental point is the least well defined in terms of angle, thus it would be expected to have the largest error associated with it and would probably be low.

Figure 6 presents a comparison of momentum distribution for a cadmium-cadmium impact. Cadmium with its low melting and vaporization points (320^{o}C and 767^{o}C), low sonic velocity and low strength is better represented by the CAMEO hydrodynamic calculations than aluminum at experimental velocities.

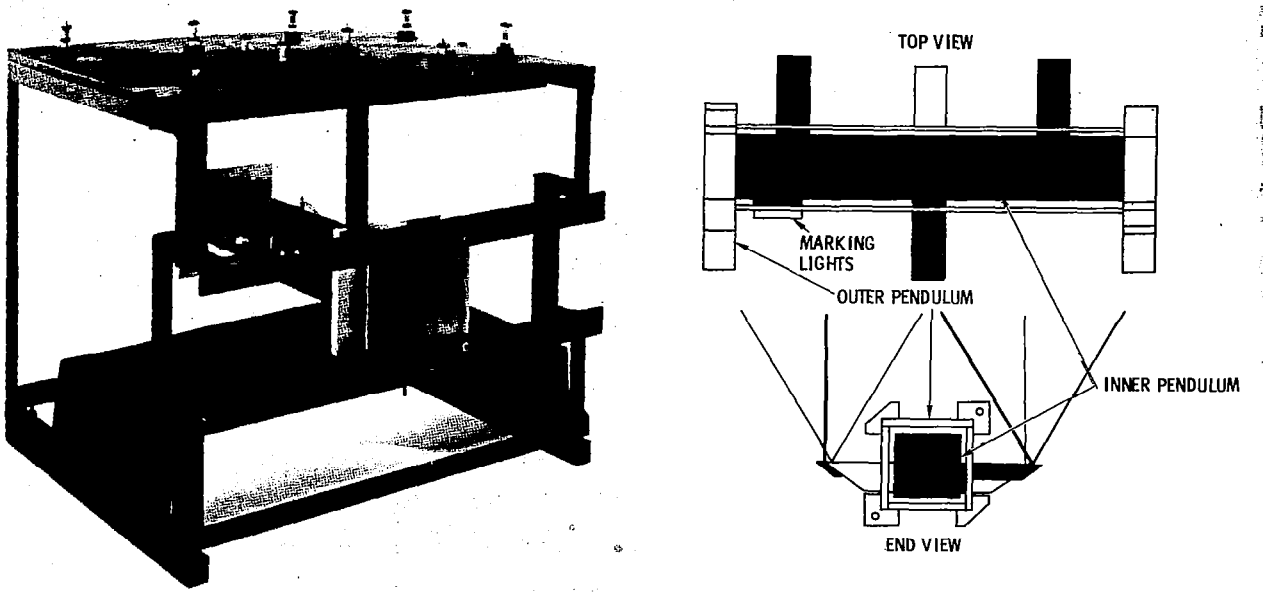

Figure 7 Dual Ballistic Pendulum, Schematic and Photograph

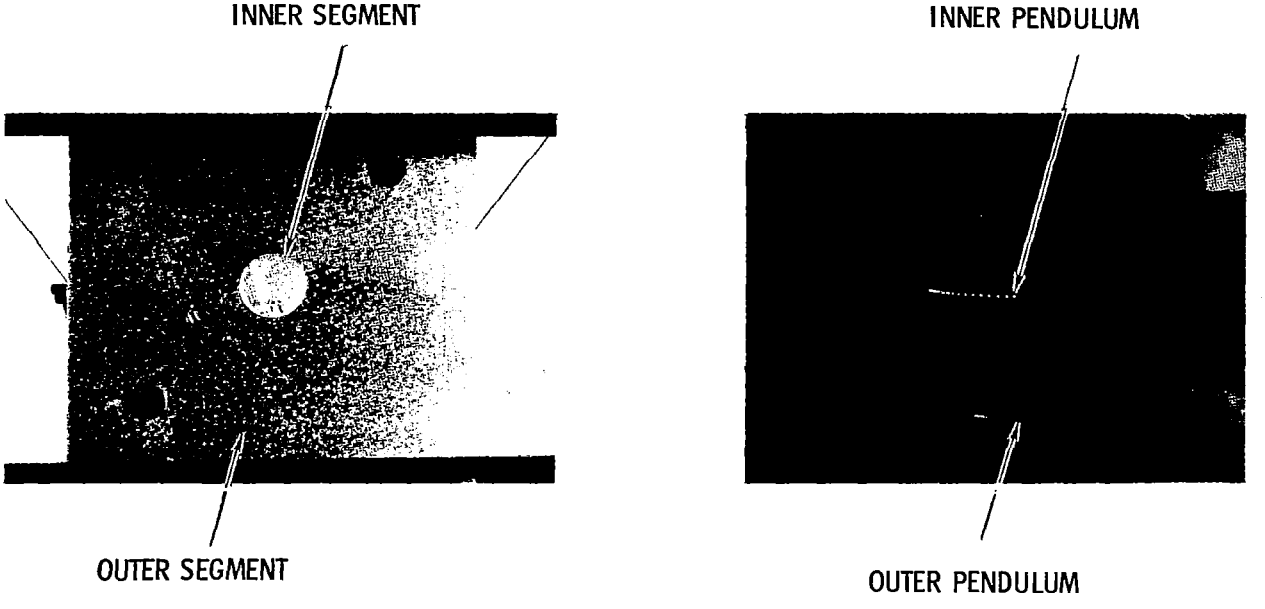

Figure 8 Pendulum Camera Trace and Segmented Target

For the conditions of impact, all the debris should be vaporized. In this figure, the computed momentum distribution is fitted to the experimental total momentum, thus the points at $\alpha = 2$ must agree. The experimental points at smaller values of α agree with the computed values quite well.

In Figures 9 through 12, the CAMEO results are compared with experiment in a different manner. In these experiments the second sheet was split, and a series of squares (1.27 cm x 1.27 cm) of the same thickness and material as the backup were lightly cemented in the gap between the halves of the backup sheet. When the projectile-shield debris struck these squares, the momentum of the debris that struck them was imparted to the squares. The momentum intensity is defined as the momentum per unit area or

$$I = \frac{mv}{A}$$

and the momentum of the squares is

$$MV = \rho A t V$$

where

ρ is the material density of the square
A is the area of the square
t is the thickness of the square
V is the velocity of the square

and the average momentum intensity felt by the square is

$$\frac{MV}{A} = I = \frac{\rho A t V}{A} = \rho t V$$

so that the velocity of the square after impact is directly proportional to the momentum intensity.

Figure 9 shows the computed and measured momentum intensities versus α for an aluminum-aluminum impact. In this figure, as in the subsequent Figures 10–12, the computed momentum intensity is presented without taking the momentum multiplication into account. As a result, it is expected that the computed points should fall below the measured points. In these figures, the computed

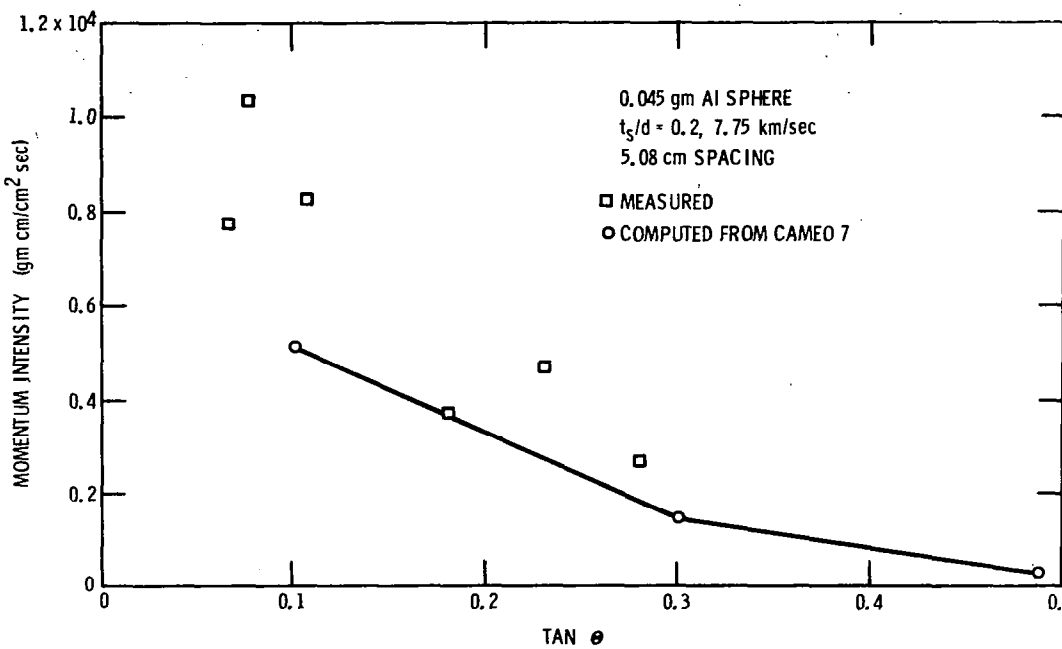

Figure 9 Momentum Intensity vs Spray Half-Angle
$t_s/d = 0.2$

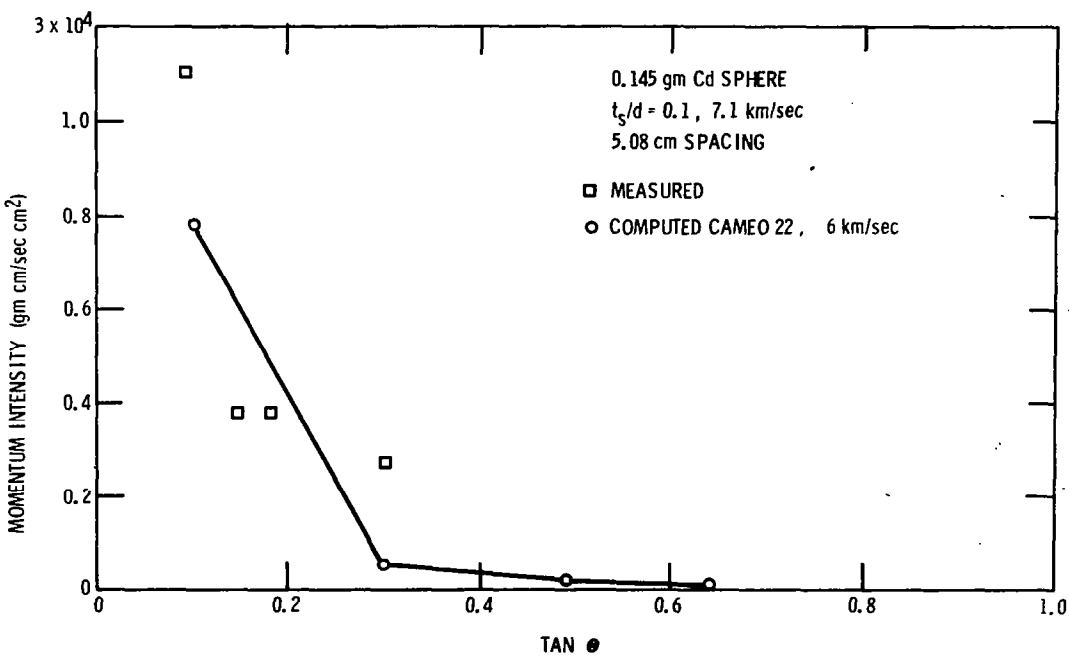

Figure 10 Momentum Intensity vs Spray Half-Angle
$t_s/d = 0.1$

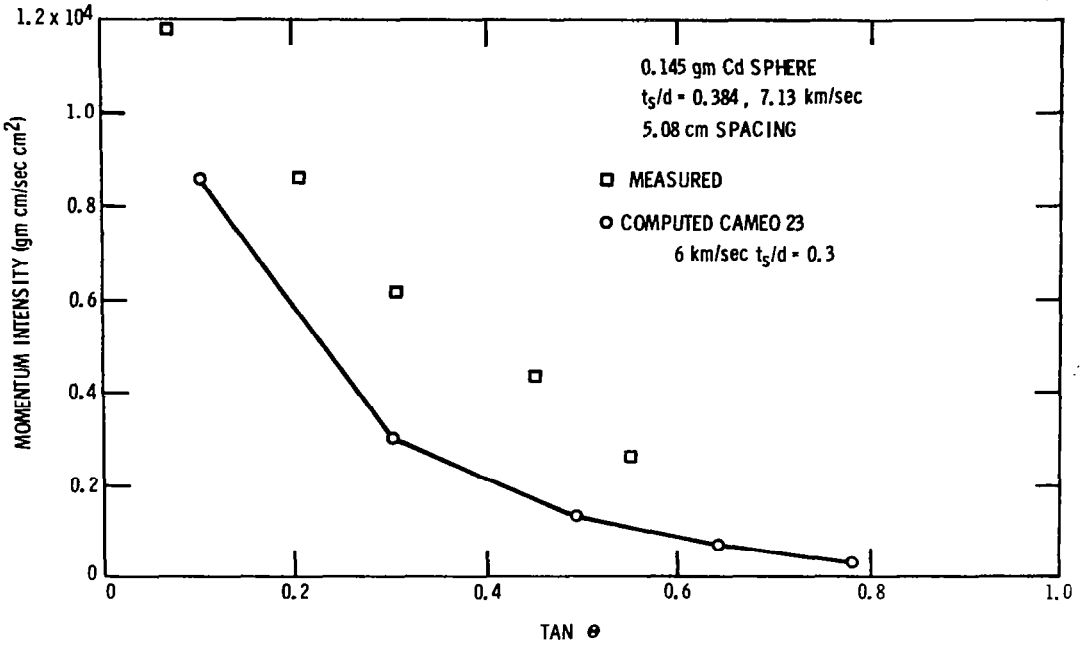

Figure 11 Momentum Intensity vs Spray Half-Angle $t_s/d = 0.384$

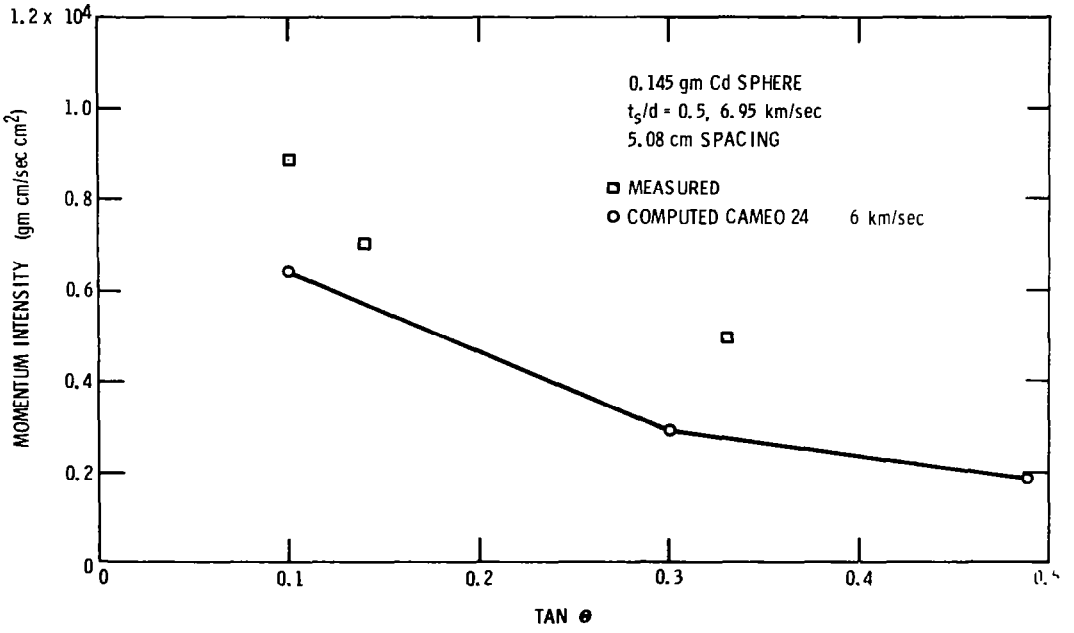

Figure 12 Momentum Intensity vs Spray Half-Angle $t_s/d = 0.5$

momentum intensities represent averages over fairly large ranges of α; also, the lines connecting the points were added for clarity and do not represent intermediate values. It can be seen that the measured data in Figure 9 compare very favorably with the computed values in magnitude and in the curve shape. Figures 10 through 12, which show comparisons of cadmium-cadmium impacts, also compare favorably.

On the basis of the comparison of computed values and measured values of momentum distribution and momentum intensities presented in Figures 5, 6, and 9 through 12, it was felt that the CAMEO code was quantitatively representative of the momentum distributions of the debris passing through the shield.

A further test of the CAMEO computations was made by examining rod impacts. The method of comparison was to predict the amount of rod fractured or "used" in passing through a thin sheet. Because the hydrodynamic calculations do not include strength effects and do not provide for fracture of material, a criterion had to be established for the determination of flow and fracture. The criterion used was a "cutoff" pressure; i.e., if the material was subjected to a pressure above some value, it would be fractured. This approximation ignores the shape of the pressure profile, which would have a significant effect upon fracture. However, in the case of a rod impacting a thin sheet, it would be expected that the shock or pressure pulse would be quite sharp (short in time duration) in both the rod and the thin sheet because of the close proximity of free surfaces. The shock reflects from these free surfaces as rarefactions which rapidly overtake the shock.

Two cases were considered:

- the impact at 5 kilometers per second of a rod three times as long as its diameter upon a thin sheet 0.5 times the rod diameter in thickness
- the impact at 5 kilometers per second of a rod ten times as long as its diameter upon a sheet 0.76 times the rod diameter in thickness.

Both the rods and the thin sheets were of 2024-T3 aluminum. The first step was to utilize the diameter of the hole formed in the $t_s/d = 0.5$ sheet to establish the

"cutoff" pressure. By examining the CAMEO cells at the edge of the shield hole a "cutoff" pressure of between 40 and 55 kilobars* was established. Using this pressure range to assign the amount of rod broken, the length of the rod remaining after impact was predicted from CAMEO. The ratio of the rod length remaining to the original rod length (L_r/L) was predicted to be between 0.536 and 0.584; the experimental ratio determined from flash X-rays was 0.54.

Proceeding to the second impact, a ratio of hole diameter to rod diameter (D/d) of between 2.66 and 2.84 was predicted from the CAMEO output as compared to an actual value of 2.75. The predicted values of L_r/L in this case were 0.857 to 0.865 and the experimental ratio was 0.84.

The excellent agreement of the CAMEO-predicted values and the experimentally determined values for the rod impacts taken with the momentum comparisons establishes a high level of confidence in the use of CAMEO computations for thin-sheet impacts.

Prior to performing data computations it was necessary to establish that termination of the computations upon reaching the maximum debris axial momentum and kinetic energy would not result in a lack of definition at later times. Examination of the axial momentum distribution of the debris at various times showed little change after the termination described above. Examples of the axial momentum distributions are shown in Figures 13, 14 and 15 for aluminum-aluminum impacts at velocities of 7.6, 30 and 50 kilometers per second. The termination in Figure 13 was 0.674 μseconds. Prior to this the full momentum had not passed through the shield. After this time there was very little change for small half angles through 2.00 μseconds. At 2.00 μseconds the mass loss through smearing or diffusion had resulted in a total momentum loss. The same effect is seen in both Figures 14 and 15. After the termination time (0.413 μsecond in Figure 14 and 0.296 μsecond in Figure 15) the entire momentum curve has been displaced downward, reflecting the diffusion mass loss.

---

* 1 kilobar = 10^9 dynes/cm^2, 1 megabar = 10^3 kilobars = 10^{12} dynes/cm^2

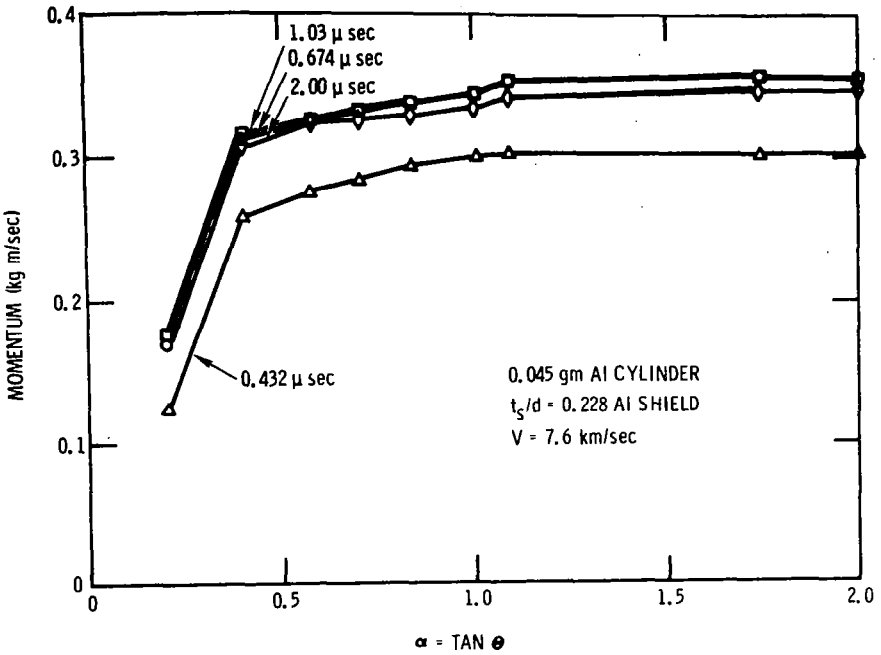

Figure 13 Momentum vs α – 7.6 km/sec – Various Times

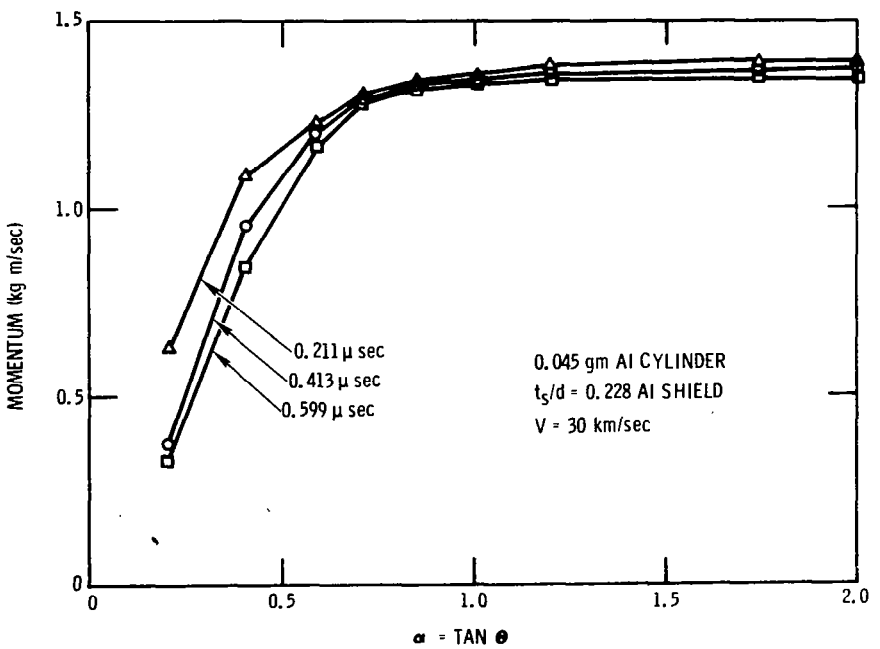

Figure 14 Momentum vs α – 30 km/sec – Various Times

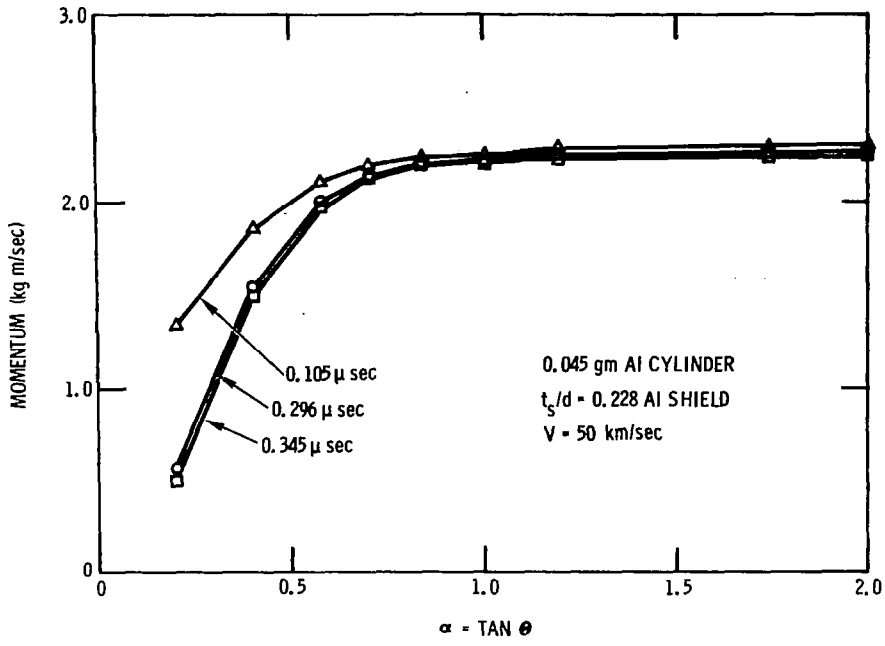

Figure 15 Momentum vs α –50 km/sec– Various Times

Finally the question of the equivalence of impacts of cylinders and spheres was examined. Computations were made with aluminum spherical projectiles of the same mass as cylinders. The spherical projectiles were not true spheres but approximation to spheres made with the toroidial zones described previously. The spheres were essentially larger than the cylinders of the same mass having larger characteristic diameters.

Figure 16 shows equivalent-mass aluminum cylinder and sphere impacts in terms of the total internal energy of debris that has passed through the shield as a function of time. As can be seen, the internal energy through the shield for the cylinder is greater at any given time than for the sphere. The time behavior of the internal energies is very similar however, with the sphere curve lagging about 0.055 μsecond behind the cylinder. Figure 17 presents the debris kinetic energy for the same two impacts; the behavior is similar to that of the internal energy, again with a time lag of about 0.055 μsecond. After about 0.15 μsecond the ratio of internal energy to kinetic energy is the same, indicating that after this time the debris passing through the shield is in the same state.

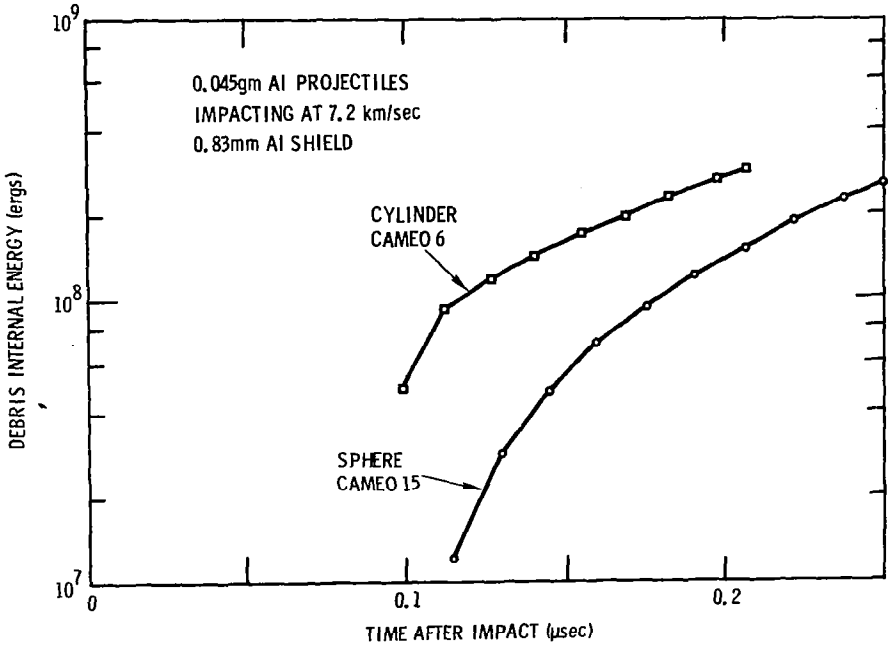

Figure 16 Debris Internal Energy vs Time for Cylinder and Sphere

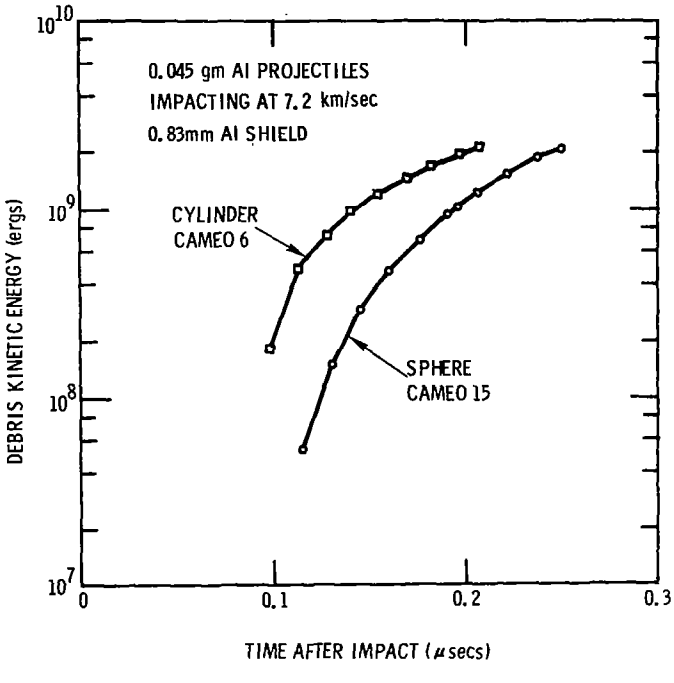

Figure 17 Debris Kinetic Energy vs Time for Cylinder and Sphere

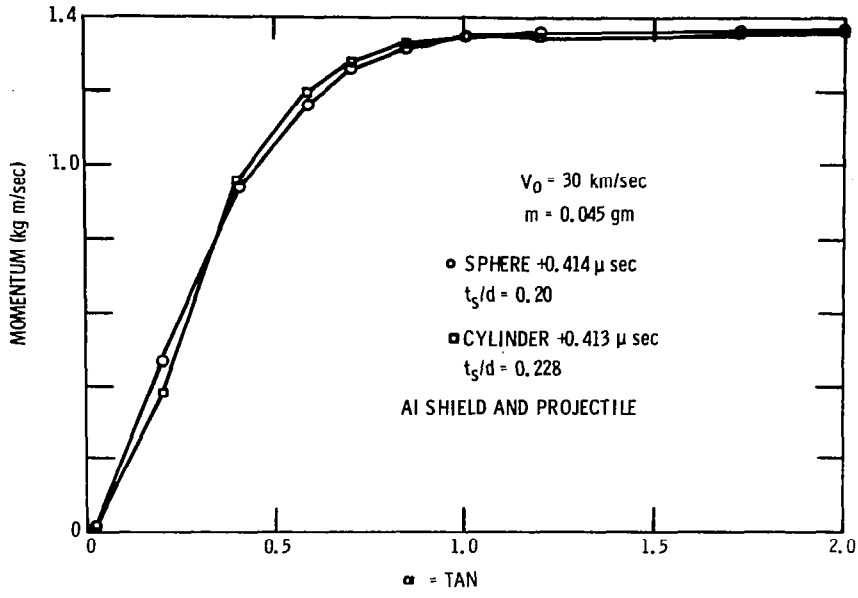

Figure 18 Momentum vs α for 30 km/sec Cylinder and Sphere

The momentum distributions for equivalent-mass cylinder and sphere impacts at 30 kilometers per second (Figure 18) show very little differences at a comparitively late time. Examination of the debris kinetic and internal energies at this time showed the kinetic energies to be within one percent and the sphere internal energy to be about nine percent higher than that of the cylinder. The debris mass was also about nine percent higher for the sphere, showing that more of the shield debris has been ejected as debris for the sphere impact but that its energy is primarily internal. The centerline debris densities and velocities for these impacts are shown in Figure 19. Because a computer print-out is not made for every cycle of computation, the times and distance of travel relative to the rear surface of the shield are not the same. Note that the density and velocity structure is essentially the same for the main body of the debris. When the debris from the sphere impact reaches the same point as the cylinder impact debris, the peak density is about the same due to further expansion of the debris. (This conclusion is reached by examination of later print-outs and interpolation.) Since the momentum will control the damage to the second sheet, there seemed to be no preference between the use of the sphere or the cylinder.

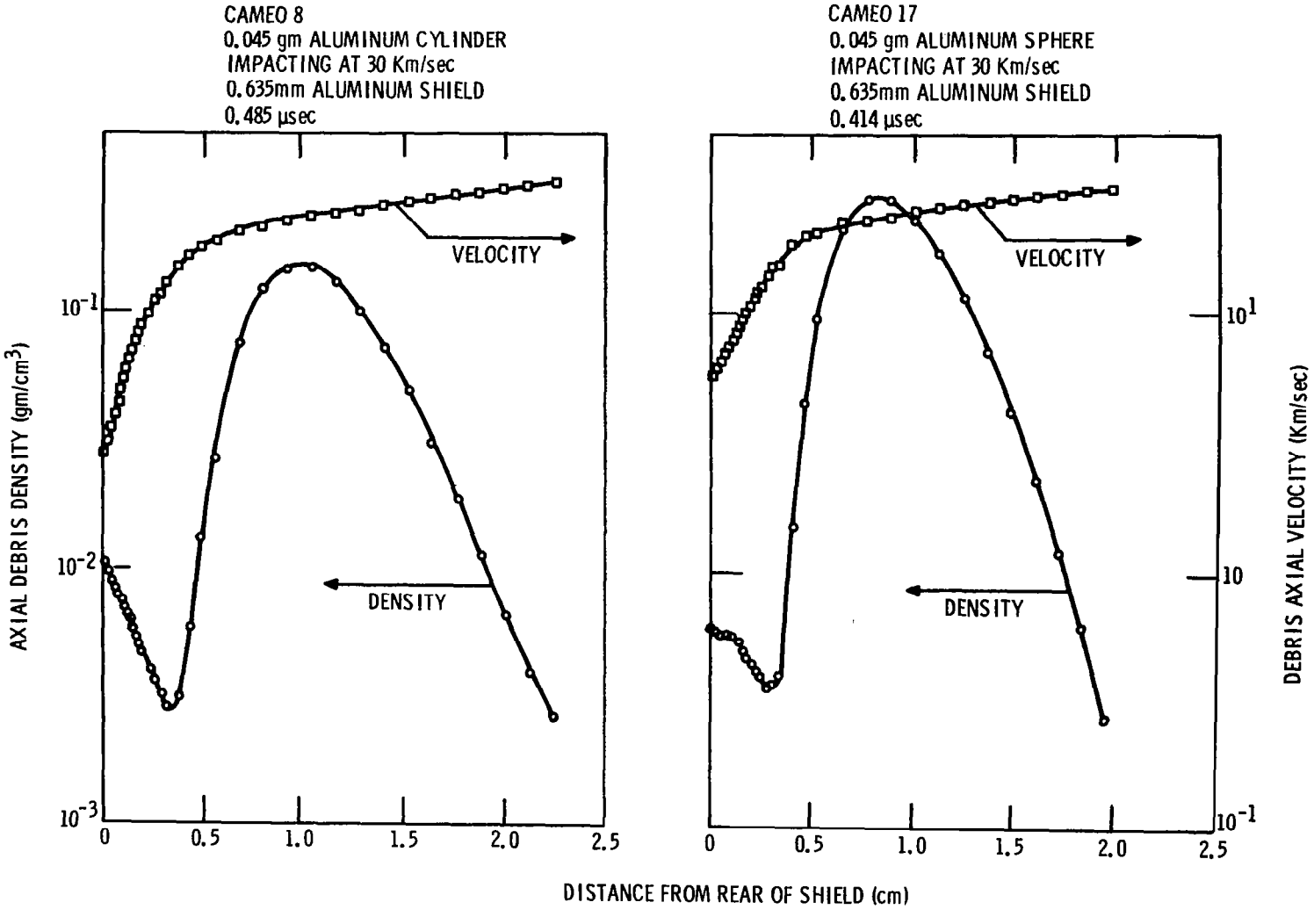

Figure 19 Cylinder and Sphere Centerline Debris Profiles

Three categories of data runs were performed: (1) Aluminum cylinders impacting the same shield at varying velocities; (2) Aluminum cylinders impacting shields of various thicknesses at a constant velocity; and (3) Cadmium spheres impacting cadmium shields of various thicknesses at a constant velocity.

The results of the first category are shown in Figure 20 as normalized axial momentum distributions. The momentum tends to be concentrated within larger half-angles as the impact velocity is increased through 22.5 kilometers per second. At velocities higher than this for the given shield thickness, the momentum again becomes more concentrated near the centerline. This would be expected, as the radial velocity of the debris for a thin shield is essentially limited to the escape velocity of the debris vapor. With increasing impact velocities the axial velocity of the debris is closely related to the impact velocity, while the radial velocity is not. Thus the debris becomes more concentrated at small half-angles. In Figure 21 the same data has been presented as momentum intensities. The momentum intensity is the momentum per unit area on a plane perpendicular to the centerline (parallel to the shield) at some arbitrary distance from the shield. At impact velocities between 22.5 and 30 kilometers per second the shield has been very efficient in distributing the momentum, while at 50 kilometers per second the debris has become more concentrated at small angles. In none of the cases considered does any appreciable amount of momentum fall outside $\alpha = 1$, or 45^{o}.

The second category of impacts considered was aluminum-aluminum impacts at 30 kilometers per second upon shields varying in thickness from 0.111 times the projectile diameter to the full diameter of the projectile. These computational results are presented in Figures 22 and 23. Figure 22 shows the axial momentum as a function of spray half-angle. As can be seen, the total amount of momentum increases as the shield thickness is increased with an enhancement of about 44 percent for the thickest shield. This increase in debris momentum is due to ejection of material from the front face of the shield. The amount of this ejecta is related to the shield thickness or hole size in the shield. As the shield is increased in thickness the total axial momentum increases and the amount of momentum at small angles decreases. The overall effect is to reduce the momentum

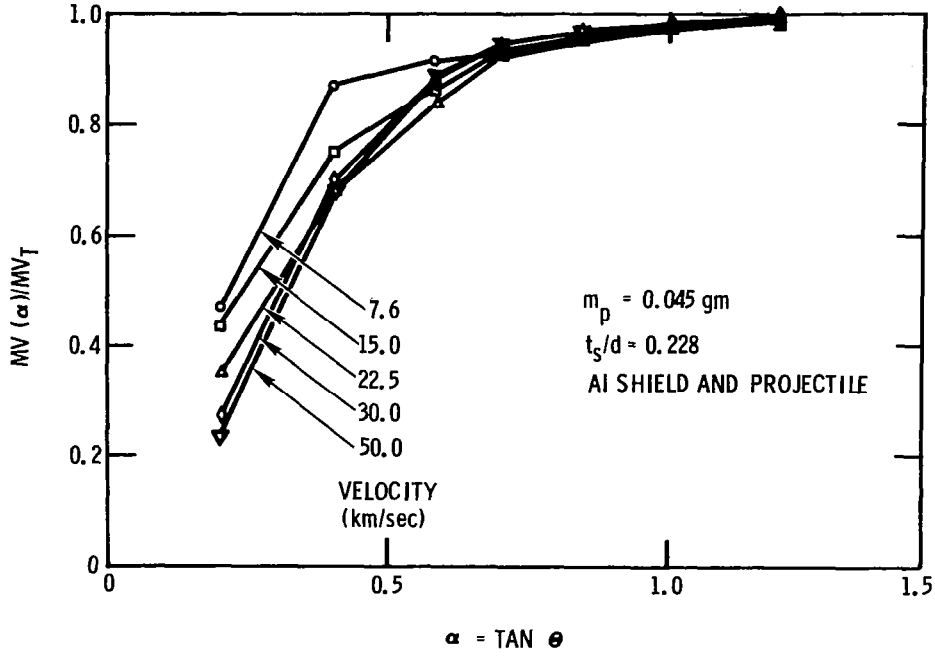

Figure 20 Normalized Momentum vs α – Various Velocities

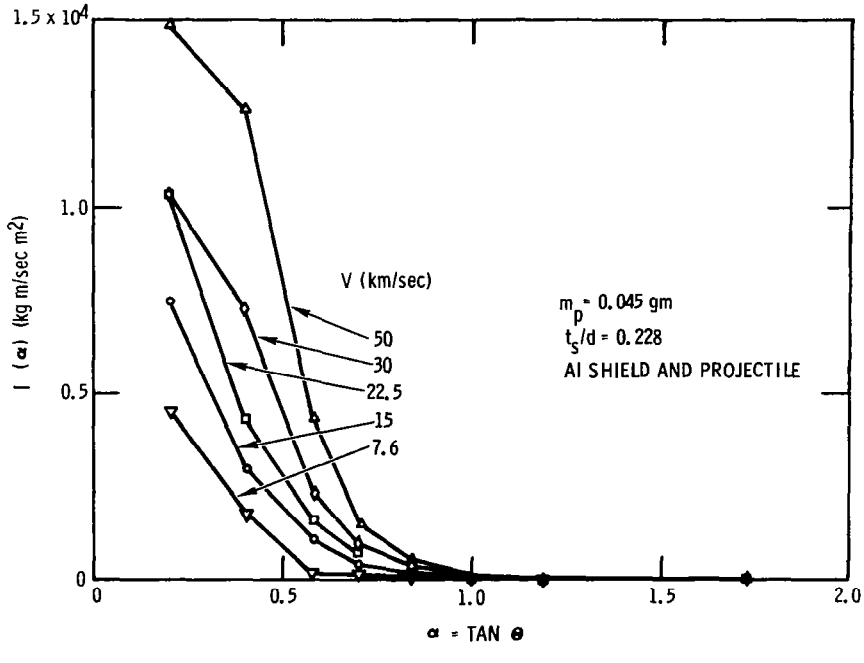

Figure 21 Momentum Intensities vs α – Various Velocities

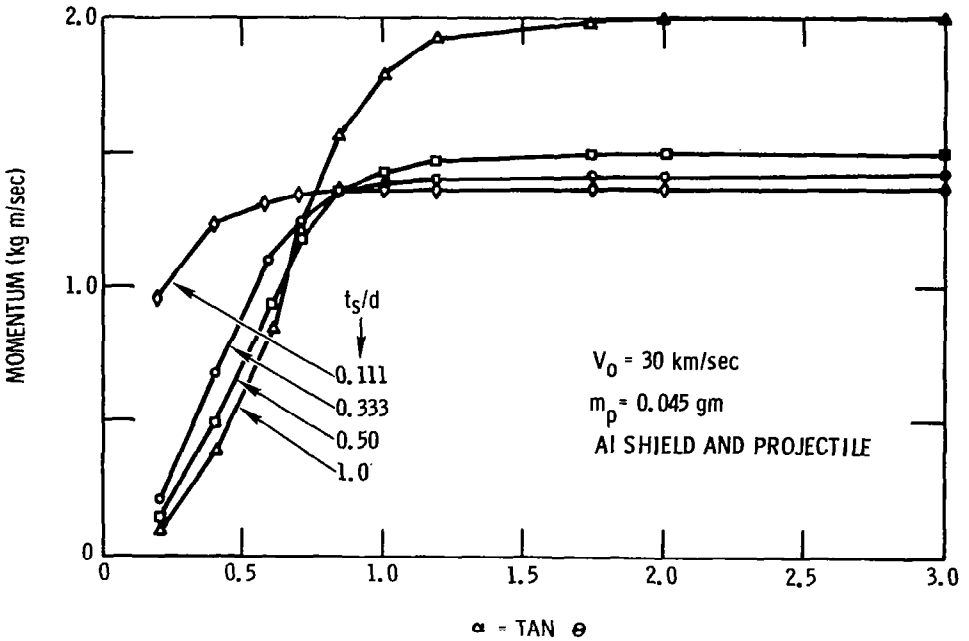

Figure 22 Momentum vs α – Various Shield Thicknesses

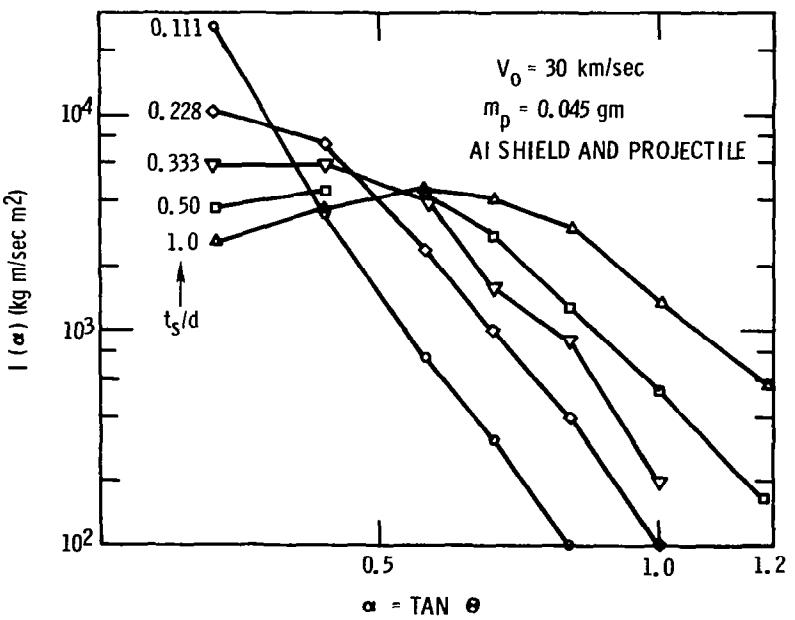

Figure 23 Momentum Intensity vs α – Various Shield Thicknesses

load per unit area (Figure 23). The momentum load at a $t_s/d = 0.5$ is almost uniform to $\alpha = 0.7$, and for $t_s/d = 1.0$ the load is more concentrated at $\alpha = 0.7$ than it is at the center of the loaded area. Once again almost all of the momentum is within $\alpha = 1.0$ or a 45-degree half-angle.

Figure 24 shows the centerline densities and velocities of the $t_s/d = 0.111$ and $t_s/d = 1.0$ impacts. Even allowing for further expansion of the debris from the thinner-shield impact, the peak density will be almost a factor of ten greater than that from the thick-shield impact. Further, there is a much greater velocity gradient in the thick-shield debris. The total result will be a more intense, shorter-duration pressure pulse generated in the second sheet by the debris from the thin shield.

Finally a group of cadmium-cadmium impacts at 6 kilometers per second were considered. Again the shield thicknesses were varied. The axial momentum distributions from these computations are presented in Figure 25. The results are qualitatively the same as for the high-velocity aluminum impacts shown in Figure 22. As the shield is increased in thickness the momentum is more effectively dispersed to larger half-angles.

With these computations, consideration will be given to the reaction of the second sheet of a thin-sheet structure. The results of the aluminum-aluminum impacts were employed to evaluate the resistance of structures to meteoroid impact. As was said earlier, the expected meteoroid is of the order of 0.5 gram per cubic centimeter. Impacts of low-density plastic and aluminum projectiles have been considered in References 10 and 11. These results show much greater heating of the projectile for underdense projectiles, and lower pressures throughout. The aluminum-aluminum impacts that have been considered herein show all the debris to be vaporized at impact velocities of 30 kilometers per second and greater. One computation for the impact of an underdense projectile was performed. In this computation the projectile was taken to be expanded aluminum vapor with a density 0.483 gram per cubic centimeter, or 0.179 times the normal aluminum density. The impact was at 30 kilometers per second upon a shield 0.635 millimeter thick. The projectile had the same mass as the normal-density aluminum cylinders of

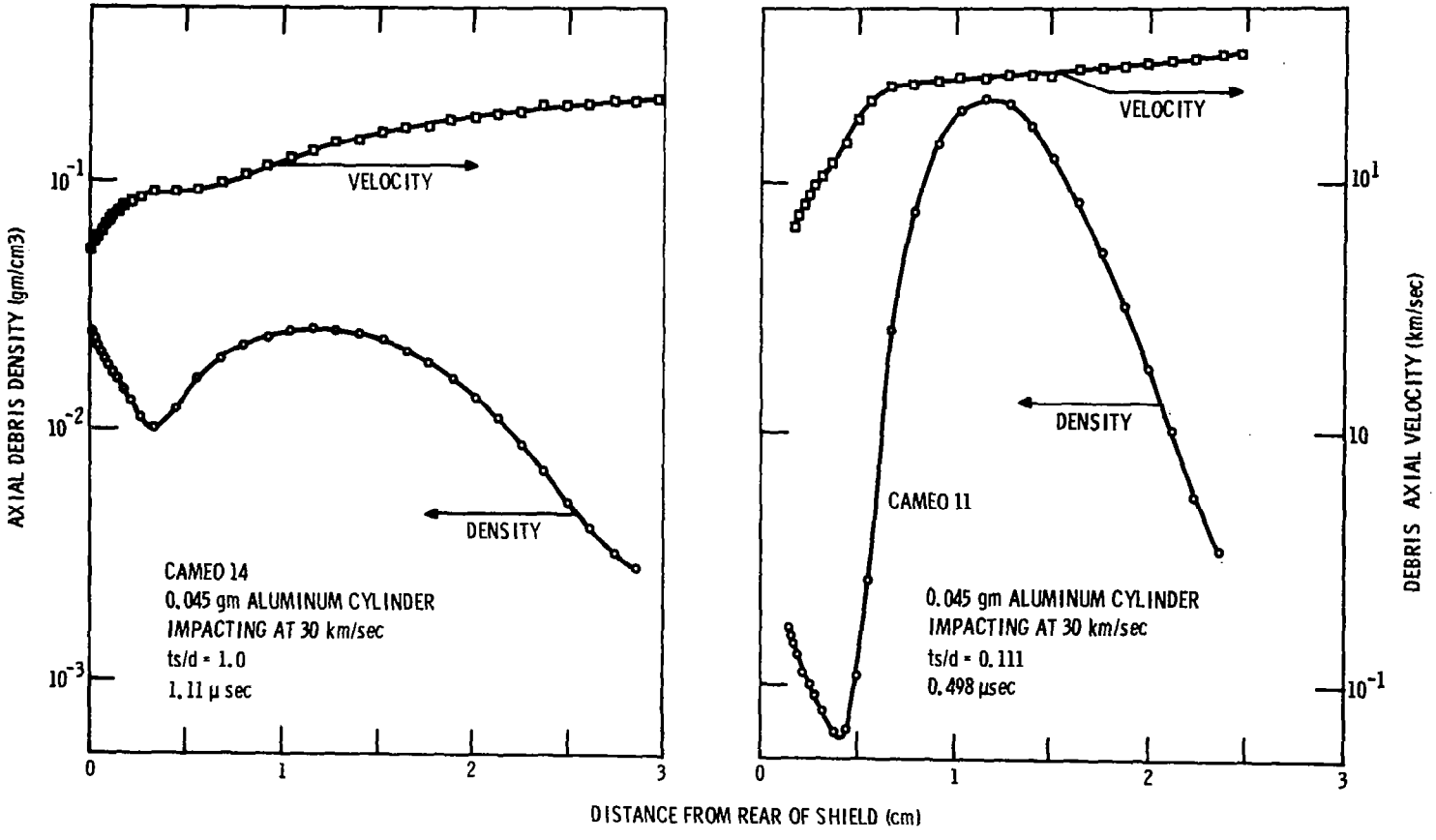

Figure 24 Centerline Debris Profiles for Two Shield Thicknesses

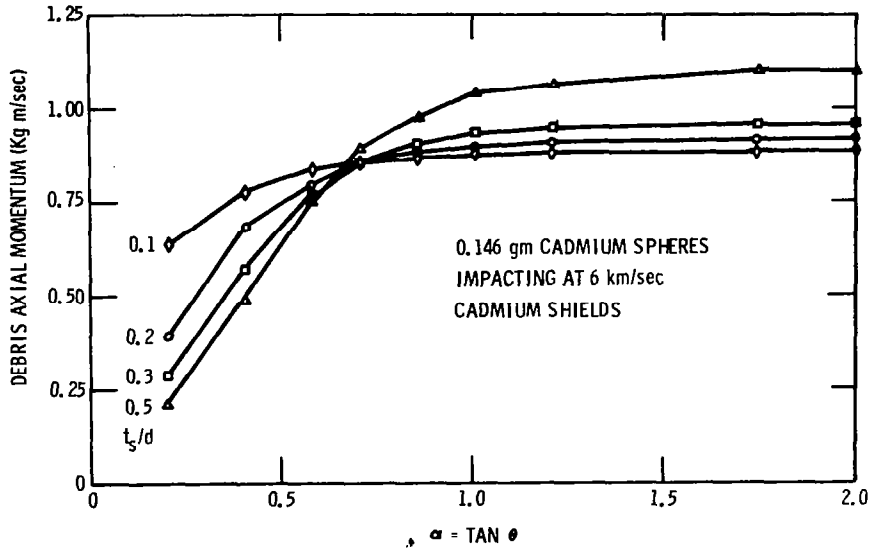

Figure 25 Momentum vs α for 6 km/sec Cadmium Impacts

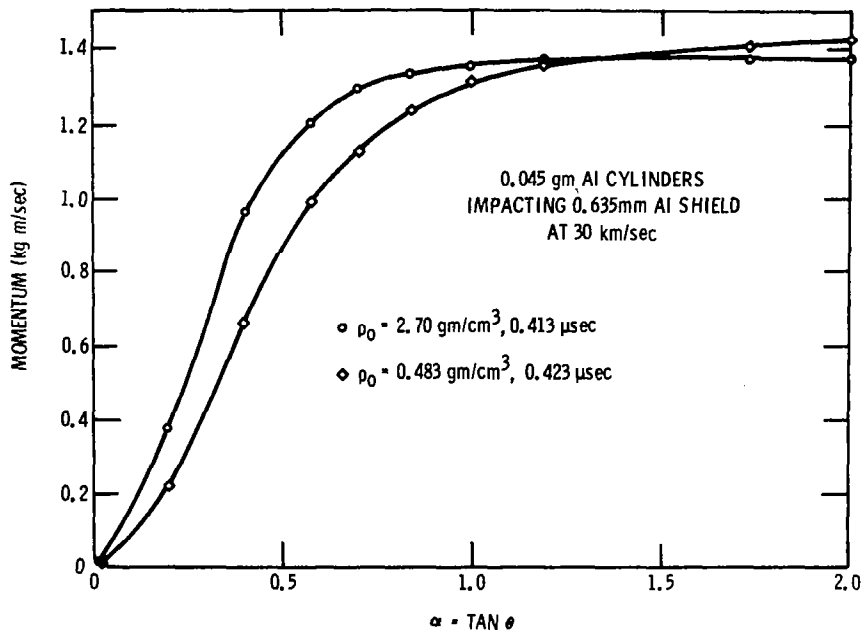

Figure 26 Momentum vs α for 30 km/sec Aluminum Impacts

CAMEO 7 through 14. This impact is the same as CAMEO 8 with the exeption of the projectile density. The first point of difference in the results is the maximum pressure of the impact, with the underdense impact showing a maximum pressure of about 2 megabars as opposed to a pressure of about 10 megabars for the normal-density impact. After about 0.4 microsecond the kinetic energy of the debris is comparable with the low-density impact, having about 90% the kinetic energy of the normal-density impact. The internal energy, however, is more than three times as great in the debris of the low-density impact. A comparison of the momentum distributions at this time is shown in Figure 26. Even though the debris from the low-density impact contains about 1.4 times as much mass as the normal-density debris, the total axial momentum is about the same. This means that the axial velocity of the debris from the low-density impact is less than for the normal-density debris. In both cases the debris would be, for the most part, vaporized.

GROSS-DEFORMATION FAILURE OF THE SECOND SHEET

A high-speed framing camera sequence of the failure of a thin-sheet target is shown in Figure 27. The second sheet is given a velocity increment and the sheet starts to deform very soon after the load is applied. For the case shown, a tensile failure has occurred after a matter of a few tens of microseconds.

Figure 28 shows a flash X-ray of a second-sheet failure. It can be seen that the central portion has failed through tension and several cracks have started to propagate in the sheet. Note that the sheet has failed through tension and no spall has formed.

To treat this problem theoretically, such factors as the magnitude, distribution, and duration of the load applied to the target must first be determined. Then the large-deformation dynamic response of the target has to be calculated, taking into account the elastic and plastic behavior of the target.

A description of the distribution of the load is available from the hydrodynamic calculations. These distributions have been utilized to determine the target response; the treatment used will be described chronologically in order to describe it as clearly as possible.

3.2mm Al SPHERE
8.07 Km/sec
0.53mm 1100-0 Al SHIELD
5.08 cm SPACING
0.81mm 7075 T6 Al BACKUP

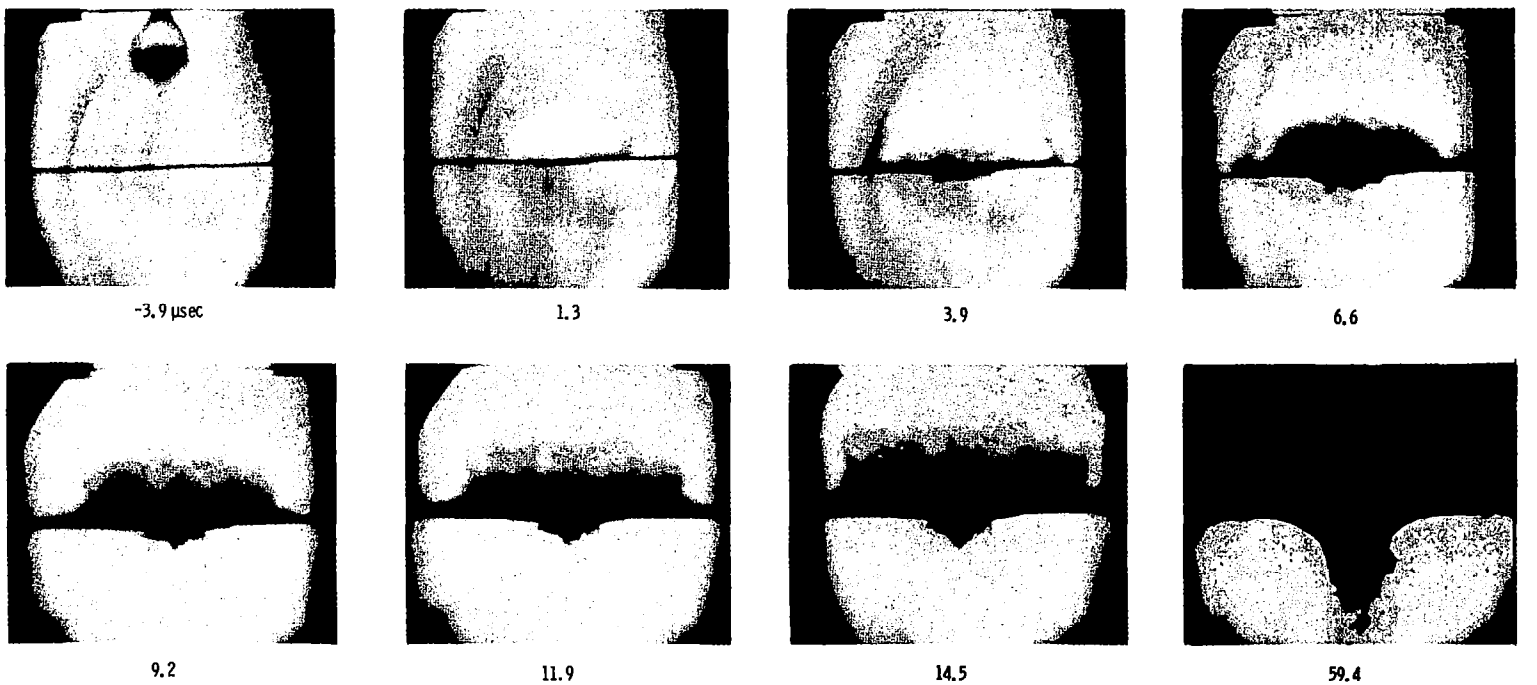

Figure 27 Framing Camera Sequence of Thin Sheet Failure

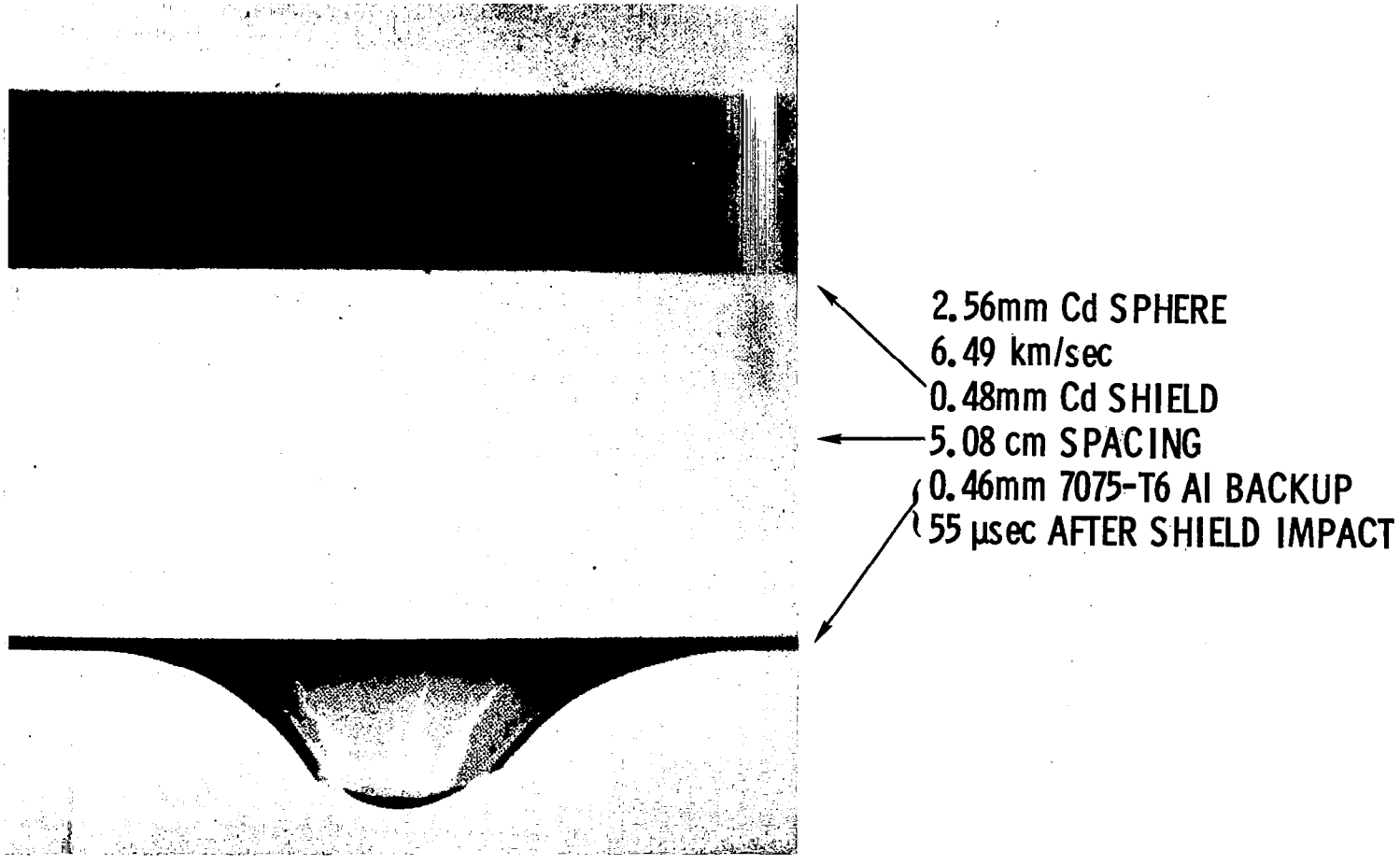

Figure 28 X-Ray Picture of Thin Sheet Failure

The following assumptions were initially made:

(a) The load is uniformly distributed over a circular area with a diameter equal to one-half the spacing.
(b) The load is applied so quickly that the loaded area is effectively given an initial velocity increment.
(c) The momentum transferred to the loaded area is equal to twice the momentum of the original particle.

The main justifications for assumptions (a) and (b) come from Figure 27, whereas a momentum multiplication factor of two, assumption (c), has been chosen for the following reasons: Since the impulsive load applied to a target increases with increasing impact velocity, the inner hull for a spacecraft must be designed to resist a meteoroid at the maximum expected velocity of 30 km/sec. At this velocity, most of the debris coming through the shield will be in gaseous form. Hence, if it is assumed that the momentum of the debris is equal to the momentum of the original particle and that perfectly elastic collisions occur between each gas atom and the target, then the momentum multiplication factor should be two.

Given the loading, the next part of the problem is to determine the response of the target (assumed to be a thin shell). However, the problem of determining dynamic deformations and stresses in thin shells involves, in general, a complex system of nonlinear differential equations. For these problems that involve both large deflections and plasticity effects, a numerical technique has been developed by Witmer, et al.[12] This technique is based on a finite difference approximation for the original differential equations. These finite difference equations are then used to describe an equivalent lumped-parameter model. For the timewise-step-by-step numerical analysis, the increments in stress resultants and stress couples are determined by idealizing the shell thickness as consisting of n concentrated layers (six layers were used in all the present calculations). Also, the material behavior used to determine the above increments can include elastic-perfectly plastic, elastic-strain hardening, or elastic-strain-hardening strain-rate-sensitive behavior.

The success of the above technique has been shown in Witmer's paper[12] in a comparison of theory and experiment for explosively loaded beams.

Figure 29 shows the situation that was first investigated to determine the motion and stress in the backup sheet.[12] In this approximation a strip (or beam) of material through the center of the loaded area was considered. The rear sheet material was taken as 7075-T6 aluminum. This material was assumed to behave in an elastic-perfectly plastic manner with a yield strength σ_0 of 4.67×10^9 dynes/cm^2 (70,000 lb/in.^{2}) and a percentage elongation to fracture of 11 percent. The first step is to calculate the initial velocity v_i imparted to the center portion of the strip. From the previous assumptions this is given by:

$$v_i = \frac{32 M_p V_p}{\pi S^2 \rho_b t_b} \tag{4}$$

where M_p and V_p are the mass and velocity of the impacting particle; S is the spacing, and ρ_b and t_b are the density and thickness of the backup target. For the initial calculation, the following parameters were used: $M_p = 0.045$ grams and $t_b = 0.8$mm.

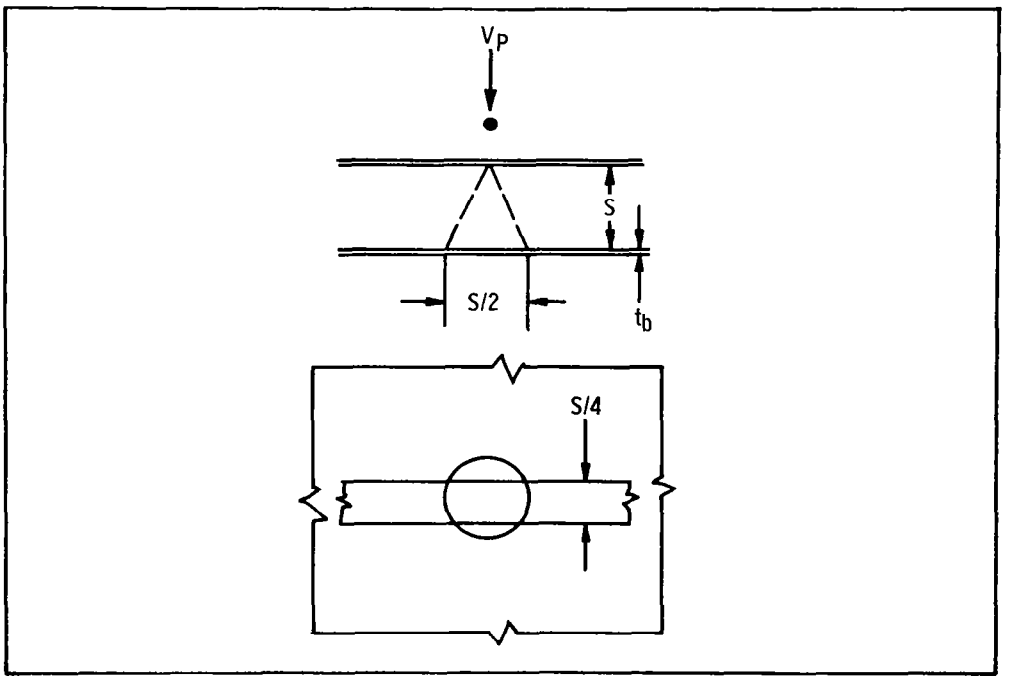

Figure 29 Strip Approximation

The results of the calculation are shown in Figures 30 and 31. The centerline deflection, the tensile strain at the edge of the loaded area, and the tensile strain at the center of the load are shown in these figures. Figure 30 includes the experimental curve of centerline deflection determined from the framing-camera photos in Figure 27, indicating good agreement between theory and experiment. Note that in Figure 31 the fracture strain is first reached at the edge of the loaded area after about seven microseconds; after this time the solution is academic. There is also some evidence of spalling in Figure 27, and such initial wave effects have been ignored for the moment.

The above calculations were repeated for a backup sheet 1.6mm thick. The results showed that the peak strain occurs at the center of the sheet, and that the sheet should not fracture. Experiment showed that only a small perforation occurs, and this is due to spallation.

With the above reasonable agreement between theory and experiment, it was decided to use the strip approximation further. Because solutions are required for an effectively infinite rear sheet, it was considered necessary to find out how long a strip is effectively infinite for the time of interest in the present problem. To do this, the first analysis (25.4cm span) was repeated for a 50.8cm span, with the result that up to about 100 microseconds no difference was found in centerline deflection, edge, or center strain for the two cases. Since in most situations of interest either the maximum or fracture strain would occur in less than 100 microseconds, it was decided that a 50.8cm span would correspond to an effectively infinite sheet and would be used in all subsequent calculations.

The strip approximation was used to determine the response of backup sheets of various thicknesses for impacts of 3.2mm particles at velocities of 7.62, 15.2, 22.8 and 30.4 km/sec. The results at 7.62 km/sec (Figures 32–34) show that there is a large difference between backup-sheet thicknesses required for no-yield failure (maximum strain less than 0.7%) and no-fracture failure (maximum strain less than 11%). Also, it can be observed that for sheet thicknesses above about 1.6 mm the maximum strain occurs at the edge of the loaded area. Similar solutions to Figures 32–34 have been obtained for the other three impact velocities.

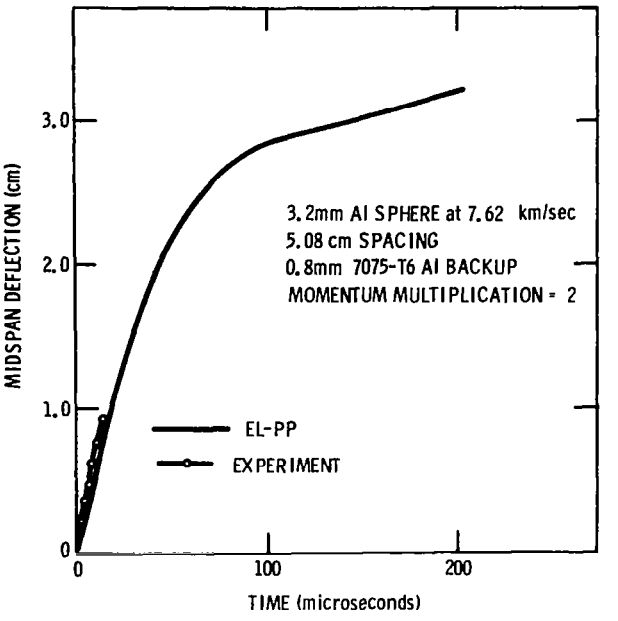

Figure 30 Centerline Displacement vs Time

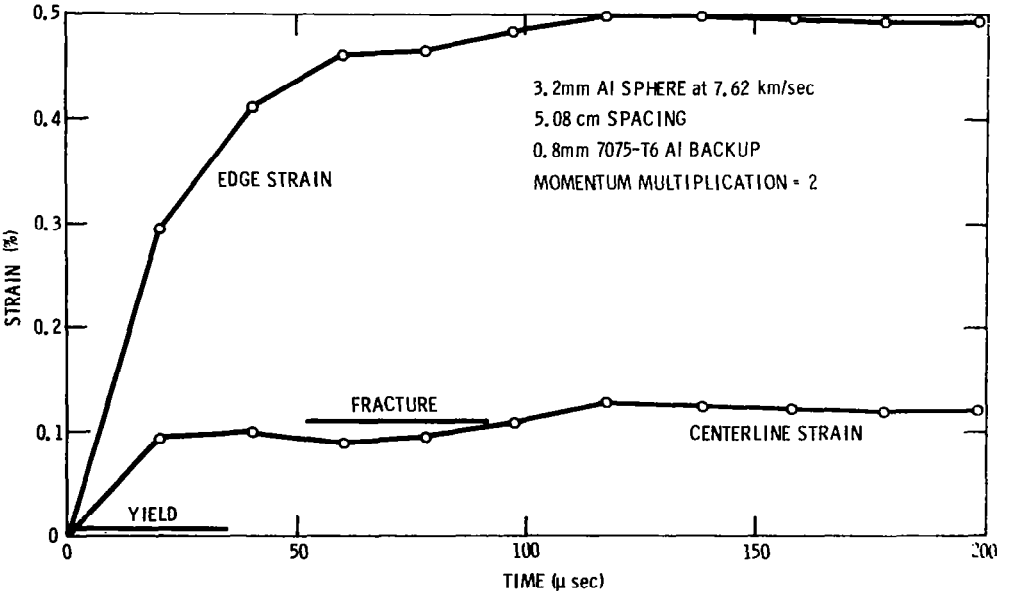

Figure 31 Centerline and Edge Strain vs Time

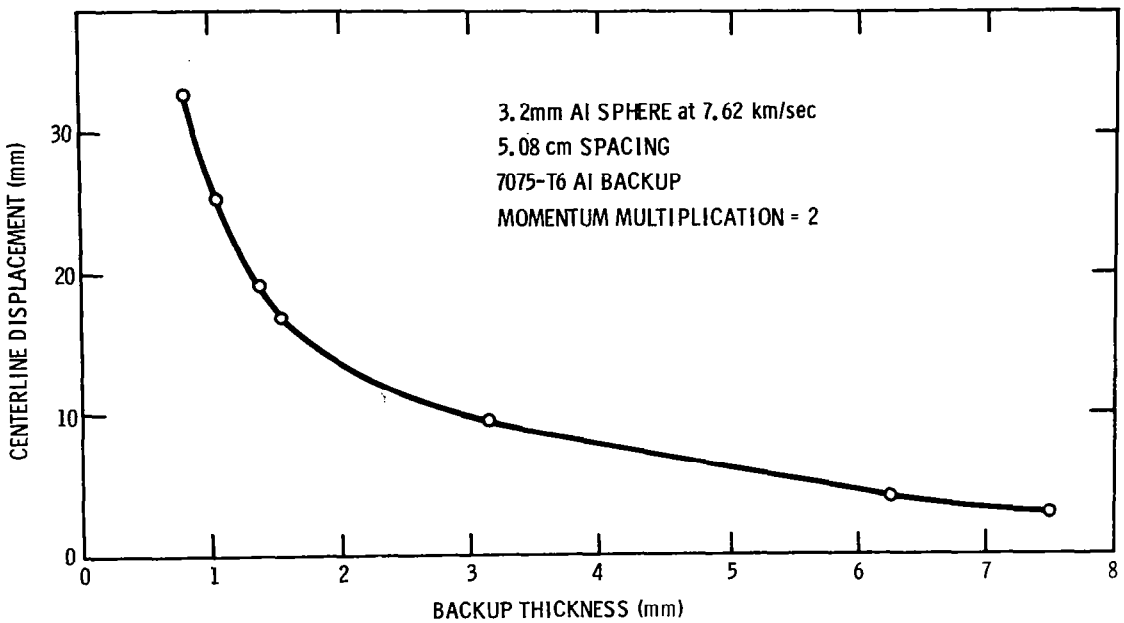

Figure 32 Centerline Displacement vs Thickness at 200 μsec

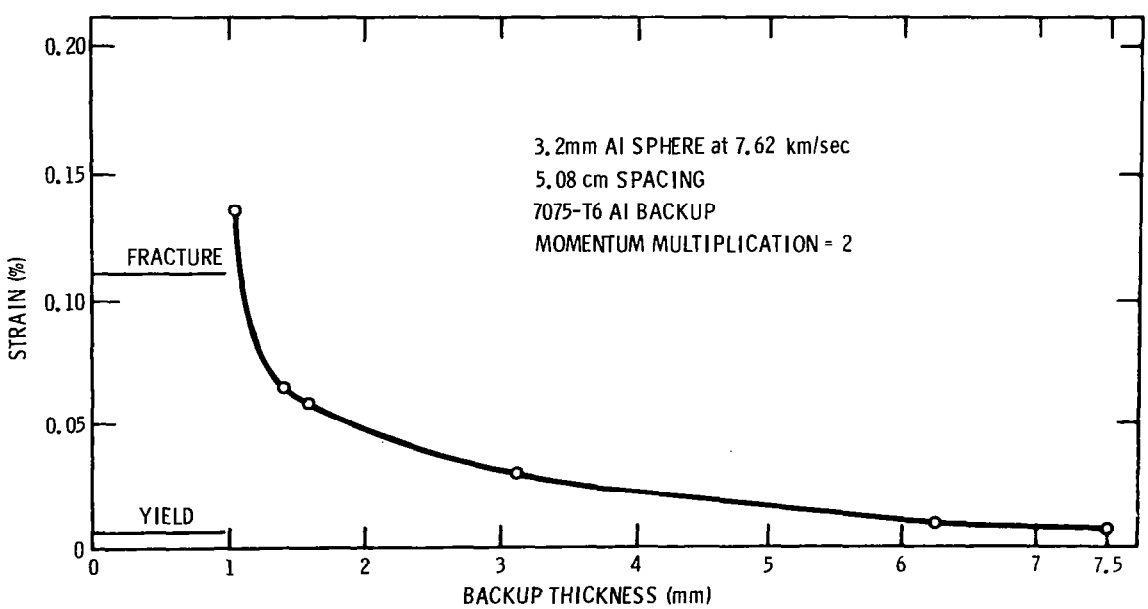

Figure 33 Maximum Centerline Strain vs Thickness

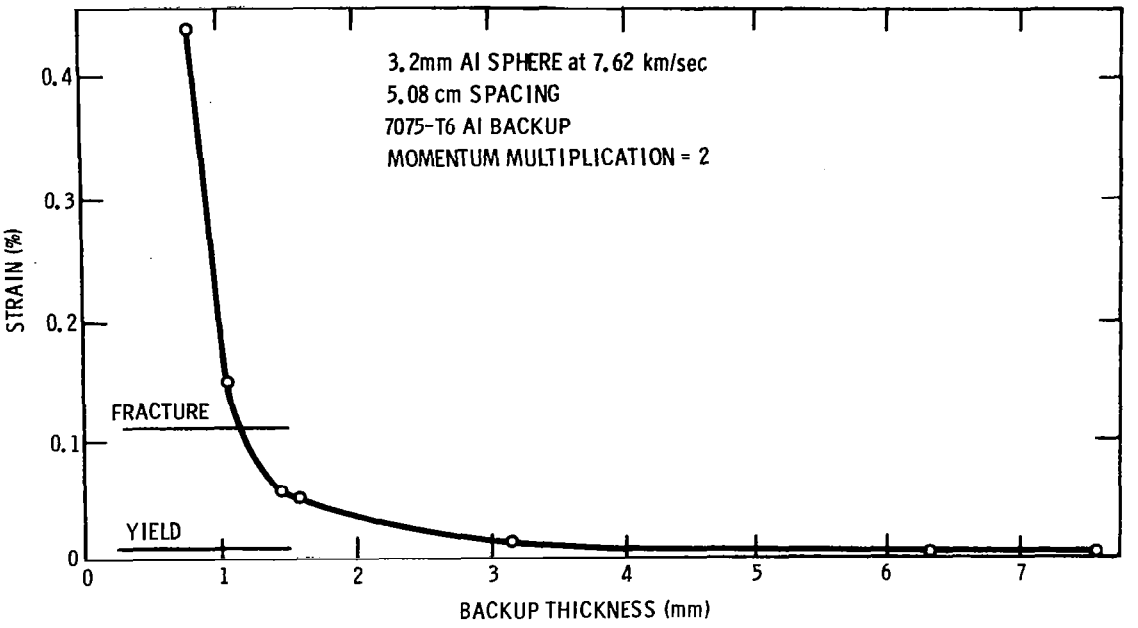

Figure 34 Maximum Edge Strain vs Thickness

The resulting curves of sheet thickness against impact velocity for failure criteria of yield, maximum strain of 2%, 4%, and 6%, and fracture are presented in Figure 35. The surprising aspect of this figure is that for each failure criterion the curve of t_b against velocity is nearly linear. This is surprising in view of the fact that the basic mechanisms are nonlinear. It is also seen from this figure that, above about 4% maximum strain at a given velocity, a small decrease in thickness produces a large strain increment. Thus it would appear wise to design for no more than a few percent maximum strain.

Figure 36 shows results similar to those of Figure 35, but for 1.02mm-diameter aluminum spheres. The same comments can be made concerning the results for this particle that were made for the 3.2mm particle. Note that the crowding of the constant maximum-strain lines is seen to increase with decreasing particle size.

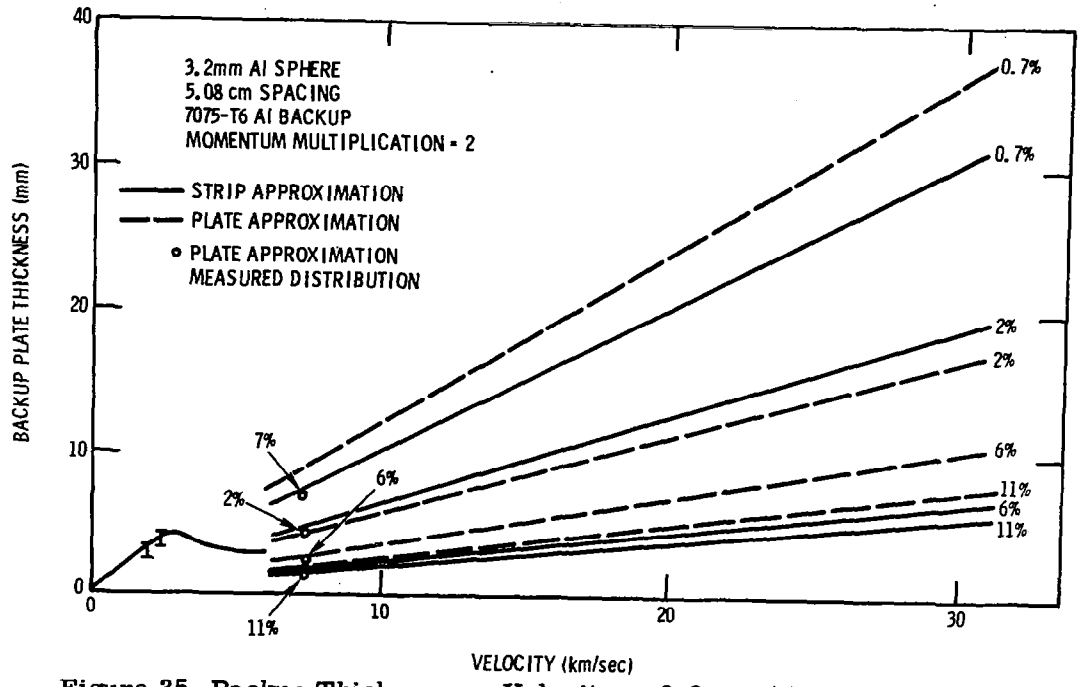

Figure 35 Backup Thickness vs Velocity — 3.2mm Aluminum Sphere

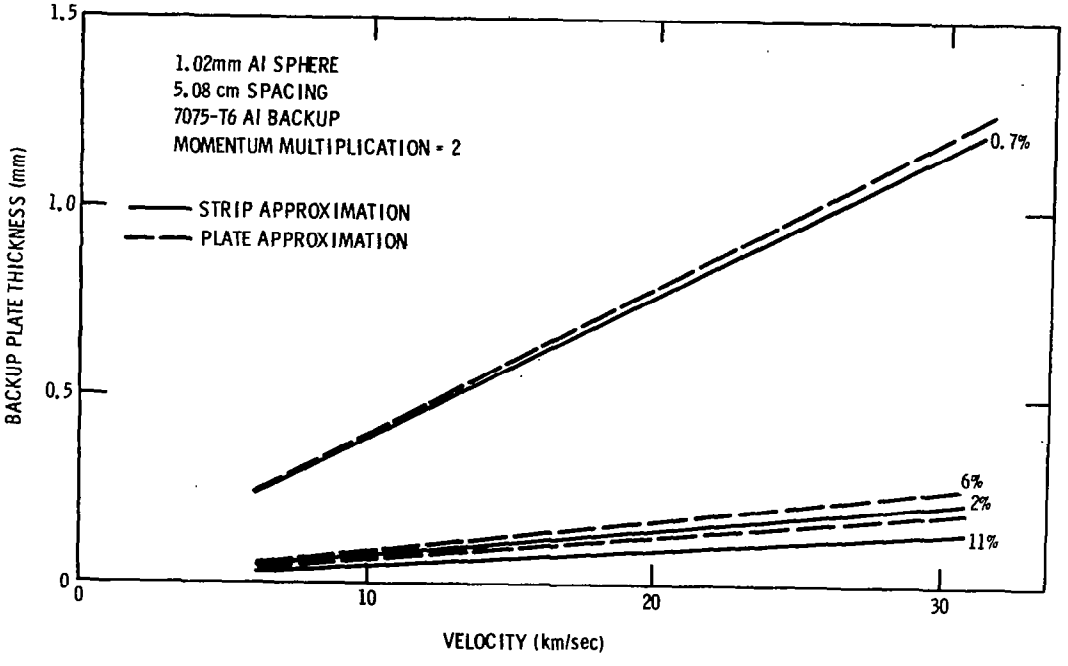

Figure 36 Backup Thickness vs Velocity — 1.02mm Aluminum Sphere

From Figures 35 and 36, the backup-sheet thicknesses for the yield and fracture criteria can be plotted against particle diameter at a number of velocities. When this is done it is found that, for either criterion, t_b is approximately proportional to the cube of the particle diameter. Thus, under these conditions, Equation (4) indicates that v_i, the initial velocity of the loaded area, is roughly constant.

Spacing of 2.54, 5.08, and 10.16 cm were investigated for an Apollo-scale particle (1.02mm diameter) at 30.4 km/sec. The results for both the yield and fracture criteria show that the sheet thickness necessary for either decreases approximately with the inverse square of spacing. This result, plus those of the preceding sections, gives rise to an approximate equation for rear-sheet thickness. For 7075-T6 aluminum this equation is given by

$$t_b = C \frac{M_p V_p}{S^2} \tag{5}$$

where $C = 415 \pm 140$ and 82 ± 14 for the yield and fracture criteria, respectively, t_b is in millimeters, M_p is in grams, V_p is in km/sec, and S is in centimeters (Note: because the exact solutions do not require v_i in Equation (4) to be exactly constant, there is not a constant value for C at a specific maximum strain).

In many space applications, the structure to be protected will be a pressurized fuel tank; hence, it was decided to investigate the effect of pre-tensioning the rear sheet (in one direction only). The computer code for the strip approximation can accommodate such pre-tensioning, and solutions were obtained for a 1.04mm particle at 30.4 km/sec with pre-tensioning of 25%, 50%, 75% and 100% of the static yield stress. The centerline displacements against time are shown in Figure 37.

These results reveal that the thickness required for the yield criterion is not very sensitive to pre-tension, the value of the yield stress being less than 10% greater than that at zero (see Figure 38). The thickness based on the fracture criterion is sensitive to the amount of pre-tension increasing by more than 60% of the yield stress.

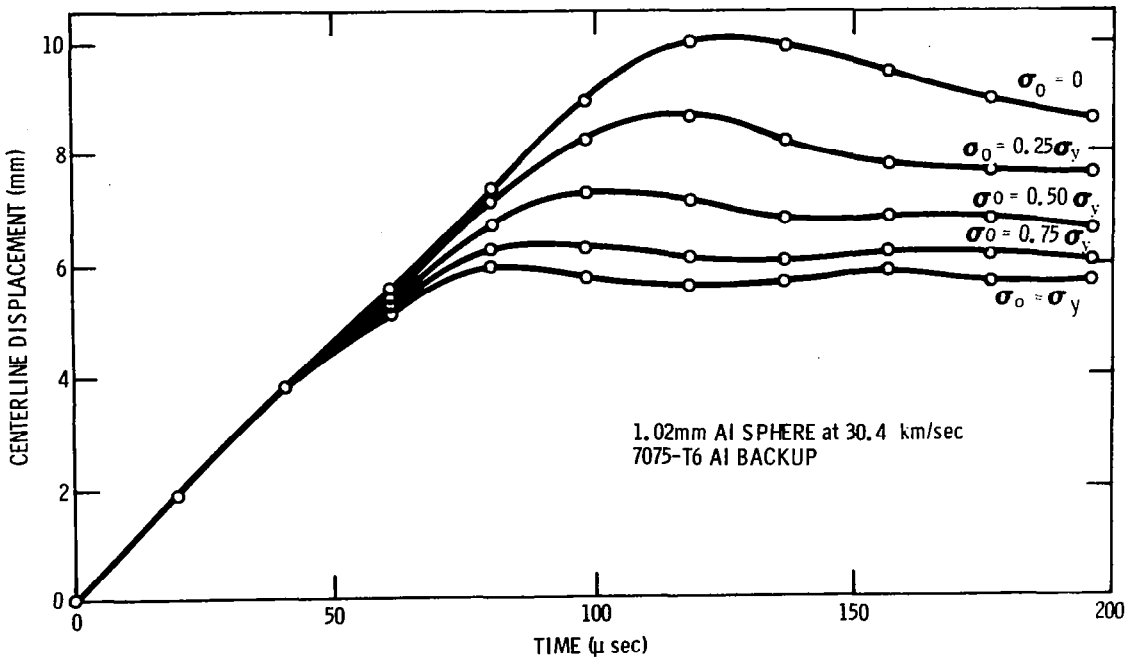

Figure 37 Centerline Displacement vs Time-Pretensioned Beam

The strip approximation has been shown to be in good agreement with experimental results; however, the complete solution should consider a centrally loaded circular plate. The numerical technique of Witmer, et al,[12] has been applied to the plate analysis and the results agree well with those from the strip approximation. Such comparisons are shown in Figures 35 and 36. Both the strip and plate treatments are more fully described in Appendix A.

Finally, the plate analysis has been used to compute the second sheet reaction utilizing the hydrodynamic momentum distributions. The strain versus sheet thicknesses for these distributions are presented for the aluminum-aluminum impacts in Figures 39 through 47. A momentum multiplication factor of two was used for all the impacts except those at 7.6 kilometers per second, where a multiplication factor of 1.3 was used (this value was experimentally determined).

Common to all of the strain-versus-thickness plots is the rapid increase in strain as the thickness decreases for strains above about 5%. This indicates that it would be unwise to design a structure near the fracture point or to accept a very large strain. Also, it was noted that for a particular strain the thickness was to a first-order proportional to the momentum intensity at $\alpha = 0.2$ in the axial momentum distribution.

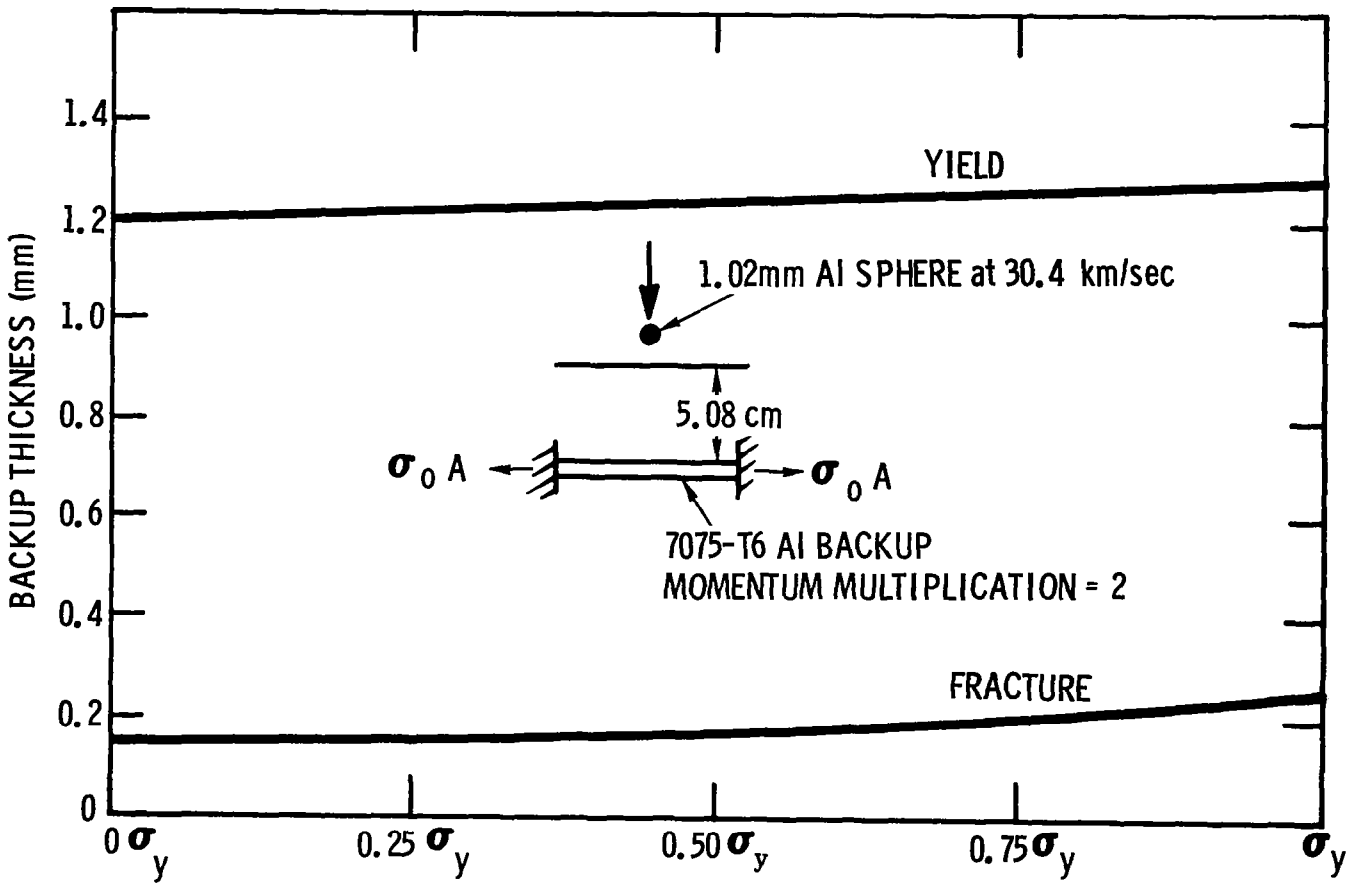

Figure 38 Backup Thickness vs Pretension Stress

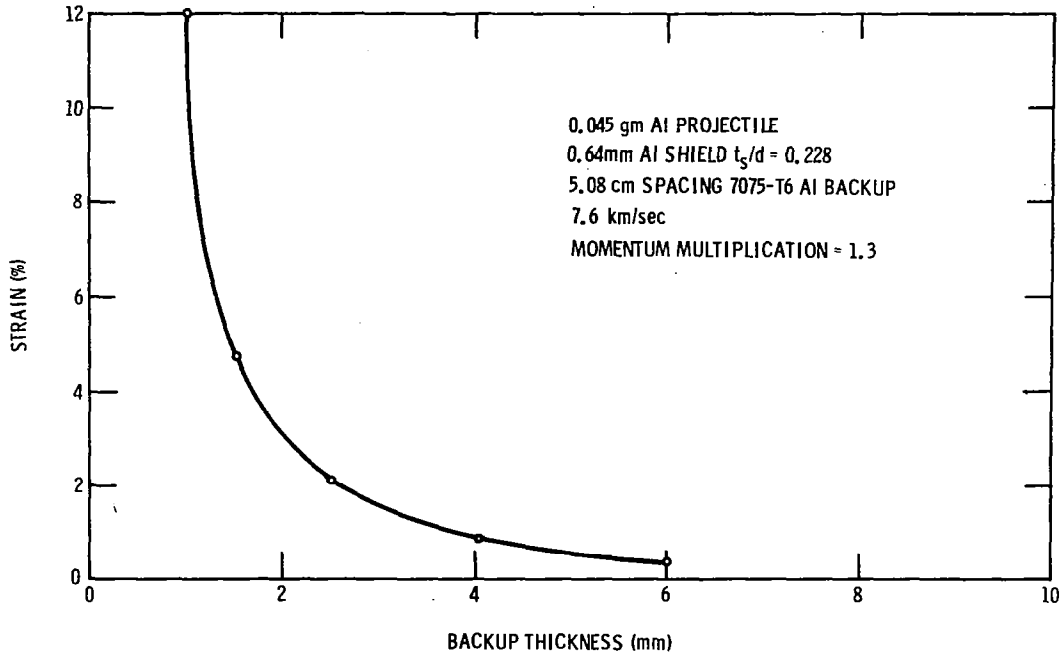

Figure 39 Strain vs Backup Thickness, 0.64 mm Al Shield at 7.6 km/sec

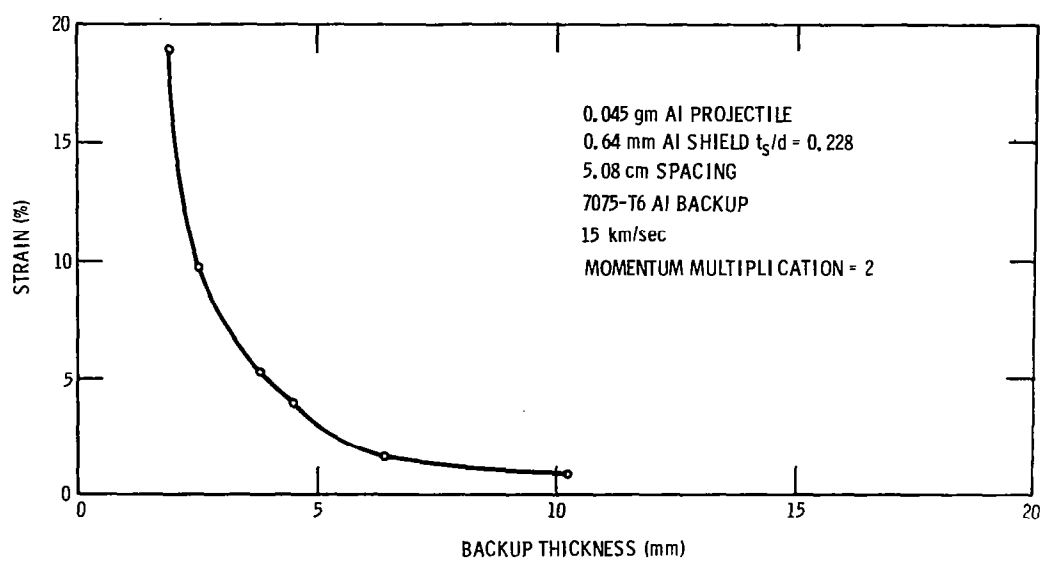

Figure 40 Strain vs Backup Thickness, 0.64 mm Al Shield at 15 km/sec

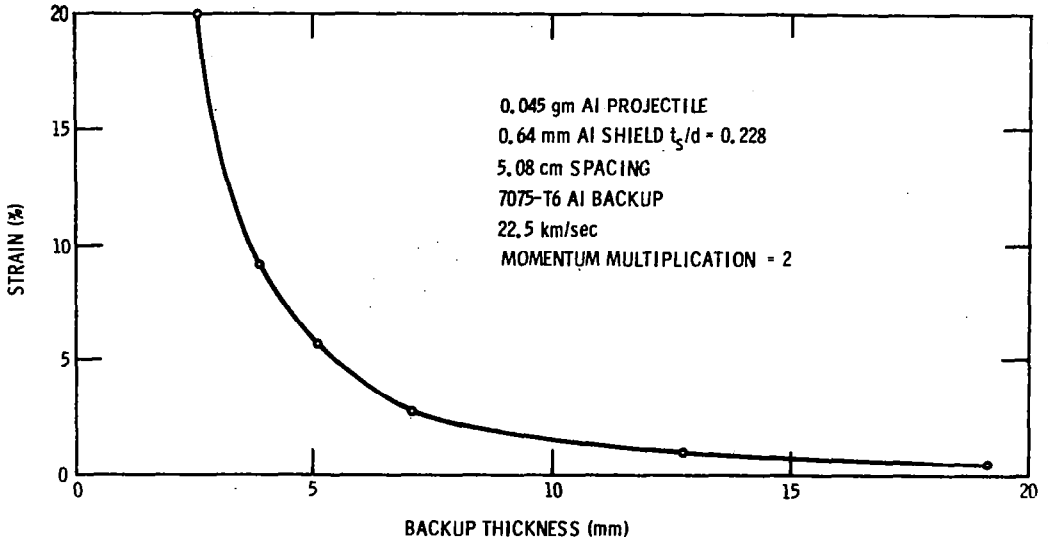

Figure 41 Strain vs Backup Thickness, 0.64 mm Al Shield at 22.5 km/sec

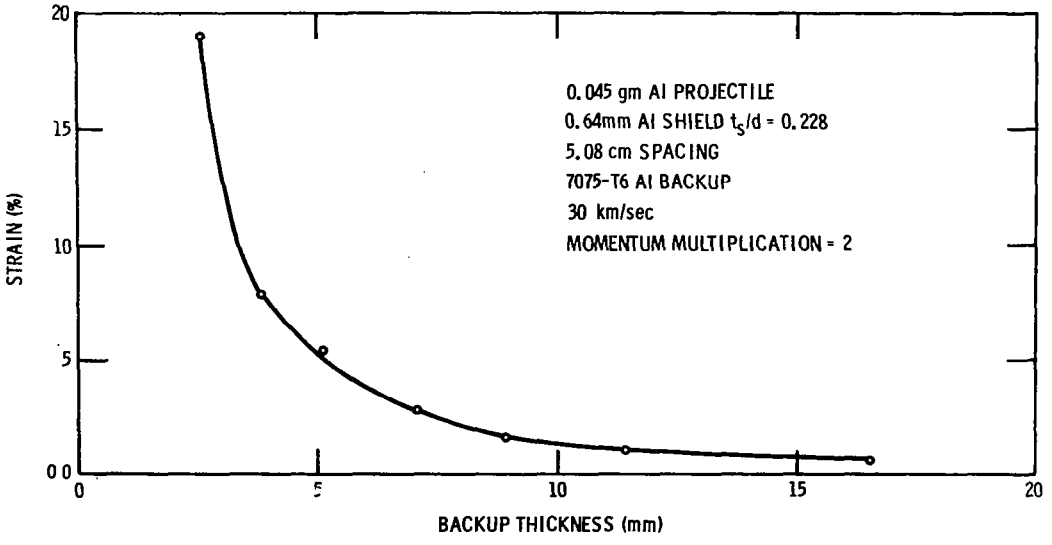

Figure 42 Strain vs Backup Thickness, 0.64 mm Al Shield at 30 km/sec

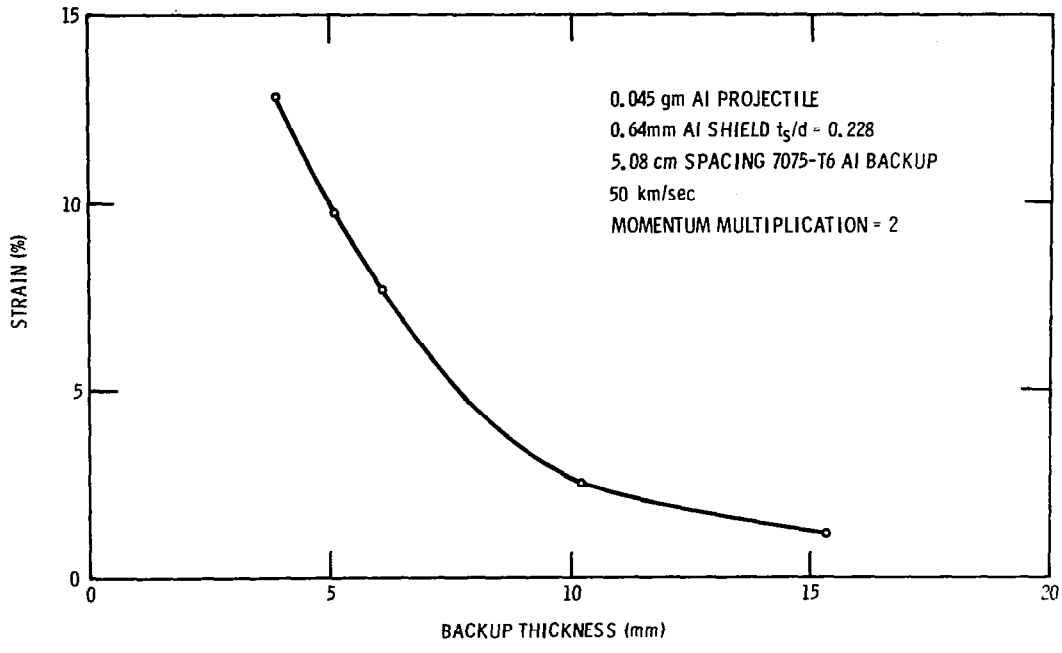

Figure 43 Strain vs Backup Thickness, 0.64 mm Al Shield at 50 km/sec

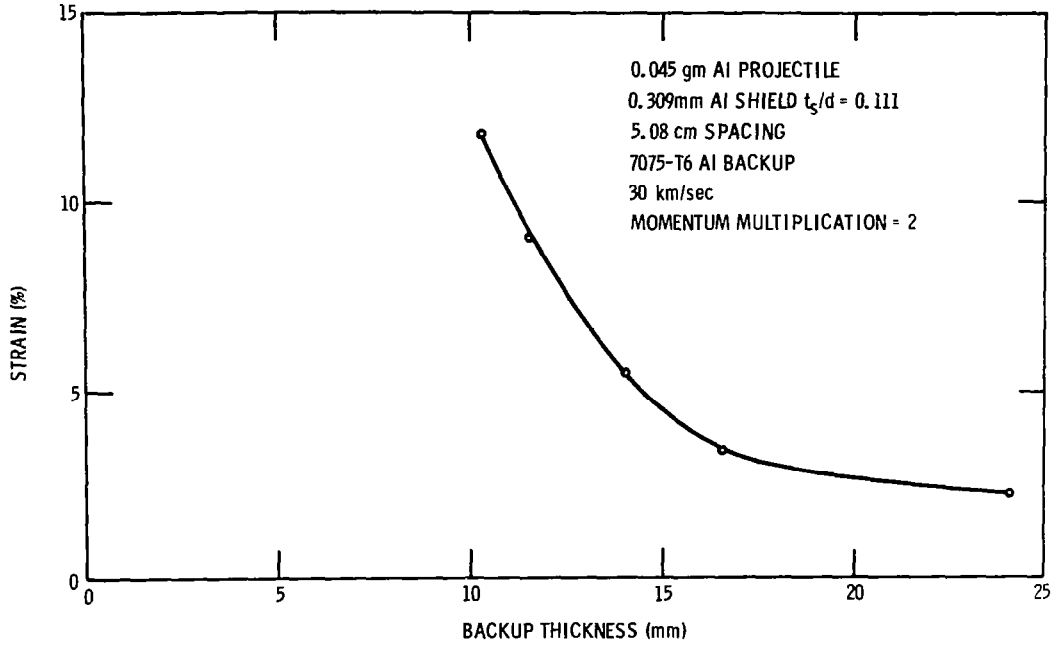

Figure 44 Strain vs Backup Thickness, .309 mm Al Shield at 30 km/sec

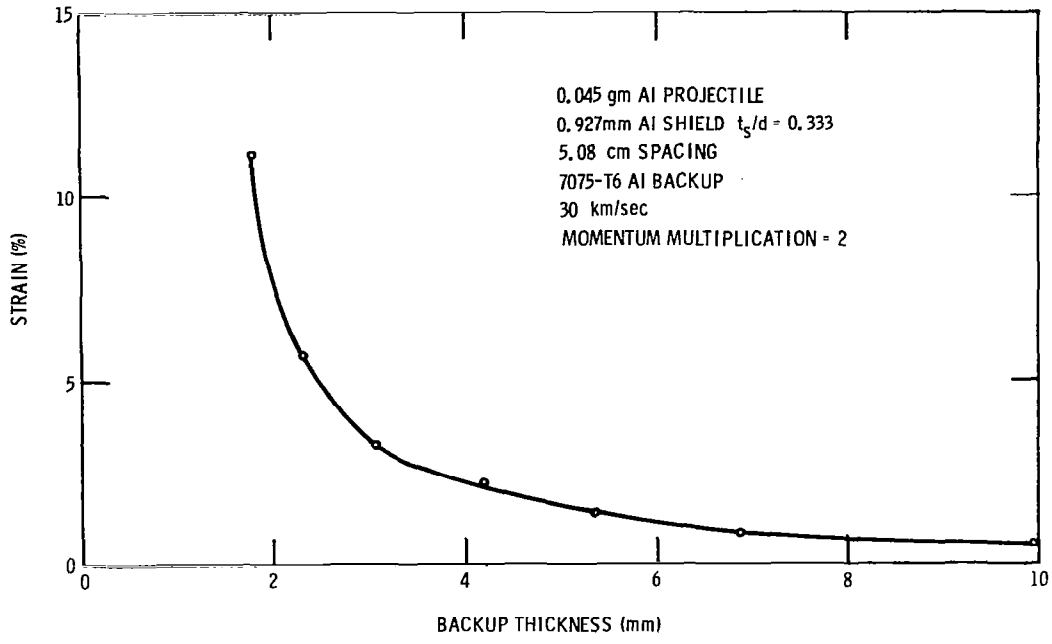

Figure 45 Strain vs Backup Thickness, .927 mm Al Shield at 30 km/sec

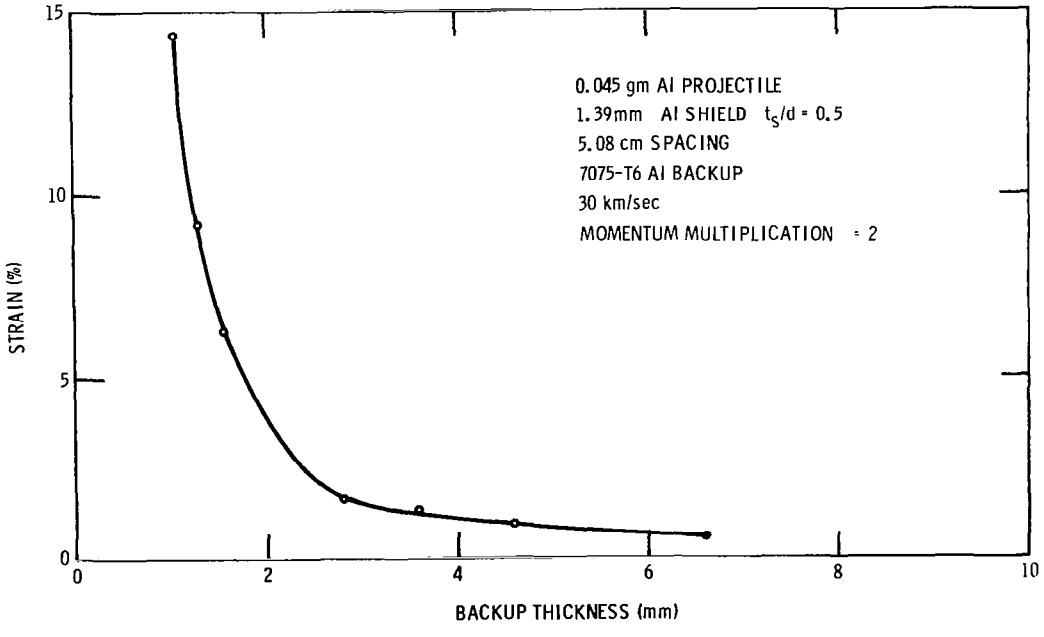

Figure 46 Strain vs Backup Thickness, 1.39 mm Al Shield at 30 km/sec

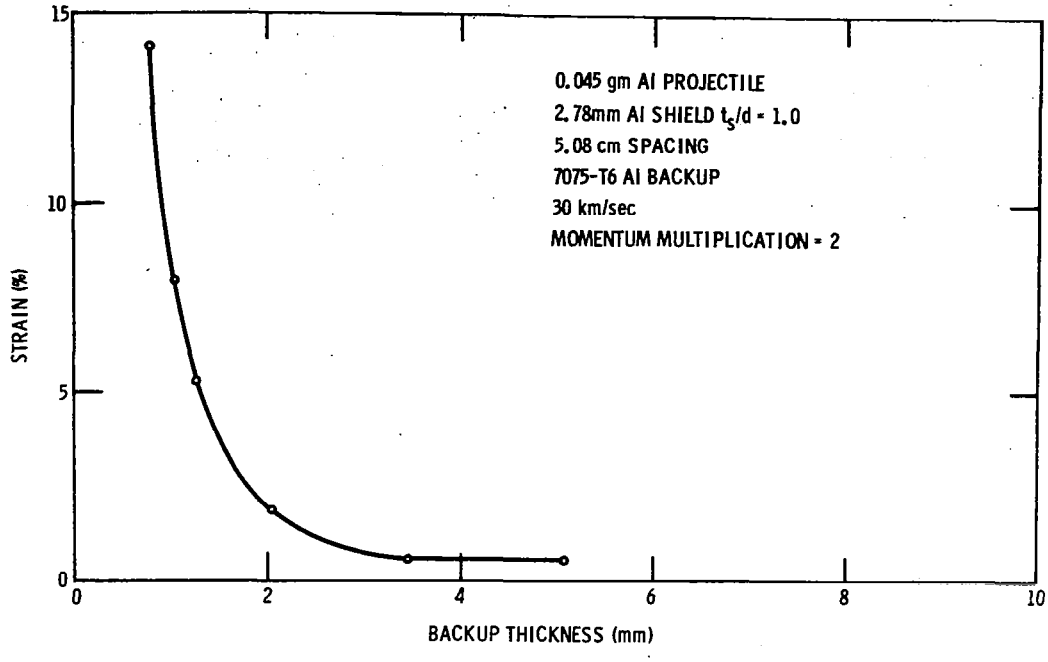

Figure 47 Strain vs Backup Thickness, 2.73 mm Al Shield at 30 km/sec

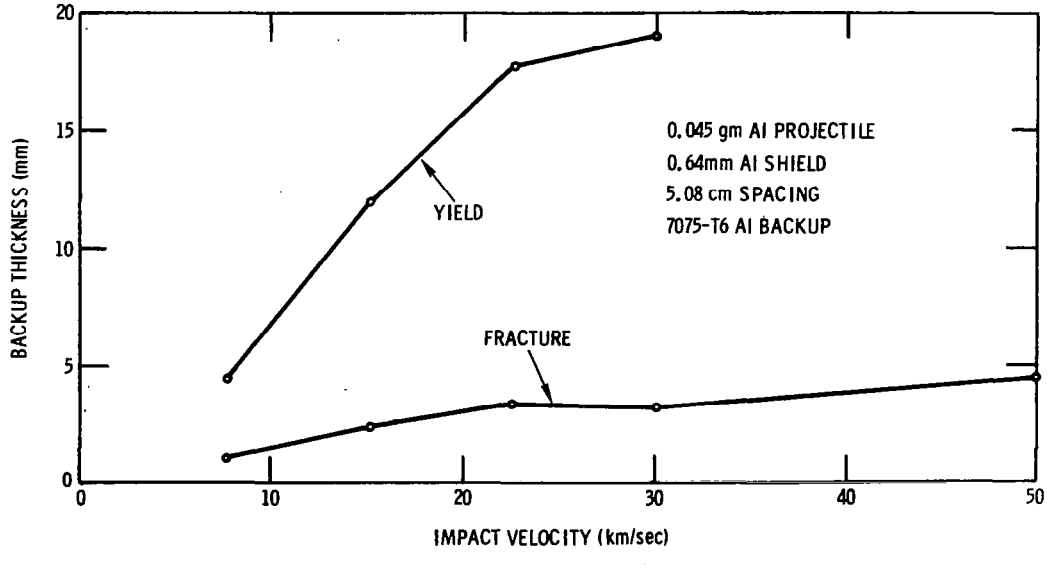

Figure 48 Backup Thickness vs Velocity – CAMEO Input

In Figure 48 the thicknesses to prevent fracture and yield are given as a function of velocity. Note that the thicknesses are no longer linear functions of the impact velocity.

If the thicknesses given in Figure 48 are compared to those in Figure 35 it can be seen that the use of the distribution has considerably reduced the thicknesses required to prevent fracture or yield. This result would seem to be due to the fact that the larger loaded area utilizes a greater amount of the second sheet material to absorb the load.

The variation of shield thickness results were used in Figure 49 to determine the total thicknesses to prevent fracture at an impact velocity of 30 kilometers per second. Here the ordinate is the total structure thickness, i.e., the shield and second- or backup-sheet thickness. The result is a broad, flat minimum from about $t_s/d = 0.3$ to 0.7. This "optimum" shield thickness is greater than that predicted in Reference 6, but the basis of the determination of "optimum" is much different in Reference 6 than it is here. Again in this figure we see that if the shield is overly thick nothing serious occurs; however, if the shield is just a little too thin a severe weight penalty must be paid to avoid fracture.

The next problem considered was whether the plate analysis results could be scaled with projectile mass and intersheet spacing. If not, it would be necessary to compute each case of interest. In Figures 50 through 54, the strain versus thickness plots are given for a number of impact conditions.

For these comparisons the "scaled input" points were obtained by scaling the input momentum distribution to the plate analysis proportional to the impacting particle mass. The original computational results were scaled directly with the particle mass to obtain the "scaled output" points. As can be seen there is practically no difference between these results, leading to the conclusion that the backup thickness for a particular t_s/d and spacing is directly proportional to the impacting projectile mass.

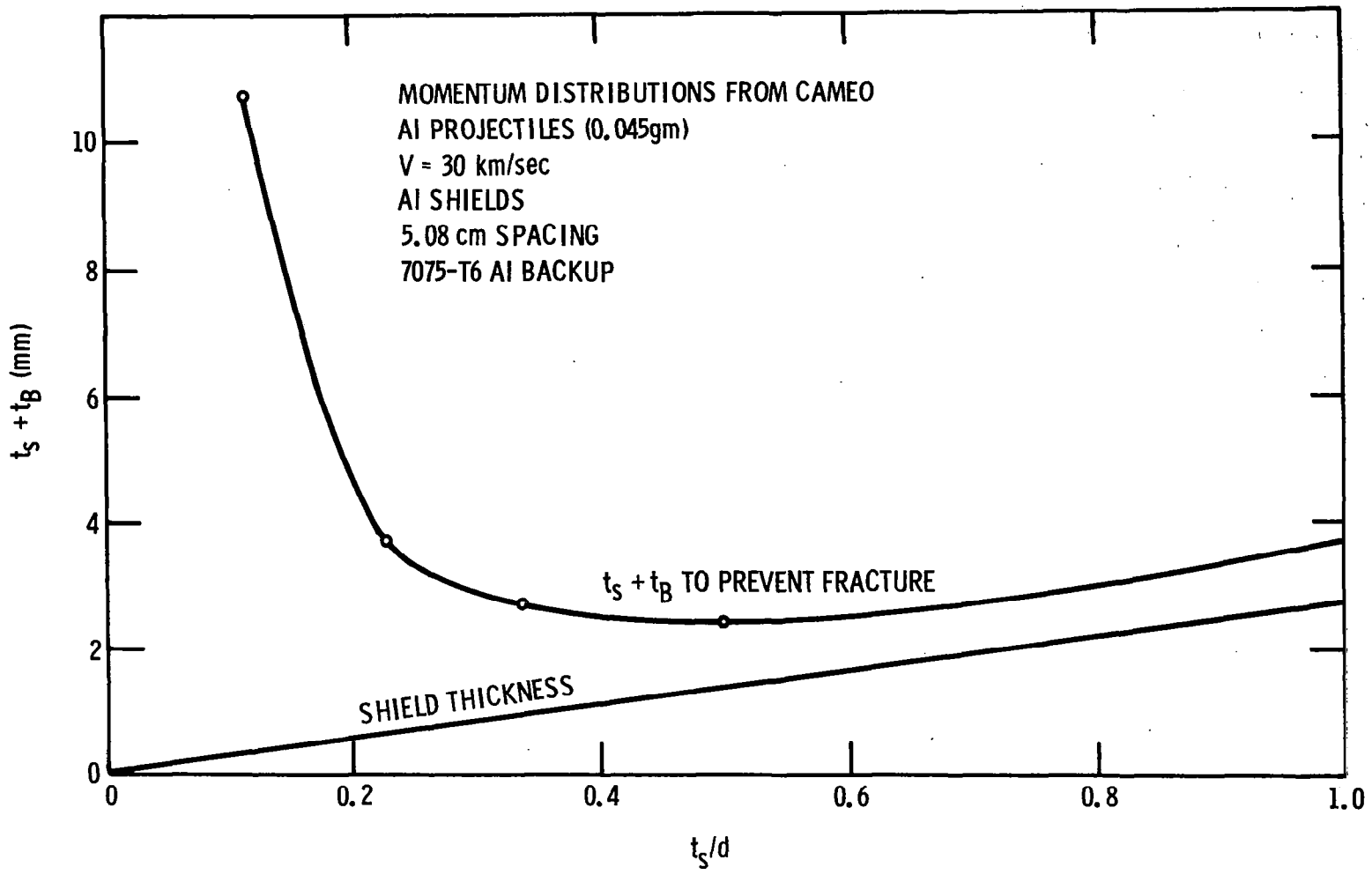

Figure 49 Total Thickness vs t_s/d – 30 km/sec

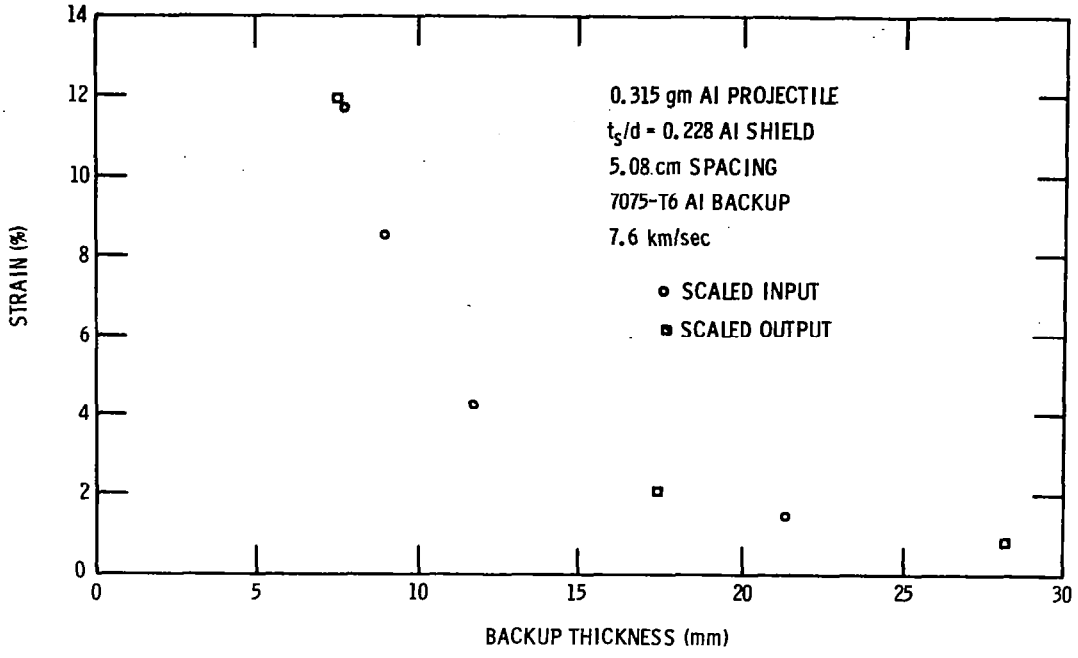

Figure 50 Strain vs Thickness – Mass Scaling, 0.315 gram

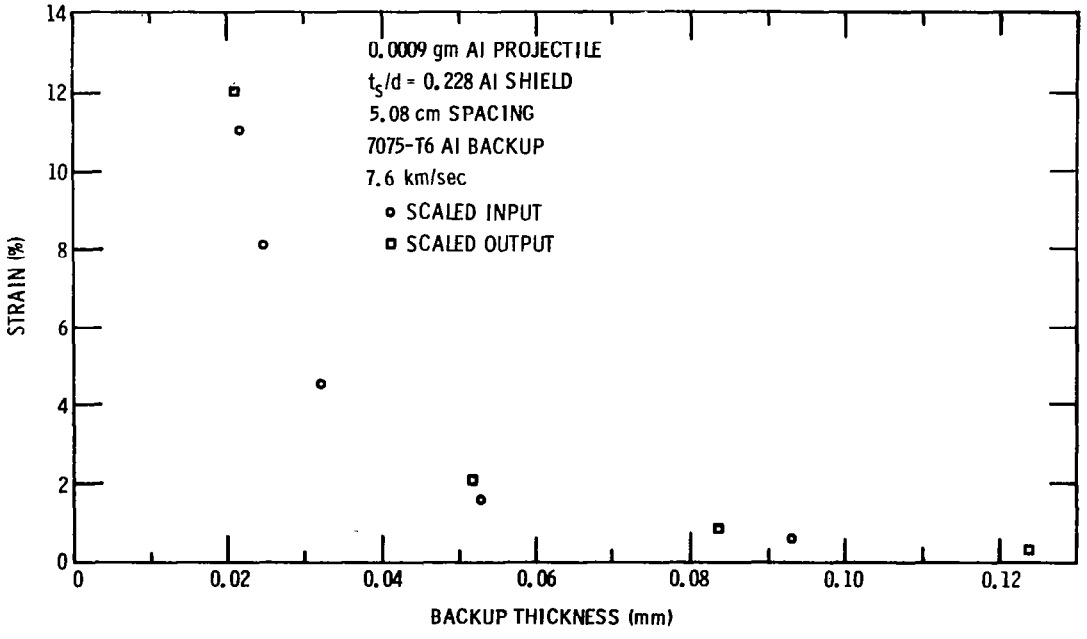

Figure 51 Strain vs Thickness – Mass Scaling, 0.0009 gram

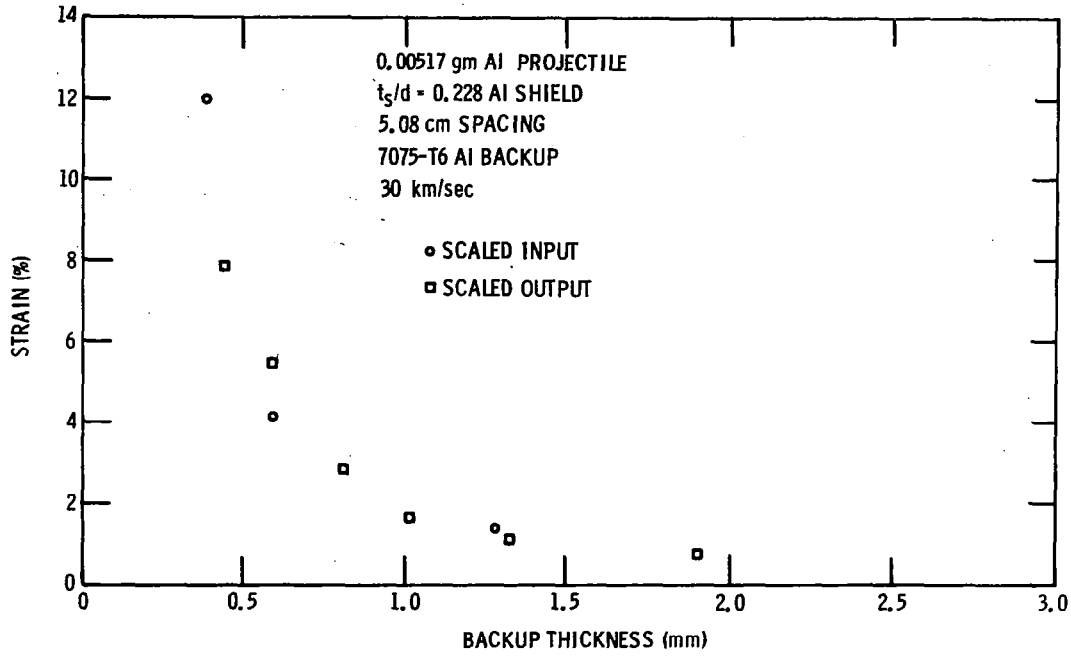

Figure 52 Strain vs Thickness – Mass Scaling, 0.00517 gram

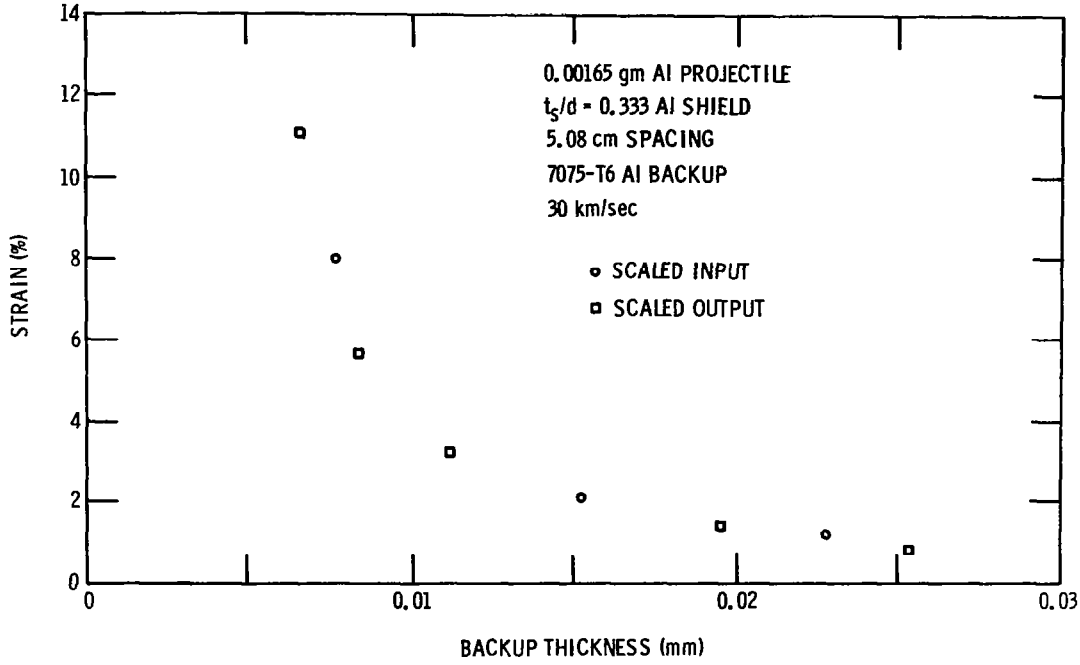

Figure 53 Strain vs Thickness – Mass Scaling, 0.00165 gram

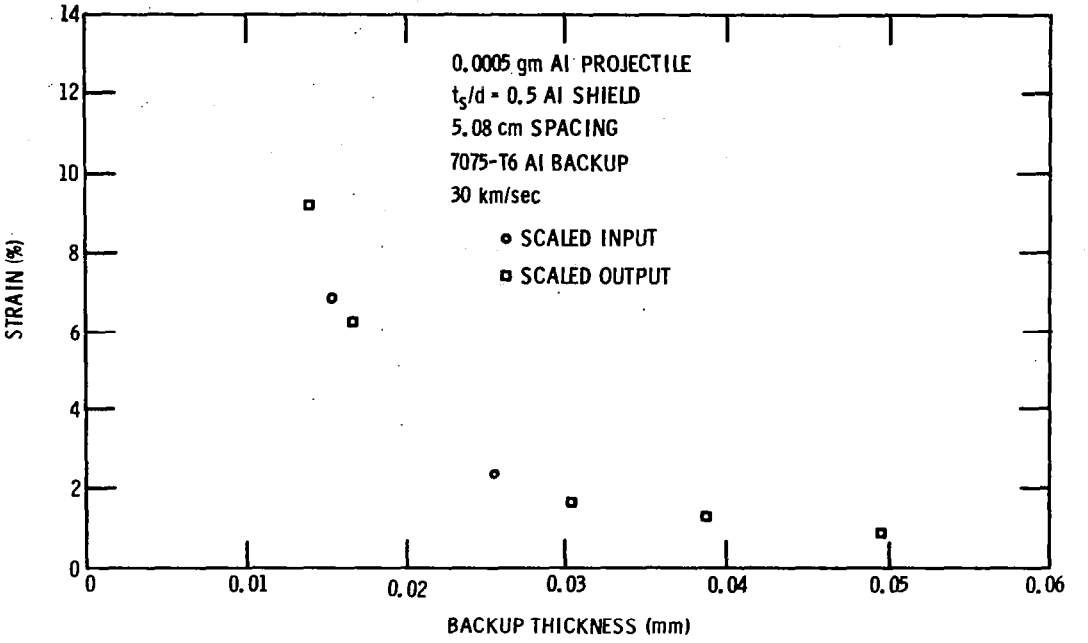

Figure 54 Strain vs Thickness – Mass Scaling, 0.0005 gram

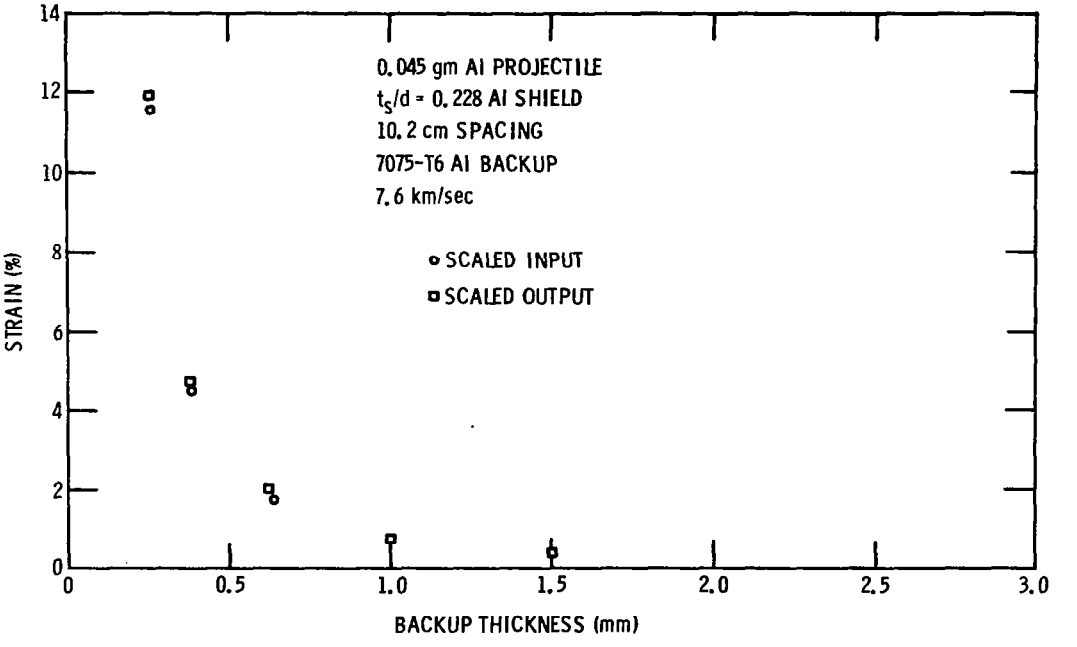

Figure 55 Strain vs Thickness – Spacing Scaling, 10.2 cm, V=7.6 km/sec

The effect of spacing with the CAMEO momentum distributions was considered in the same manner as the effect of projectile mass. These results are shown in Figures 55 through 59. Here the original results were scaled as one over the square of the spacing. Again there is essentially no difference between the "scaled input" and "scaled output" results, with the conclusion that the results can be scaled as backup thickness proportional to one over the square of the spacing. The combination of these results leads to the backup thickness for a particular t_s/d being directly proportional to the impacting particle mass divided by the square of the spacing.

The above results are based on the assumption that the debris that strikes the second sheet is in a liquid or vapor form with a density much less than that of the impacting particle or shield. This will not be the situation if the spacing between the sheets is small compared to the particle size. This corresponds to the CAMEO calculations for the early time flow before the debris is "set". For the debris in this form, cratering of the second sheet will take place. Secondly it has been assumed that the velocity vectors of the debris all pass through the impact centerline exactly at the rear surface of the shield. This is not the case in the CAMEO results, where the debris appears to be coming from along the centerline within the shield or particle. Thus the debris is not spreading quite as rapidly as has been assumed. The results as presented should not be applied to large particles impacting thin shields with short spacings to the second sheet (less than eight particle diameters) or to very large spacings.

Using the scaling results, it is possible to express the thickness to prevent fracture for impacts at 30 kilometers per second as a function of the shield thickness, particle size, and spacing as

$$t_f = \frac{M_p}{0.045} \left(\frac{5.08}{S}\right)^2 \left[\frac{0.0102}{(t_s/d)^2} + 0.079\right] \qquad (6)$$

where

M_p is the particle mass in grams

S is the spacing in centimeters

t_s is the shield thickness in centimeters

t_f is the second sheet fracture thickness in centimeters.

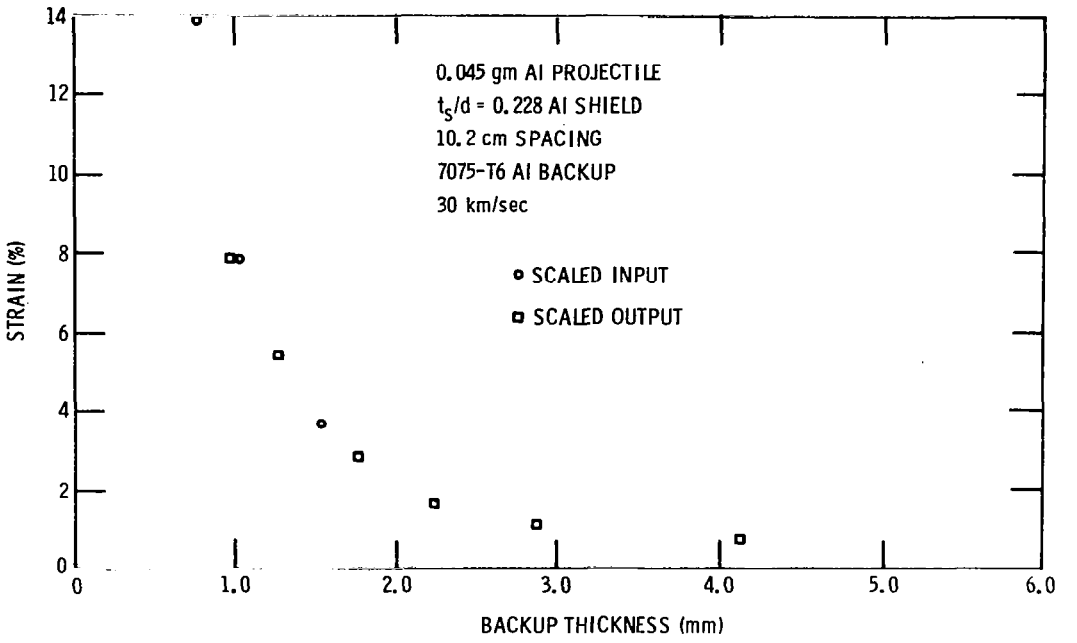

Figure 56 Strain vs Thickness – Spacing Scaling, 10.2 cm, V=7.6 km/sec (t_s/d = 0.228)

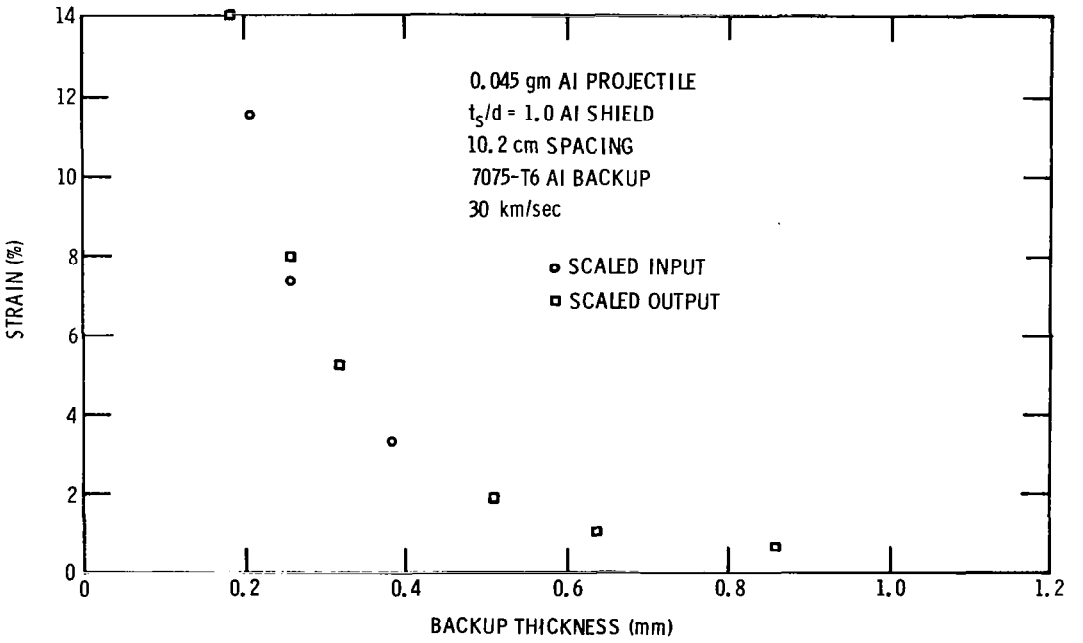

Figure 57 Strain vs Thickness – Spacing Scaling, 10.2 cm, V=7.6 km/sec (t_s/d = 1.0)

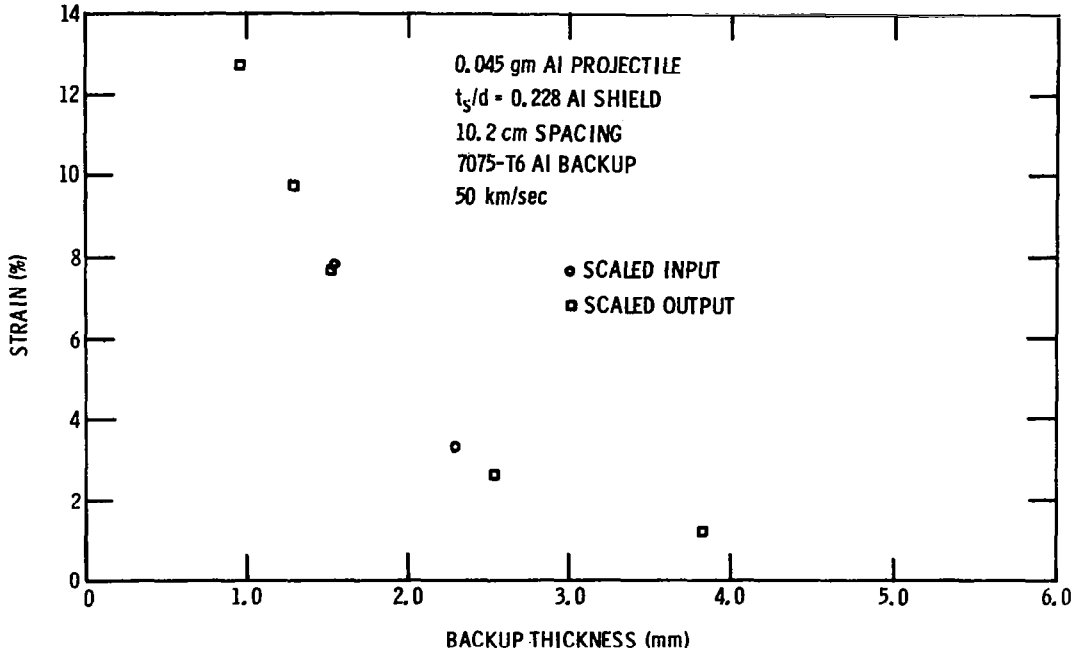

Figure 58 Strain vs Thickness – Spacing Scaling, 10.2 cm, V=50 km/sec

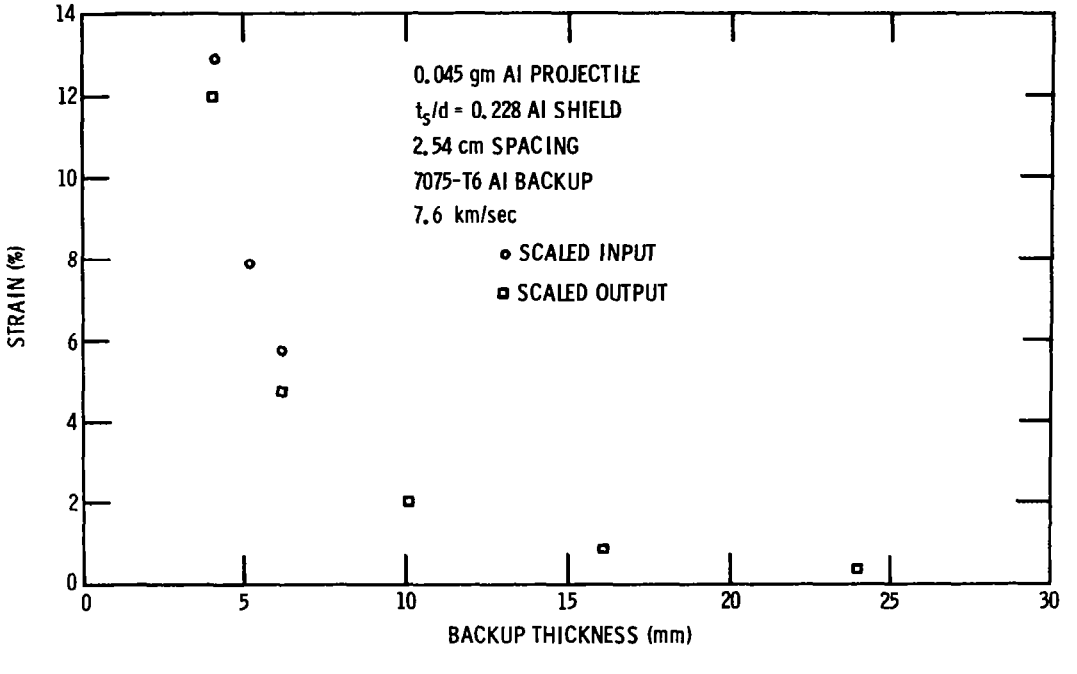

Figure 59 Strain vs Thickness – Spacing Scaling, 2.54 cm, V=7.6 km/sec

Equation (6) shows that the dominant factors in determining the thickness to prevent fracture are the projectile mass and the spacing, with the shield thickness to projectile diameter ratio becoming important only if it is small. Use of the equation is restricted to 30 km/sec impacts in which the spacing is fairly large (greater than eight projectile diameters), the debris is underdense and molten or vaporized, and the shield thickness ratio is in the range of about 0.1 to 1.0.

This result applies to aluminum on aluminum impacts with the second sheet material of 7075-T6 aluminum. The formula can be used to evaluate the resistance to fracture of the second sheet of a two-sheet structure with the t_s/d ratio computed on the basis of the equivalent-mass aluminim particle. It would be unwise to design a two-sheet structure on the basis that it just resist fracture, because of the sensitivity of the maximum strain near the fracture point.

The combination of the CAMEO hydrodynamic computations and the plate analysis were applied to cadmium-cadmium impacts to provide the basis for an experimental check. In these computations a momentum multiplication factor of 1.4 was used.

This value was determined from experiment. Four shield thicknesses were computed for an impact velocity of 6 kilometers per second. The fracture thicknesses versus shield-thickness ratios are shown in Figure 60, together with experimentally determined fracture thicknesses. In all cases the fracture thicknesses found experimentally are much less than those predicted.

It is felt that this discrepancy is probably due to the way in which the debris transfers its momentum to the second sheet. A momentum transfer ratio of 1.4 has been observed experimentally and it was assumed that the debris delivered 1.4 times its momentum to the second sheet independent of spray half-angle. The debris is more concentrated at small spray half-angles and there is an indication, from framing camera records (Figure 61), that the leading edge of the debris reflects after striking the second sheet. In this figure the reflected front can be seen after the debris has struck the second plate. This material travels back to the shield and some of it passes through the hole and overtakes the debris ejected

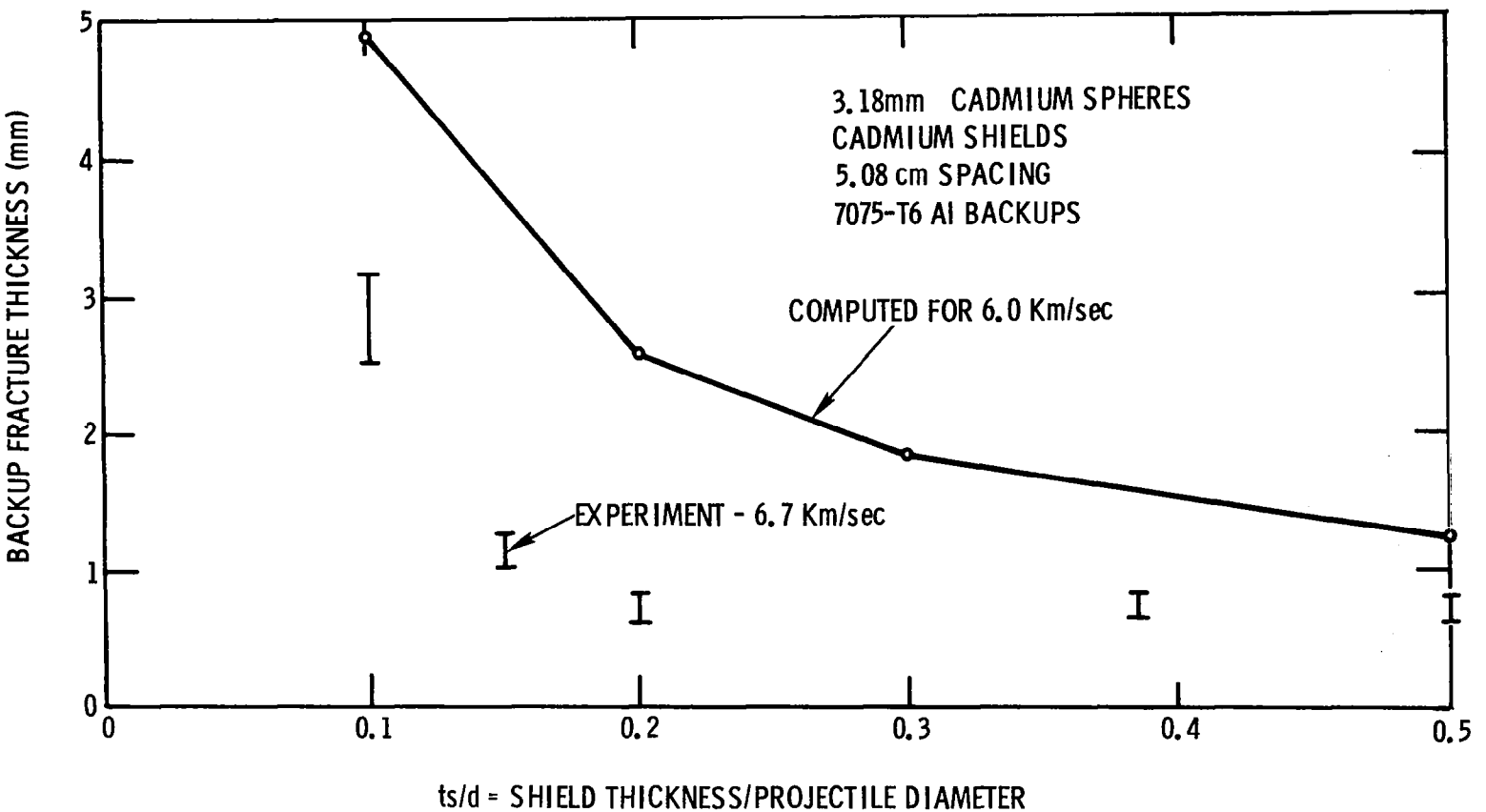

Figure 60 Backup Thickness vs t_s/d – 6 km/sec Cadmium Impacts

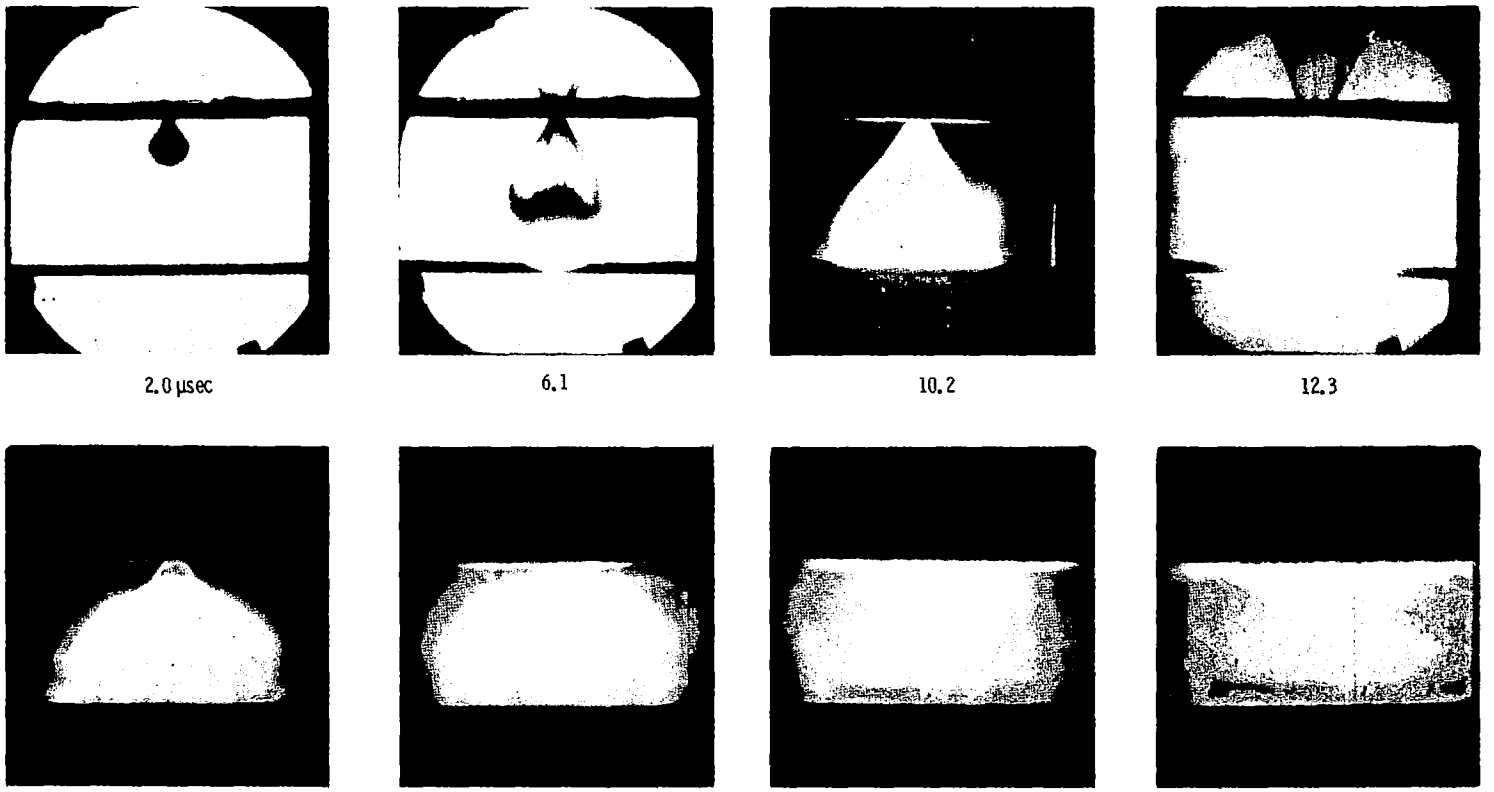

Figure 61 Framing Camera Sequence of Cadmium Impact

from the shield, causing light to be given off (the last two frames). The passage of the front of the debris back through the later debris would be expected to reduce the momentum transfer. Since the interaction would be greatest where the debris is most dense, the small spray half-angle debris would be affected the most. The reaction of the loaded plate is very dependent upon the small spray half-angle load, and this interaction is probably the cause of the low experimental values. Stated another way, the momentum multiplication factor is probably a function of spray half-angle. (There is some indication of this in the results shown in Figures 9 through 12.)

A number of scaling experiments were also performed with cadmium-cadmium impacts. When the projectile mass was reduced by one half with a shield thickness ratio of 0.2, the fracture thickness was reduced from 0.64–0.81 millimeters to 0.46–0.64 millimeters. The results of varying the fracture thickness with spacing are given in Table II below.

Table II
CADMIUM-CADMIUM IMPACTS AT 6.7 km/sec

t_s/d	t_f 5.08 cm spacing	t_f 10.2 cm spacing	t_f 2.54 cm spacing
0.1	2.28–3.18mm	0.41–0.64mm	–
0.2	0.64–0.81	0.25–0.64	–
0.385	0.64–0.81	0.25–0.38	2.54–3.18mm

These results are in good agreement with the mass and spacing scaling predictions.

SPALL FAILURE

The impact of the projectile-shield debris upon the second sheet generates a shock wave in the second sheet. This wave upon reflection can cause fracture or spall of the second sheet. Analysis of this problem requires consideration of the strength of the second sheet. This problem has been treated by use of the two-dimensional elastic-plastic analysis described in Appendix B.

The debris distributions from the CAMEO computations were utilized as the input to the spall calculations. The second-sheet treatment included the effects of strength, while the impacting cloud of debris was treated as purely hydrodynamic.

The results of CAMEO 8 were used to determine if the gross-deformation-failure thickness determined above would spall. This is the impact of a 0.045 gram aluminum projectile upon an aluminum sheet 0.635 millimeters thick. A second sheet of 7075-T6 aluminum is spaced 5.08 centimeters from the first sheet or shield. The second-sheet thickness is 3.18 millimeters. This computation showed a rise to a compressive stress of about 70 kilobars in the second sheet. The pulse duration was very long and multiple reflections occurred within the sheet. The maximum tensile stress was found to be about 7 kilobars. The 7075-T6 aluminum would spall with a tensile stress of about 13 kilobars.

These results show that the shape and duration of the pressure pulse applied to the sheet have overriding importance in determining whether the sheet will spall. This pulse is determined by the debris cloud that strikes the plate. From the computation it is expected that for this impact:

a) Less spacing will cause spall, greater spacing will not
b) Larger projectile masses will cause spall, less mass will not
c) Thinner (t_s/d) shields will cause spall, thicker shields will not
d) Higher projectile densities will cause spall, lower densities will not.

Spall here refers to fracture of the material. This does not mean that material will be detached from the surface, but only that there will be an internal fracture. This provides a conservative estimate of spall damage.

INTERACTION OF DEBRIS WITH A SHIELDED TARGET — EXPERIMENTAL

Experimental studies in support of the theorteical studies described in the previous section have been performed with a light-gas gun at impact velocities up to eight kilometers per second. This section describes some of the results of these experiments. Appendix C presents the raw data from all the experiments.

Momentum Multiplication

Extensive experiments utilizing a ballistic pendulum were carried out to measure the momentum transfer to the second sheet as a function of impact parameters. Initial experiments involved the measurement of momentum applied to the backup while varying the bumper thickness and the impact velocity in aluminum-aluminum impacts. The results of these experiments are summarized in Figure 62. The thin bumpers (0.305 mm, 0.635 mm and 1.02 mm) gave very similar results. The ratio of the measured momentum applied to the backup sheet divided by the incident projectile momentum increased with velocity up to about 5 kilometers per second, then remained constant throughout the rest of the experimental range. The thicker shield, 1.6 mm, exhibited a continued increase in the momentum multiplication ratio throughout the experimental range. Since it has been argued that the momentum multiplication ratio for the thin-sheet impact case has an upper bound of 2.0, and semi-infinite impact has no upper bound,[10] it is to be expected that the momentum multiplication ratio should show an increase for the thicker targets.

The momentum multiplication values presented in Figure 62 cover the range of solid-debris impact through completely melted debris. There appears to be no sharp change in behavior in this transition, with perhaps the exception of a change of slope at about 5 kilometers per second corresponding to the onset of melting in aluminum-aluminum impact.

Experiments were performed in which the second sheet was of 1100-0 aluminum in place of the 7075-T6 aluminum used in all other tests. No difference in momentum multiplication was observed.

As a test of the effect of spacing upon the momentum multiplication ratio, experiments were conducted with spacings less than the 5.08-centimeter spacing of the previously described experiments. The values obtained in these experiments were identical, within the ±4% error of the measurements, to the values obtained with the 5.08-centimeter spacing (Table III) with the exception of two measurements made with 1.27mm spacing which gave higher values.

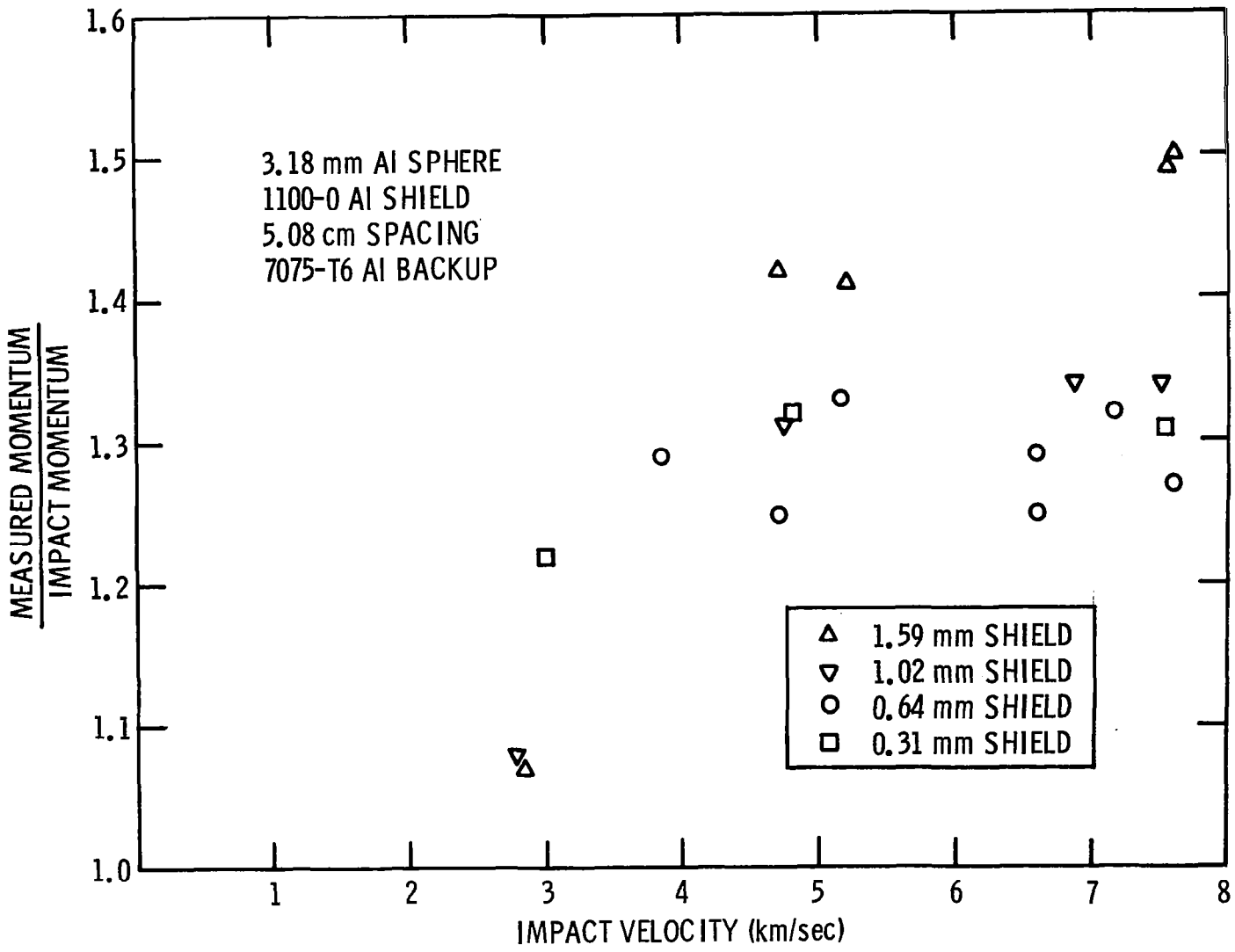

Figure 62 Momentum Multiplication vs Velocity

Table III
EFFECT OF SPACING

Shot No.	Shield Thickness (mm)	Impact Velocity	Spacing (cm)	Momentum Multiplication
D-1852	0.64	5.82	2.54	1.36
1556	↓	7.32	↓	1.35
1225	1.02	5.88	↓	1.43
1851	↓	7.62	↓	1.39
1854	1.60	5.64	↓	1.32
1853	↓	7.86	↓	1.45
1560	0.64	5.86	1.27	1.70
1352	↓	7.07	↓	1.35
1336	↓	7.29	↓	1.68
1557	↓	7.35	↓	1.34
1850	↓	7.47	↓	1.29

No explanation for these anomalous measurements has been found. This spacing is four projectile diameters and the debris is overdense when it strikes the second sheet, causing some cratering. It is not clear why this would not result in reproducible momentum transfer.

On the basis of these experiments it is concluded that spacing has no effect on momentum transfer for spacings greater than eight projectile diameters.

The value of the momentum multiplication factor attained for the aluminum-aluminum thin-sheet impact case was much less in the case of the three thinnest shields than the value of 2.0 postulated as the upper bound. The aluminum-aluminum impact represented a liquid debris impact and it was felt that perhaps the impact of vapor debris would more closely approach the value of 2.0. Experiments were performed with cadmium and lead projectiles and shields in which the debris striking the backup sheet was in vapor form. The results of these experiments are shown in Table IV. As can be seen, the values attained are again much less than 2.0.

Table IV
CADMIUM-CADMIUM AND LEAD-LEAD IMPACTS

Shot No.	Shield Thickness (mm)	Impact Velocity (km/sec)	Momentum Multiplication
D-1230	0.33	3.60	1.26
1453		5.18	1.28
1019		5.61	1.34
1889		6.83	1.42
1884	0.48	7.01	1.39
1046	0.64	3.18	1.21
1324		5.38	1.41
1326		5.70	1.40
1327		5.76	1.38
1045		6.40	1.41
1454		6.40	1.39
1580	1.22	3.69	1.39
1581		5.18	1.48
1888		6.89	1.52
1883		7.01	1.48
3.18mm Cadmium Spheres 5.08 cm Spacing			
1891	0.48	4.91	1.31
1890		6.89	1.39
2.57 mm Cadmium Spheres 5.08 cm Spacing			
1820	0.89	4.51	1.43
1819		4.85	1.48
1822	1.78	4.18	1.24
1821		4.36	1.24
3.18 mm Lead Spheres 5.08 cm Spacing			

The experiments performed with 0.64mm cadmium shields represented a transition from liquid debris striking the backup (the test at 3.18 kilometers per second) to vapor debris. The value of the momentum multiplication ratio reached a value of 1.4 at 5.38 kilometers per second and remained unchanged throughout the

experimental range. The experiments performed with the 0.33mm cadmium shields covered the transition from solid debris to liquid debris. Again the highest value attained is far less than 2.0. The 1.22mm cadmium shields and the lead tests represent vapor debris impacts, and again the momentem ratio is much less than 2.0.

Low-Density Projectiles

Four sets of experiments were performed using low-density and underdense materials for projectiles. The first series of tests was performed using Inlyte as the projectile material. This material is composed of very small hollow glass spheres held together in a plastic matrix. The projectiles used had a bulk density of 0.73 grams per cubic centimeter. The values of momentum multiplication obtained for impacts against aluminum shields (Table V) are about the same as observed for aluminum-aluminum impacts. Examination of the backup sheets showed fragment damage (probably from shield fragments) and no evidence of melting of the aluminum.

Table V
LOW-DENSITY IMPACTS

Shot No.	Projectile	Shield Thickness (mm)	Impact Velocity (km/sec)	Momentum Multiplication
D-1391	4.90mm Inlyte	0.64	4.69	1.20
1394	0.73 gm/cm^3	0.64	7.91	1.24
1393	↓	0.305	4.68	1.25
1575	4.19mm Nylon	0.64	4.11	1.45
1561	1.18 gm/cm^3	0.64	7.50	1.52
1349	↓	1.02	6.31	1.55
1371	↓	1.02	7.13	1.51
1653	2.62mm Foam Cu	0.64	5.99	1.36
1344	4.88 gm/cm^3	1.02	3.29	1.46
1345	↓	1.02	5.15	1.24
1652	↓	1.02	6.61	1.39
1650	2.62mm Foam Ni	0.64	6.50	1.43
1346	4.88 gm/cm^3	1.02	5.03	1.35

The second series utilized foamed copper and nickel as the projectile material. These foamed metals have approximately one-half the density of the fully dense materials. With the projectiles, the momentum ratios were about the same as for aluminum-aluminum impacts. The backup targets showed some evidence of melted aluminum from the shield and some cratering. The foam material with its many internal surfaces would not be expected to transmit the shock very well, and incomplete projectile breakup results with a fairly thin sheet. With the 1.02-millimeter shield this was less evident than with the 0.64-millimeter shield.

Nylon projectiles were used in the last series of tests. The nylon is fully dense with a density of 1.18 grams per cubic centimeter. In contrast to the underdense Inlyte, copper, and nickel, the momentum ratio was quite high (Table V). The second sheets showed damage similar to that observed with the Inlyte projectiles with many small craters apparently caused by shield fragments. Here there was no evidence of melted aluminum. Because of the similarity in the damage to the second sheet for the nylon and Inlyte impacts, it must be concluded that the differing values of momentum transfer must be due to some property of the projectile.

Throughout all the momentum measurements no value of momentum multiplication over 1.55 was observed for impacts with intersheet spacings of eight projectile diameters or greater. For intersheet spacings of four projectile diameters two values of momentum multiplication of about 1.7 were observed. In no case was a momentum multiplication ratio near 2.0 observed. The lack of attainment of momentum multiplication ratios near the limit of two can be accounted for by a probably lack of perfectly elastic vapor impact on the second sheet and internal interaction of the debris cloud as it strikes the second sheet.

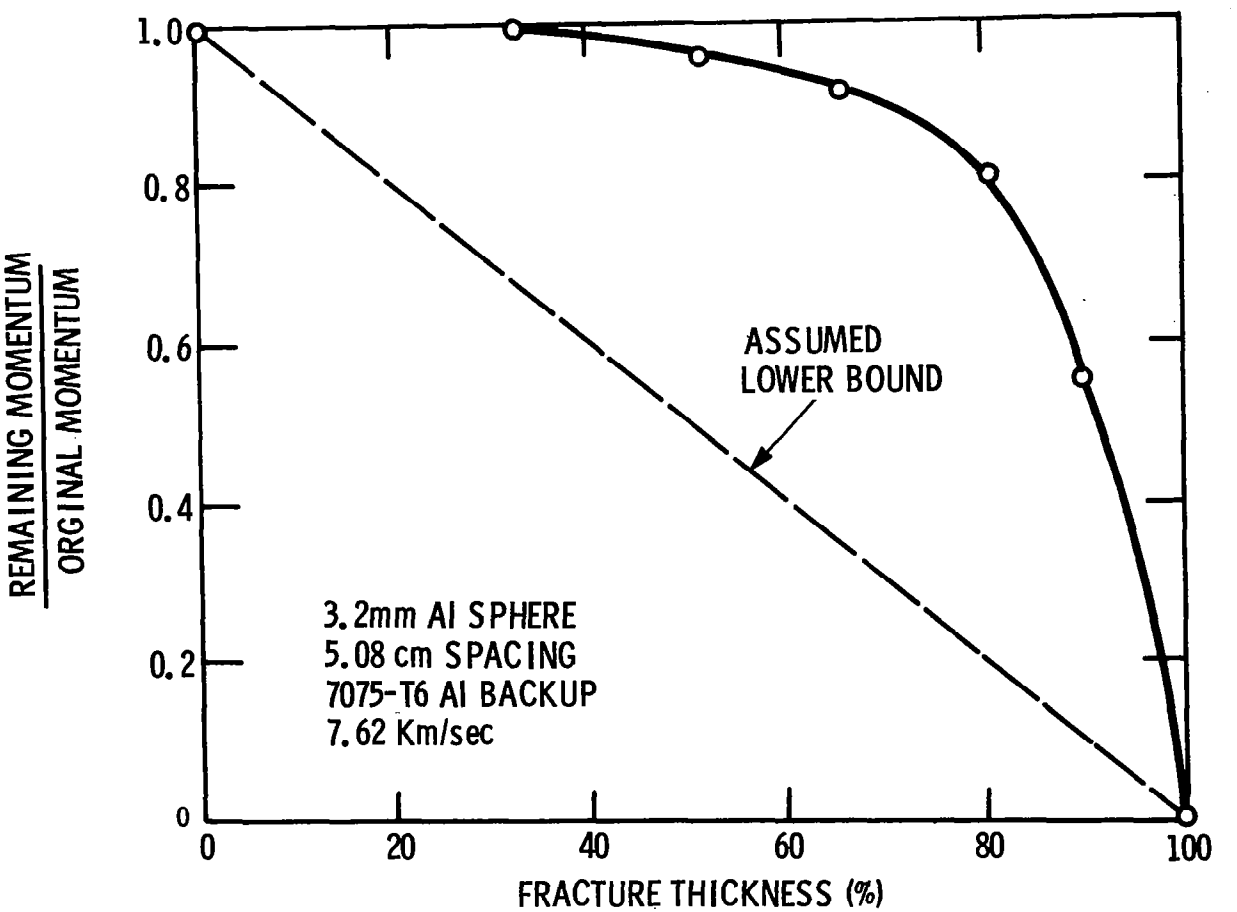

Figure 63 Remaining Momentum vs Backup Thickness

STRUCTURES

The foregoing has dealt with simple structures, two sheets, subjected to normal impacts. This section will deal with more complex structures and non-normal impacts. These situations lend themselves, to a greater or lesser degree, to analysis.

FILLERS

Under some conditions it is desirable to introduce a filler material between the sheets of a two-sheet structure. This filler material can take the form of a honeycomb for structural rigidity or additional sheets or foamed material for thermal insulation. In general the addition of mass to a structure increases its resistance to impact damage but studies of fillers, honeycombs in particular, have indicated that they may make the structure more vulnerable.[13]

The first of these fillers considered was additional sheets between the two primary sheets. The strip analysis was used to examine the amount of momentum that passed through a sheet when the sheet was less than the fracture thickness. When fracture occurred in any of the six layers in the strip, the momentum of the broken segment was summed. The result of this procedure is shown in Figure 63. These results indicate that the use of multiple sheets offers little or no advantage over single backup sheets, as there is no significant decrease of momentum through the second sheet until the second sheet is of approximately 90% of the fracture thickness.

A series of experiments was conducted to test the validity of this approach. The first three experiments utilized the ballistic pendulum behind various thicknesses of the second sheet to attempt to measure the momentum delivered through the second sheet. The results of these tests are summarized in Table VI.

Table VI
MOMENTUM THROUGH BACKUP

Shot Number	D-1437	1400	1442
Velocity	8.05 km/sec	7.60	7.50
% of Fracture Thickness	32	50	100
Momentum Through Backup (Actual)	1.38	0.65	0.47
Momentum Through Backup (Predicted)	0.99	0.95	0
All tests 3.18-mm aluminum spheres, 5.08-cm spacing, 7075-T6 aluminum backups			

The poor agreement between the experiments and the predictions is due in part to spall from the second sheet and also to the momentum multiplication in the catch material on the ballistic pendulum.

On the basis of these experiments a lower bound was set on the momentum coming through the loaded sheet as the momentum fraction remaining being equal to one minus the sheet thickness to true fracture thickness ratio. This lower bound is indicated in Figure 63 by the dotted line. Using this lower bound it is possible to analyze two cases of multiple sheets. Both cases require that the first sheet or shield breaks up, melts or vaporizes the impacting projectile and spreads the debris such that the blast loading analysis is applicable.

First assume that no spread of the debris takes place after the fracture of the second sheet. The situation is illustrated in Figure 64.

In this diagram P_n is arbitrary and t_c is defined as the fracture thickness for a second sheet spaced at S for a two-sheet structure. The true fracture thickness of the n^{th} sheet is T_n. From the scaling results

$$T_1 = \left(\frac{S}{S_1}\right)^2 t_F$$

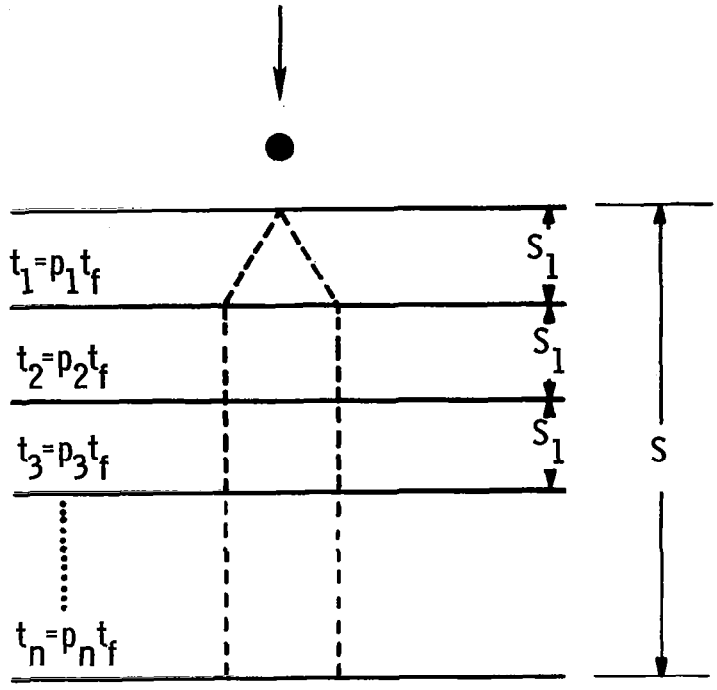

Figure 64 Schematic of Multisheet Impact

then

$$\frac{t_1}{T_1} = \frac{P_1 t_F}{\left(\frac{S}{S_1}\right)^2 t_F} = P_1\left(\frac{S_1}{S}\right)^2$$

Then the momentum fraction remaining after fracture of this sheet is

$$\frac{M_1}{M_o} = \frac{\text{Momentum to next sheet}}{\text{Original Momentum}} = 1 - P_1\left(\frac{S_1}{S}\right)^2$$

$$T_2 = \left[1 - P_1\left(\frac{S_1}{S}\right)^2\right] T_1 = \left[1 - P_1\left(\frac{S_1}{S}\right)^2\right]\left(\frac{S}{S_1}\right)^2 t_F$$

$$\frac{t_2}{T_2} = \frac{P_2\, t_F}{\left[1 - P_1\left(\frac{S_1}{S}\right)^2\right]\left(\frac{S}{S_1}\right)^2 t_F} = \frac{P_2\left(\frac{S_1}{S}\right)^2}{\left[1 - P_1\left(\frac{S_1}{S}\right)^2\right]}$$

$$\frac{M_2}{M_o} = \left[1 - \frac{P_2\left(\frac{S_1}{S}\right)^2}{1 - P_1\left(\frac{S_1}{S}\right)^2}\right]\left[1 - P_1\left(\frac{S_1}{S}\right)^2\right] = 1 - P_1\left(\frac{S_1}{S}\right)^2 - P_2\left(\frac{S_1}{S}\right)^2$$

Generalizing,

$$\frac{M_{n-1}}{M_o} = 1 - P_1\left(\frac{S_1}{S}\right)^2 - P_2\left(\frac{S_1}{S}\right)^2 - \cdots - P_{n-1}\left(\frac{S_1}{S}\right)^2$$

$$= 1 - \left(\frac{S_1}{S}\right)^2 \left(P_1 + P_2 + \cdots + P_{n-1}\right)$$

$$T_n = \left[1 - \left(\frac{S_1}{S}\right)^2 \left(P_1 + P_2 + P_3 + \cdots + P_{n-1}\right)\right] T_1$$

$$= \left[1 - \left(\frac{S_1}{S}\right)^2 \left(P_1 + P_2 + P_3 + \cdots + P_{n-1}\right)\right] \left(\frac{S}{S_1}\right)^2 t_F$$

and

$$\frac{t_n}{T_n} = \frac{P_n}{\left[1 - \left(\frac{S_1}{S}\right)^2 \left(P_1+P_2+P_3+\cdots+P_{n-1}\right)\right]\left(\frac{S}{S_1}\right)^2}$$

If the last sheet is not to fracture $t_n = T_n$ so

$$P_n = \left[1 - \left(\frac{S_1}{S}\right)^2 \left(P_1 + P_2 + P_3 + \cdots + P_{n-1}\right)\right] \left(\frac{S}{S_1}\right)^2$$

Then the total of the p is

$$\sum_{i=1}^{n} P_i = \sum_{i=1}^{n-1} P_i + \left(\frac{S}{S_1}\right)^2 \left[1 - \left(\frac{S_1}{S}\right)^2 \left(P_1 + P_2 + P_3 + \cdots + P_{n-1}\right)\right]$$

$$= \sum_{i=1}^{n-1} P_i + \left(\frac{S}{S_1}\right)^2 - \sum_{i=1}^{n-1} P_i$$

$$= \left(\frac{S}{S_1}\right)^2$$

If n sheets are better than two, the sum of the p must be less than one; so

$$\sum_{i-1}^{n} P_i < 1$$

or

$$\frac{S}{S_1}^2 < 1$$

or

$$S < S_1$$

which is not so. Therefore two sheets are better than n for the case where the debris is channeled after fracturing the second sheet.

For the second case assume that the debris continues to spread after each sheet fractures and that the sheets are uniformly spaced (Figure 65).

With the notation as above

$$T_1 = \left(\frac{S}{S_1}\right)^2 t_F$$

$$\frac{t_1}{T_1} = P_1 \left(\frac{S_1}{S}\right)^2$$

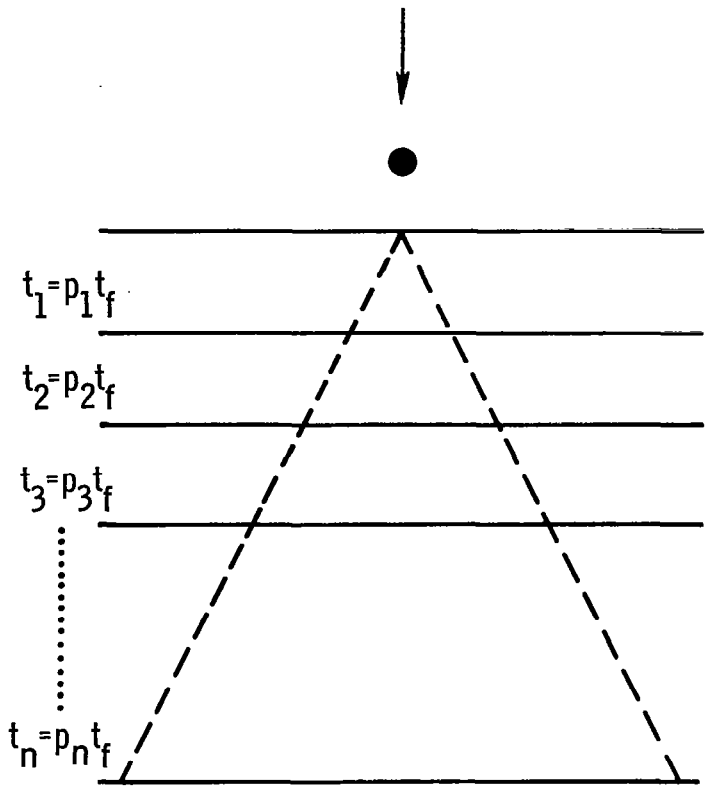

Figure 65 Multisheet Impact Schematic With Debris Spreading

$$\frac{M_1}{M_o} = 1 - P_1\left(\frac{S_1}{S}\right)^2$$

$$T_2 = \left[1 - P_1\left(\frac{S_1}{S}\right)^2\right]\left(\frac{S}{2S_1}\right)^2 t_F$$

$$\frac{t_2}{T_2} = \frac{P_2\left(\frac{2S_1}{S}\right)^2}{\left[1 - P_1\left(\frac{S_1}{S}\right)^2\right]}$$

$$\frac{M_2}{M_o} = \left\{1 - \frac{P_2\left(\frac{2S_1}{S}\right)^2}{\left[1 - P_1\left(\frac{S_1}{S}\right)^2\right]}\right\} \quad \left[1 - P_1\left(\frac{S_1}{S}\right)^2\right] = 1 - P_1\left(\frac{S_1}{S}\right)^2 - P_2\left(\frac{2S_1}{S}\right)^2$$

Generalizing, the momentum fraction to the last sheet is

$$\frac{M_{n-1}}{M_o} = 1 - P_1\left(\frac{S_1}{S}\right)^2 - P_2\left(\frac{2S_1}{S}\right)^2 - P_3\left(\frac{3S_1}{S}\right)^2 - \cdots - P_{n-1}\left(\frac{n-1\ S_1}{S}\right)^2$$

$$= 1 - \left(\frac{S_1}{S}\right)^2 \left[P_1 + 2^2P_2 + 3^2P_3 + \cdots + (n-1)^2\ P_{n-1}\right]$$

$$T_n = \left\{1 - \left(\frac{S_1}{S}\right)^2 \left[P_1 + 2^2P_2 + 3^2P_3 + \cdots + (n-1)^2P_{n-1}\right]\right\} \left(\frac{S}{nS_1}\right)^2 t_F$$

$$\frac{t_n}{T_n} = \frac{P_n}{\left\{1 - \left(\frac{S_1}{S}\right)^2 \left[P_1 + 2^2P_2 + \cdots + (n-1)^2P_{n-1}\right]\right\}\left(\frac{S}{nS_1}\right)^2}$$

$$P_n = \left\{1 - \left(\frac{S_1}{S}\right)^2 \left[P_1 + 2^2P_2 + \cdots + (n-1)^2P_{n-1}\right]\right\}\left(\frac{S}{nS_1}\right)^2$$

Then the sum of all the p is

$$\sum_{i=1}^{n} P_i = \sum_{i=1}^{n-1} P_i + \left(\frac{S}{nS_1}\right)^2 - \frac{1}{n^2}\sum_{i=1}^{n-1} i^2P_i$$

But $S = n\ S_1$ so

$$\sum_{i=1}^{n} P_i = 1 + \sum_{i=1}^{n-1} P_i\left(1 - \frac{i^2}{n^2}\right)$$

If n sheets are better than two the sum of the p must be less than one or

$$\sum_{i=1}^{n-1} P_i\left(1 - \frac{i^2}{n^2}\right) < 0$$

which cannot be so. Therefore two sheets are better than n for the sheets uniformly spaced and with the debris spreading after the fracture of each sheet.

Further generalization of the second case with the sheets placed arbitrarily an S distance from the shield leads to the sum of the p as

$$\sum_{i=1}^{n} P_i = \sum_{i=1}^{n} P_i + \left(\frac{S}{\bar{S}}\right)^2 - \sum_{i=1}^{n-1} a_i^2 P_i$$

$$= 1 + \sum_{i=1}^{n-1} P_i (1 - a_i^2)$$

Again for n sheets to be better than two

$$\sum_{i=1}^{n} P_i < 1$$

or

$$\sum_{i=1}^{n-1} P_i (1 - a_i^2) < 0$$

or at least one of the a_i must be greater than one. This says that one of the intersheet spacings must be greater than S . Therefore for all cases two sheets are better than n within a given spacing, provided the mode of failure is blast loading.

Experiments with aluminum-aluminum and cadmium-cadmium impacts supported the conclusion that two sheets provide more protection than n . In some cases the addition of a third sheet increased the vulnerability of a structure. An impact of a 3.18-millimeter-diameter cadmium projectile at 6.5 kilometers per second upon a 0.64-millimeter cadmium shield with 5.08 centimeters spacing to a 7075-T6 aluminum second sheet 1.02 millimeters thick did not cause failure of the second sheet. However, when a 7075-T6 aluminum sheet 1.02 millimeters thick was inserted between the shield and second sheet, all three sheets failed.

Examination of Figure 66 gives an indication of the reason for this. As can be seen the sheet upon failure seems to cause a restriction in the spread of the debris. This causes a higher load per unit area upon the next sheet than would occur if the debris were allowed to spread.

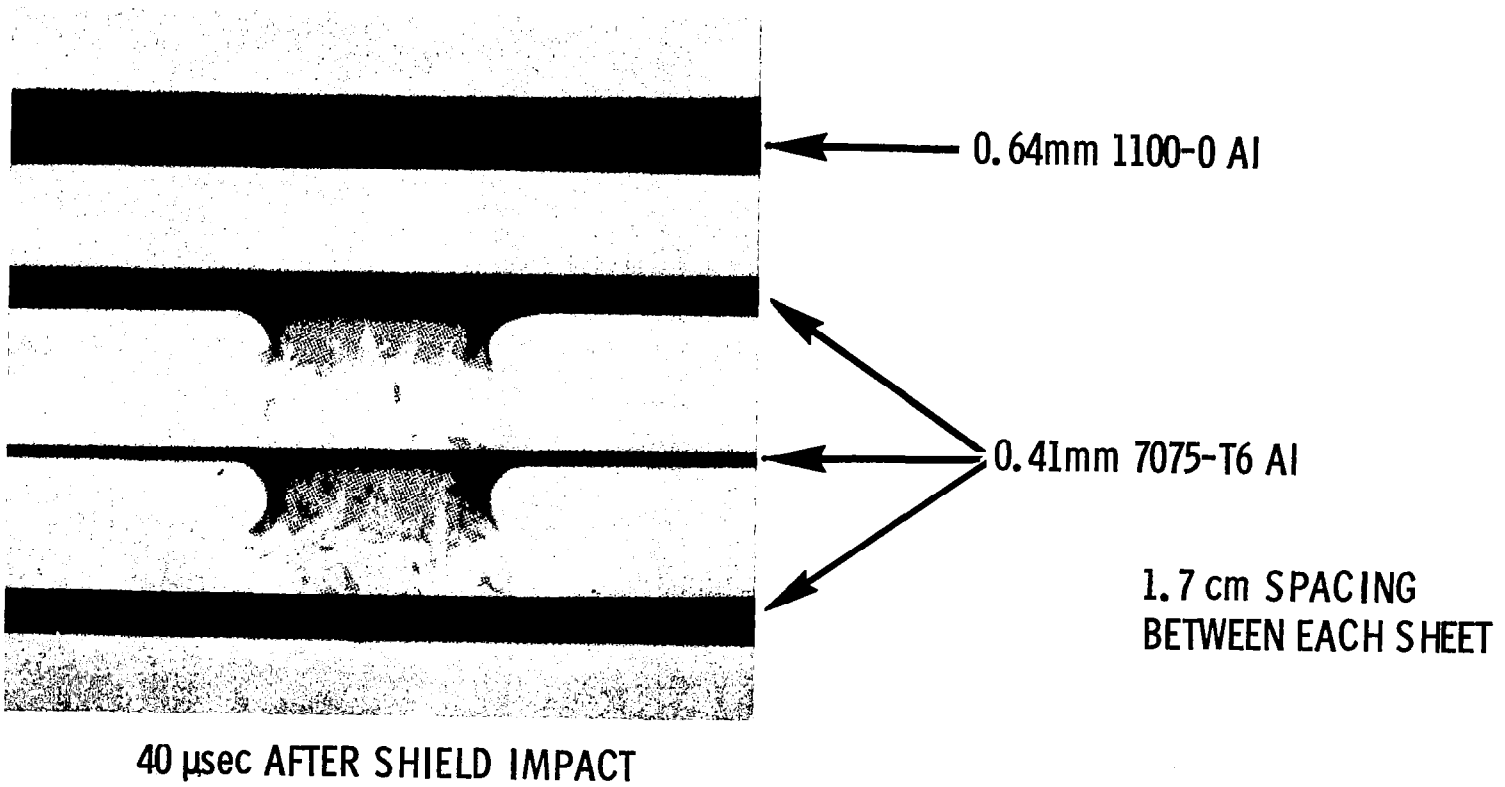

Figure 66 X-Ray of Multisheet Failure

Figure 66 also shows that debris from the sheet that has failed will impact the next sheet. This solid debris is not accounted for within the blast-loading treatment. If the primary damage mechanism is the impact of this solid debris, the blast-loading analysis will not apply.

Experimentally, the only advantage that multiple sheets offered was to catch spall fragments from the preceding sheet.

HONEYCOMBS

The second filler to be considered was the honeycomb added between two sheets, such as on the Apollo Service Module.

To obtain an understancing of the reaction of the honeycomb to the debris passing through a shield, the two-dimensional hydrodynamic computation results were examined. The debris in the cases of interest is in a liquid or vapor form and expands radially at a maximum velocity of about one-half of the axial velocity. This debris would be expected to impulsively load the honeycomb from the inside. Any particulate debris from the late stages of hole formation in the shield would not impact the honeycomb until after the impulsive loading had taken place.

The basic questions to be considered with the honeycomb are whether the honeycomb cell will break and, if it does, will the projectile-shield debris be channeled. To attempt to answer these questions a somewhat simplified analysis was performed. The honeycomb cell was assumed to be a circular cylinder rather than a hexagon. The impact was assumed to take place normal to the shield and in the center of the circular cell. The radial momenta were then taken from the two-dimensional hydrodynamic calculations and used to calculate the impulse delivered to the circular cell. Given the wall thickness of the cell, the maximum radial velocity of the cell wall can be obtained. This velocity can then be compared with the radial velocity of the debris. The velocity of the cell wall computed is not the actual radial velocity but rather the velocity it would have if all the debris radial momentum were instantaneously imparted to it. This is not actually the case, as the debris impacts over some period of time. It is possible that the

debris first striking the wall and rebounding interferes with that debris that is trailing. Thus if the maximum radial velocity of the cell wall is less than the debris radial velocity the debris will strike the wall, rebound and be channeled. For the debris not to be channeled the computed velocity of the cell wall must be at least equal to the debris radial velocity.

In the case where the debris is channeled, the backup thickness requirements can be obtained from the plate calculations made with the uniform S/2 momentum distribution. If the debris is not channeled, the backup thickness requirements will be somewhere between the thicknesses with no filler and the channeled thicknesses. Based upon this analysis a honeycomb will be a detriment to the meteoroid-protection capabilities of any two-sheet structure.

The analysis performed states implicitly that the honeycomb damage mechanism is controlled by the momentum and velocity of the debris. The debris velocity is a function of the impact velocity, thus a velocity-scaled honeycomb experiment is not possible. It was necessary for this reason to perform experiments to test the analysis, and no attempt was made to simulate high-velocity impacts.

The experiments that were performed utilized cadmium-cadmium impacts so that the debris would be in the heated liquid or vapor state to effectively blast load the cell interior. The honeycomb was represented by a thin circular tube of 6061-T6 aluminum. The impacts were in most cases in the center of these cells, and the reaction of the cell is typified by the framing camera sequences shown in Figures 67 and 68. Figure 69 shows flash X-rays of similar impacts a few microseconds after the first-sheet impact. From these figures it can be seen that the cell wall starts to expand very soon after impact and soon breaks. However, the cell wall has not achieved a high enough velocity to get out of the way of the debris. As can be seen in Figure 69 the cell wall has broken but the debris is well channeled down the tube. By channelling the debris the load applied to the second sheet is very much restricted in expanse, producing a very high momentum intensity. This high-intensity loading requires that the thickness of the backup sheet be increased to resist any given level of damage.

14.4mm DIAMETER
0.25mm THICK 6061-T6 Al TUBE
SIMULATED HONEYCOMB CELL

3.18 mm Cd SPHERE
0.33 mm Cd SHIELD

5.08 cm SPACING
3.18 mm 7075-T6 Al BACKUP
6.92 Km/sec

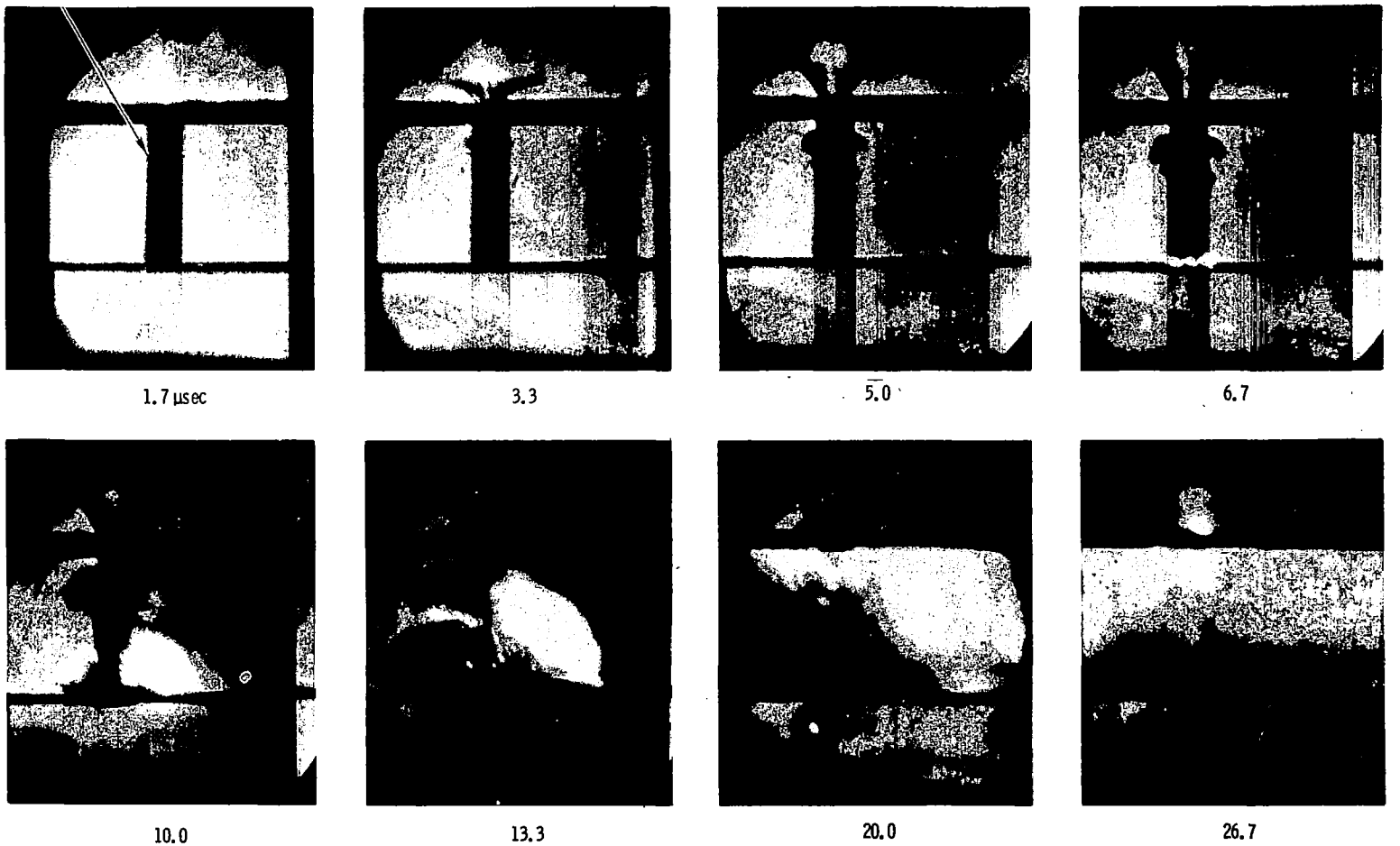

Figure 67 Framing Camera Sequence of Simulated Honeycomb Impact

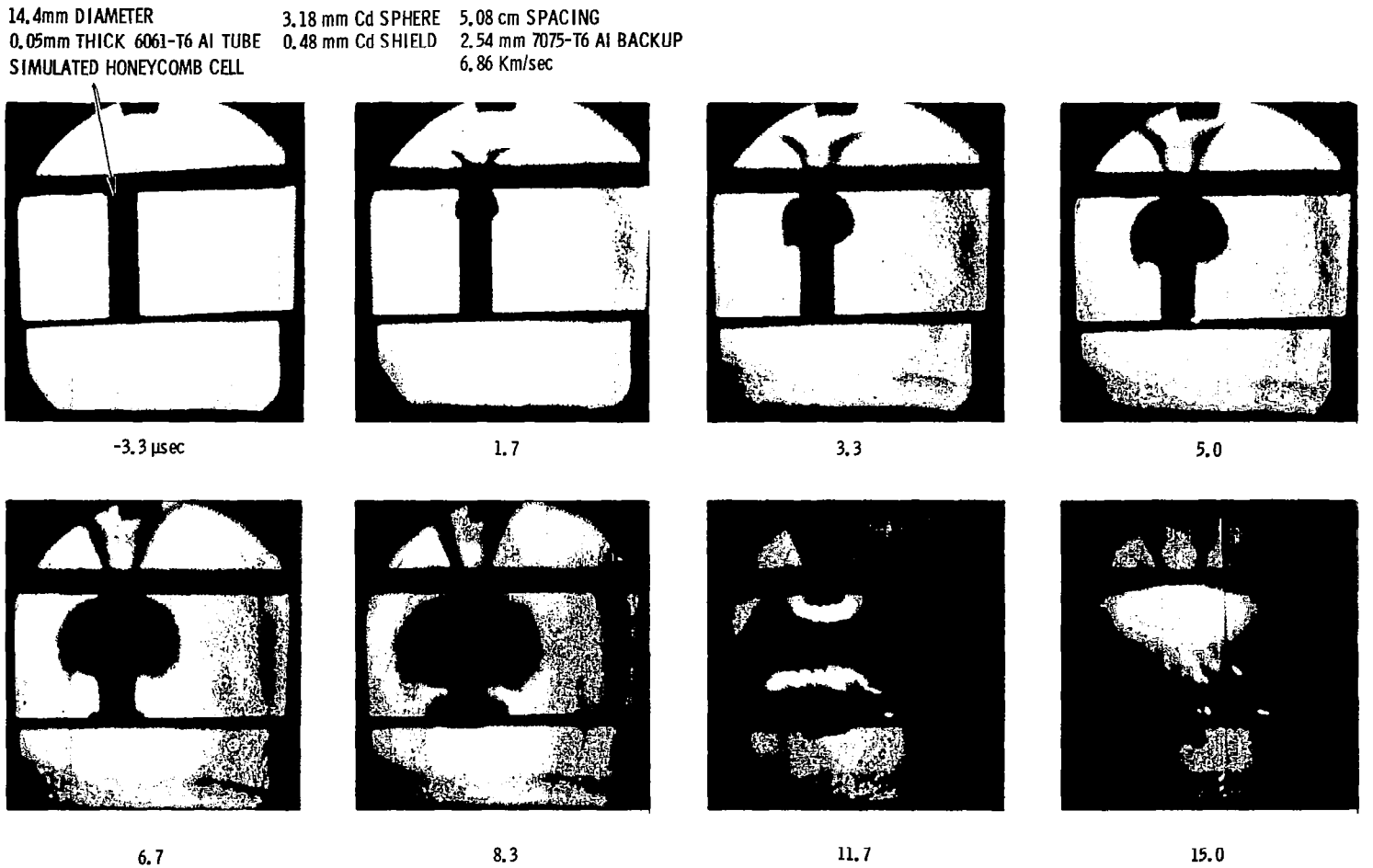

Figure 68 Framing Camera Sequence of Simulated Honeycomb Impact (Continued)

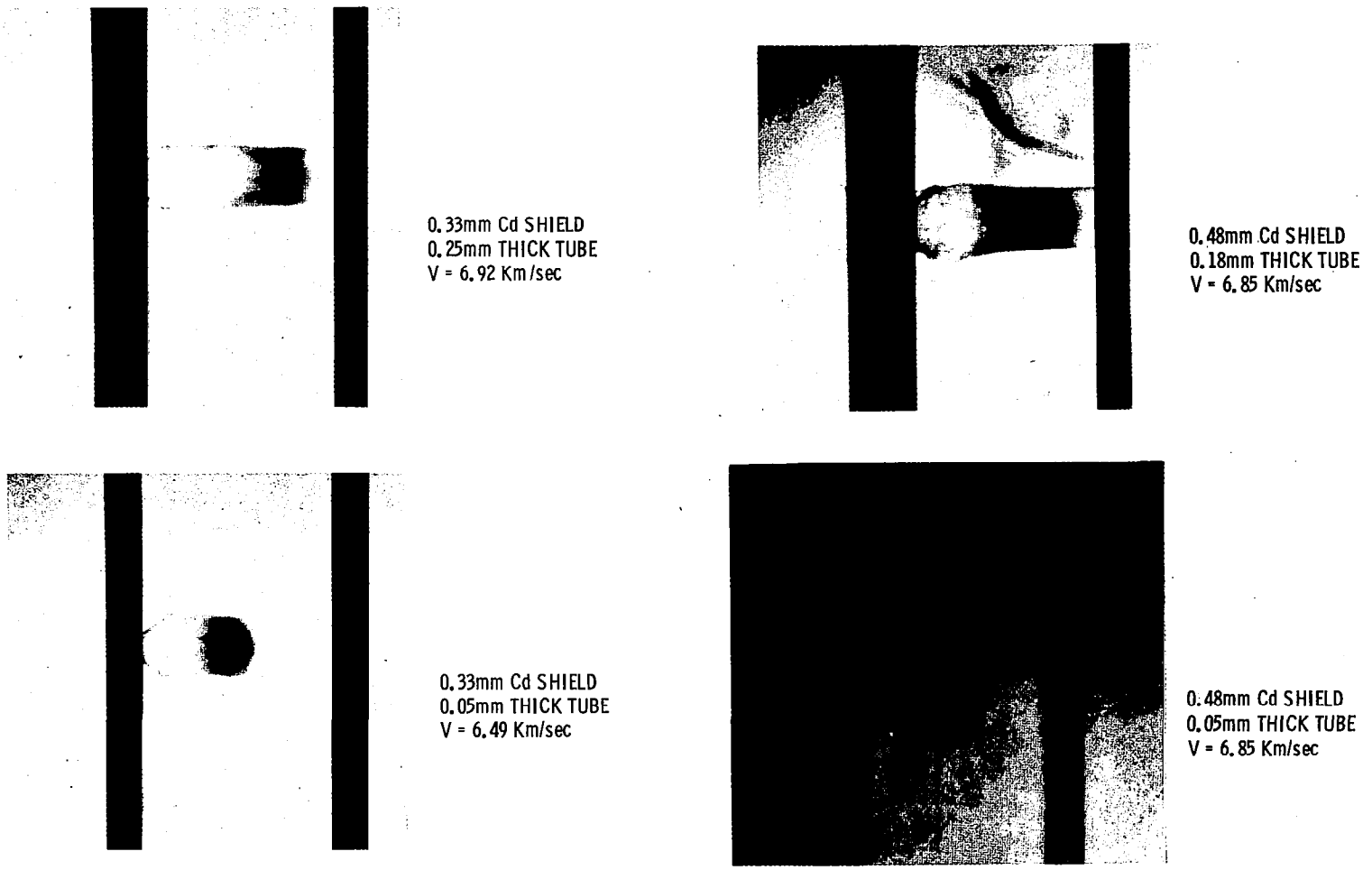

Figure 69 Flash X-Rays of Honeycomb Cell Channeling Effect

The radial momenta from CAMEO 23 and 24 were used to compute the tube wall thicknesses which would be expected to channel or not to channel the debris for cadmium-cadmium impacts. For an impact at six kilometers per second and a shield $t_s/d = 0.5$, a tube 1.27 centimeters in diameter and 0.41 millimeters thick would channel the debris while a tube thickness of 0.05 millimeters would not. For $t_s/d = 0.3$ the tube thicknesses are 0.2 and 0.02 millimeters respectively. Experiments performed with the above conditions within the range of tube sizes resulted in failure of the tube and channeling of the debris (see Table VII).

Table VII
3.18 mm CD SPHERES – 5.08 cm SPACING
ALL CADMIUM SHIELDS – 7075-T6 ALUMINUM SECOND SHEETS

Shot No.	Velocity (km/sec)	Shield Thickness (mm)	Second Sheet Thickness (mm)	Tube		Damage
				Diameter (mm)	Thickness (mm)	
D-1921	6.85	0.48	4.82	14.5	0.18	Perforation
1922	6.98	0.48	6.35	14.5	0.18	Perforation
1912	6.83	0.48	2.54	14.5	0.18	Perforation
1910	6.83	1.22	2.54	14.5	0.18	Perforation
1909	6.50	0.33	3.18	14.5	0.05	Perforation
1913	6.85	0.48	2.54	14.5	0.05	Perforation
1952	6.67	1.60	2.54	14.5	0.05	Perforation
1905	6.95	1.22	1.02	14.5	0.41	Perforation
1906	6.92	1.22	1.02	14.5	0.41	Perforation
1907	6.85	1.22	1.02	14.5	0.05	Perforation
1946	6.67	0.48	2.54	24.6	0.15	Perforation
1947	6.55	0.48	2.54	8.4	0.15	Perforation
1948	6.48	1.22	2.54	8.4	0.15	Perforation
1908	6.92	0.33	3.18	14.5	0.25	Perforation

As would be expected, larger-diameter tubes and thinner shields also caused channeling. The second-sheet failures are typified by those shown in Figure 70; the failure in these cases seems to be a shear failure with the portion of the second sheet under the honeycomb all thrown out almost intact. As can be seen by the damage to the third sheets, this fragment can cause considerable further damage.

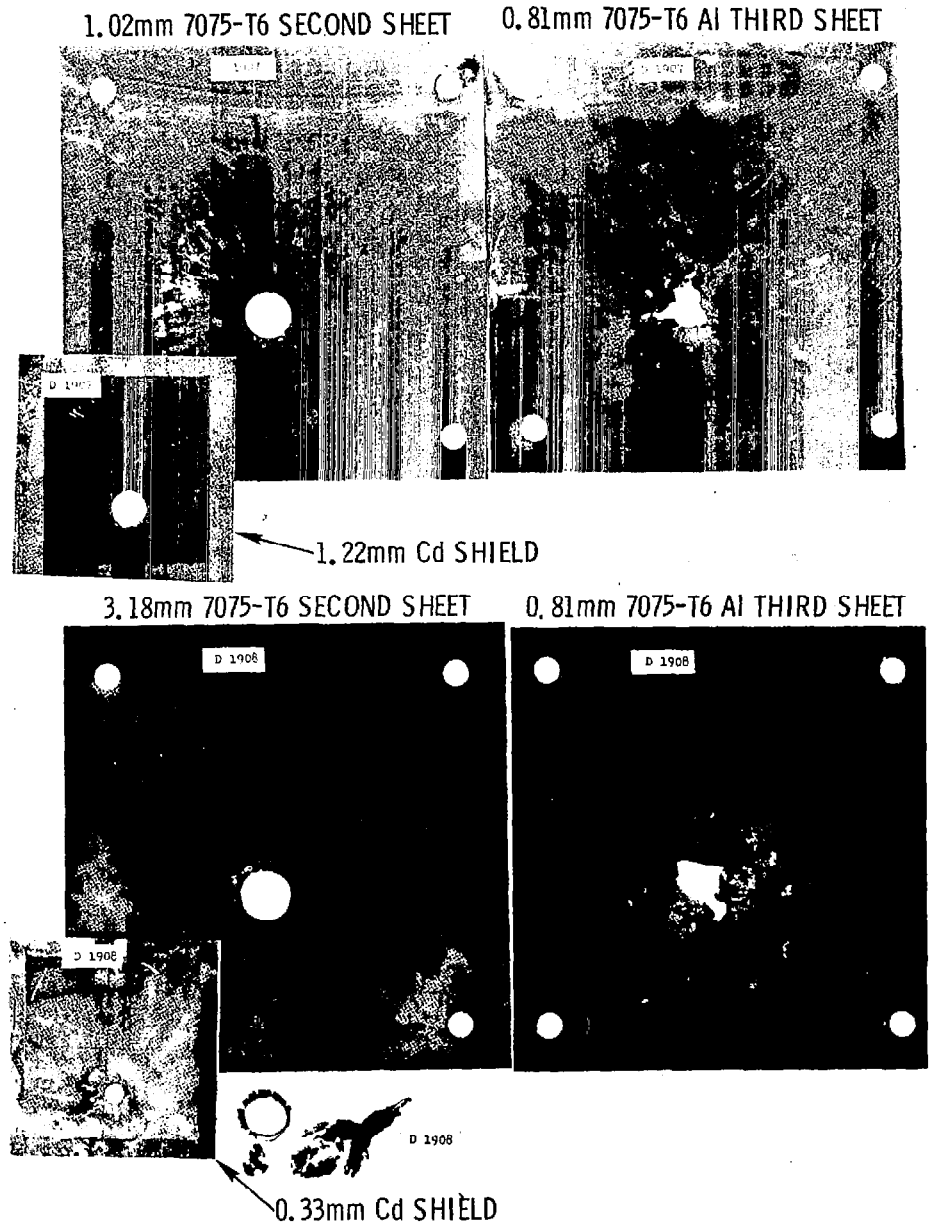

3.18mm Cd SPHERES - 5.08 cm SPACING
6.85 km/sec
14.4mm DIAMETER
0.05mm THICK 6061-T6 Al TUBE

6.92 km/sec
14.4mm DIAMETER
0.25mm THICK 6061-T6 Al TUBE

Figure 70 Targets Showing Effect of Variations in Honeycomb Wall Thickness

With a $t_s/d = 0.15$ cadmium shield and a 0.18-millimeter tube wall thickness, the second sheet had to be between 4.82 and 6.35 millimeters thick to avoid failure. Using the results of the blast loaded plate in Figure 35, the backup thickness to prevent fracture was computed to be 10.8 millimeters. This is compared to a fracture thickness of between 1.0 and 1.27 millimeters for the same structure without the tube. This honeycomb then results in an increase of at least a factor of 3.8 in the backup thickness required to prevent failure.

When the simulated honeycomb was subjected to oblique impacts the debris was still channeled to some extent but the main body of the debris impacted the side of the tube, caused it to fail, and then continued to spread.

It is concluded from the analysis and from these tests that a honeycomb will not increase the meteoroid-impact resistance of a structure and can result in a serious degradation of its resistance to failure.

LOW-VELOCITY IMPACT

The predictions of second-sheet failure made earlier have assumed that the debris passing through the shield essentially blast-loads the second sheet. This assumption is true only if the impact occurs at velocities sufficient to cause the debris to consist of very small particles or a vapor. For aluminum-aluminum impacts this condition is achieved when the debris contains molten material, say at 7 kilometers per second. At velocities lower than this incomplete fragmentation of the projectile occurs and the fragments passing through the bumper can inflict substantial damage on the rear sheet.

To investigate this effect, several tests were conducted with 3.18mm aluminum projectiles at low velocities. Figure 71 shows the penetration results for these experiments along with results at higher velocities. Also shown are the thicknesses to prevent perforation and/or spall over the range of velocities. It can be seen that for this structure (0.64mm 1100-0 aluminum shield with 5.08cm spacing to a 7075-T6 aluminum backup) that a peak in penetration and necessary thickness to prevent second-sheet rear-surface damage occurs at about 2.5 kilometers per

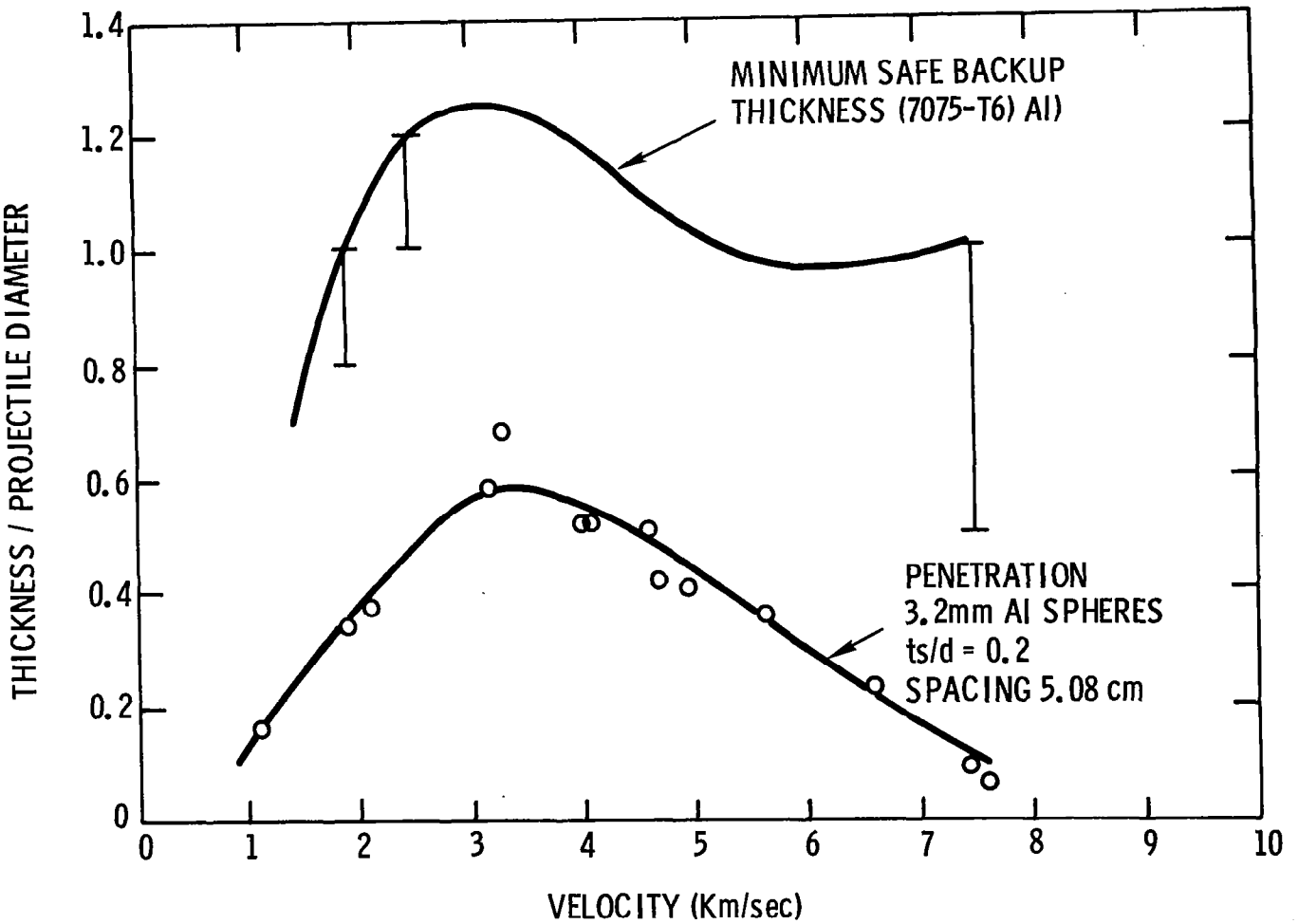

Figure 71 Backup Thickness Necessary to Prevent Perforation

second. At higher velocities the thickness decreases as the projectile is well fragmented, then increases again as the blast loading becomes more severe. The thickness to stop the projectile at 2.5 kilometers per second is the same as that required to stop the same projectile at 10 kilometers per second (see Figure 47).

The thickness of backup for various shield thicknesses to prevent perforation was determined. These thicknesses are given below in Table VIII.

Table VIII
SHIELD THICKNESS DATA

$\frac{t_s}{d}$	$\frac{t_s+t_B}{d}$	Velocity (km/sec)
0.20	> 1.00 < 1.20	1.90
0.20	> 1.20 < 1.40	2.48
0.32	> 1.12 < 1.32	2.60
0.50	> 1.01 < 1.30	2.12

All but the first set are for the low-velocity maximum penetration. Although the values are not determined very accurately, there appears to be a trend toward lower values for thicker shields.

It is important to note that fracture thicknesses for blast-loading failure scale with projectile mass while the low-velocity results should scale directly with projectile diameter. Also, the low-velocity results are expected to be independent of intersheet spacing.

OBLIQUE IMPACTS

It would be expected that most meteoroid impacts will not occur normal to the surface of a structure. Consideration of such oblique impacts is not possible with a two-dimensional treatment such as CAMEO because the impact is not axisymmetric. Kreyenhagen, et al,[14] have used a two dimensional analog of an oblique

impact which demonstrates some features of the process. In their computations an infinite-length aluminum cylinder strikes a thin aluminum plate at 6.1 kilometers per second at an angle of 80-1/2^{o} from the normal to the plate. The maximum pressure generated is about 330 kilobars, whereas a normal impact would result in a maximum pressure of about 800 kilobars. The projectile material does not pass through the sheet and the debris to the rear of the sheet is all shield material, leaving the sheet normally at low velocity. For this impact there would be no "in line" damage to the second sheet, i.e., there would be no damage to the second sheet along an extension of the original flight path. Impacts at smaller angles of obliquity will allow projectile debris to pass through the shield and this material can cause "in line" damage.

A cadmium-cadmium impact at an angle of 30^{o} from the normal to the shield is shown a few microseconds after impact in Figure 72. For the impact conditions here there certainly will be "in line" damage. Note that the debris here is concentrated in the front of the debris as opposed to the case of the normal impact shown in Figure 1, where the debris is spread through the length of the bubble of debris. This concentration of the debris would be expected to deliver a more intense pressure pulse of shorter duration in the second sheet for the oblique impact, and would be more likely to cause rear surface spall from the second sheet.

Initially experiments were performed with aluminum-aluminum impacts at angles of obliquity of 30^{o}, 45^{o}, and 60^{o} measured from the normal to the surface of the shield. These experiments, at impact velocities in excess of 7 kilometers per second, showed that the major source of damage was fragment impact to the second sheet. For normal impacts against these structures fragment damage is very minor due to the melting of the debris. The lesser degree of fragmentation is expected because of lower peak pressures associated with oblique impacts. Examination of the second sheets from these experiments, shown in Figure 73, reveals that the amount of fragmentation of the debris decreases as the angle of obliquity is increased (as evidenced by the crater sizes). Note that the second sheet of the target struck at 45^{o} shows the greatest damage. This would seem to be due to the increase in lateral dispersion as the angle is increased, eventually offsetting the decrease in debris fragmentation.

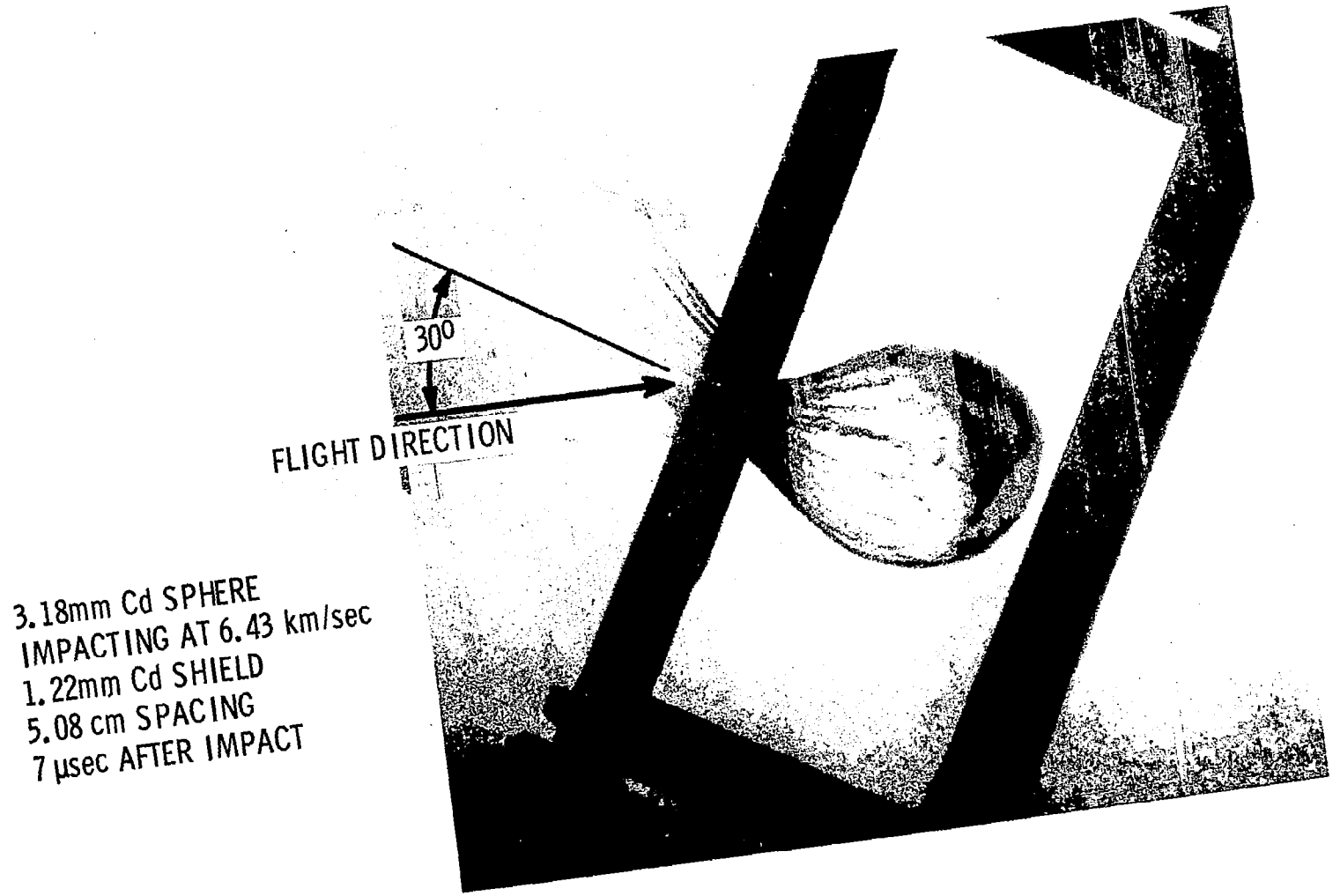

Figure 72 Flash X-Ray Showing Effect of Oblique Impact

3.18mm Al SPHERES
IMPACTING AT FROM 7.26 to 7.53 km/sec
0.64mm 1100-0 Al SHIELD
5.08 cm SPACING
1.60mm 7075-T6 Al BACKUPS

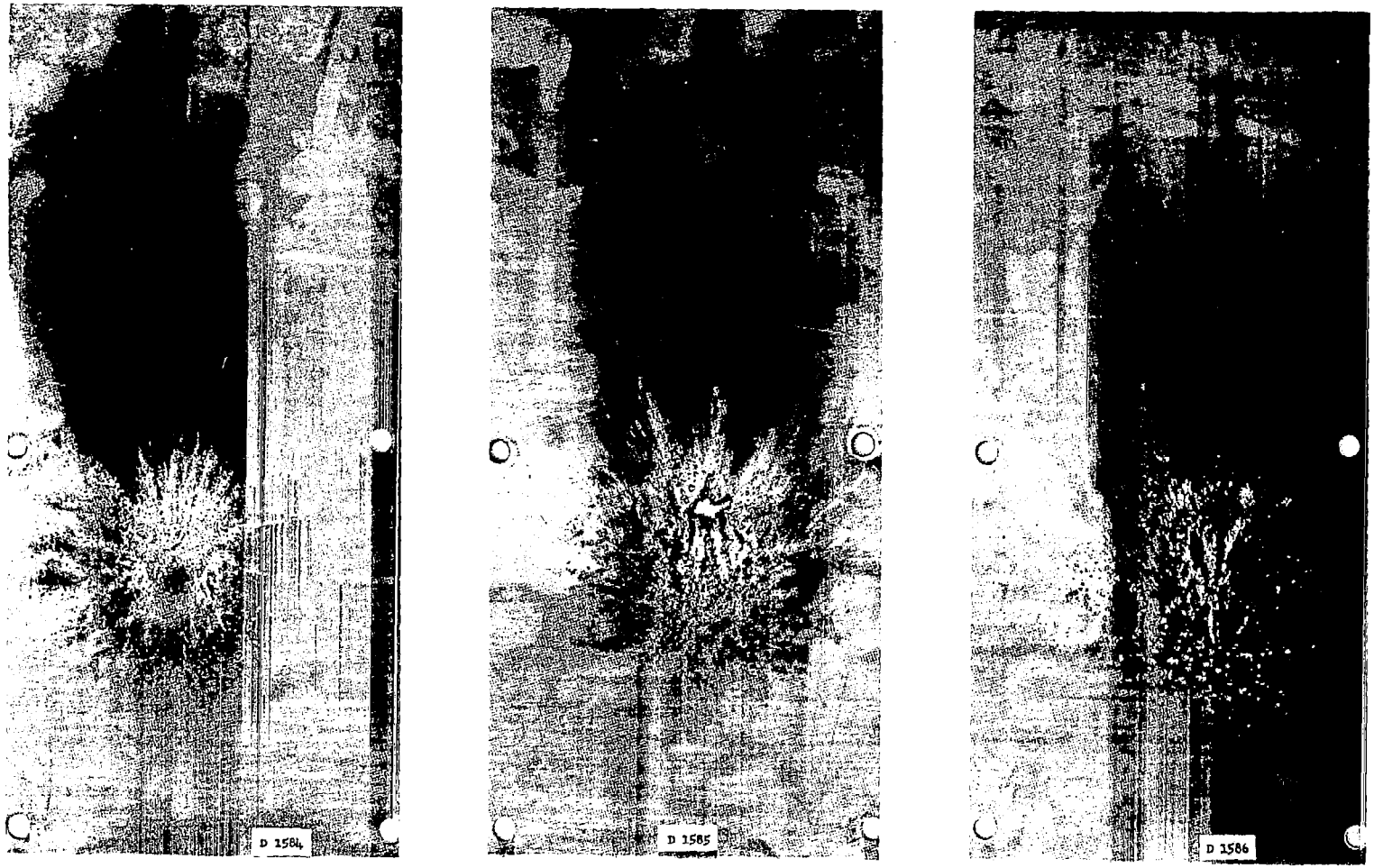

30^0 45^0 60^0

Figure 73 Backup Targets Showing Effects of Oblique Impact

Further tests were performed in excess of 7 kilometers per second to determine what the second sheet requirements were to prevent failure. A summary of these experiments is presented in Table IX. In all cases of failure the cause was fragment impact. This observation from examination of the targets was supported by flash X-rays of the debris. The term "safe" in Table IX means that the second sheet was intact.(leak proof) and no material was detached from the rear surface.

Table IX
OBLIQUE IMPACTS SECOND SHEET DAMAGE
3.18 mm Al Spheres -- 5.08 cm Spacing

Angle of Obliquity	Shield Thickness (mm) 1100-0 Al		
	0.64	1.02	1.60
30	Rear Spall	Safe	Safe
45	Perforation	Perforation	Perforation
60	Rear Spall	Perforation	Perforation
1.60 mm 7075-T6 Al Second Sheets, 7.26 to 7.59 km/sec			
30	Rear Spall	–	–
45	Rear Spall	Safe	Safe
60	Safe	Safe	Safe
3.18 mm 7075-T6 Al Second Sheets, 7.50 to 7.65 km/sec			
30	Safe	–	–
45	Safe	–	–
60	–	–	–
6.35 mm 7075-T6 Al Second Sheets, 7.60 to 7.65 km/sec			

Comparison of the total structure ($t_s + t_b/d$) required to prevent failure from high-velocity oblique impacts with the structures required to prevent failure from low-velocity normal impacts show that, for the aluminum-aluminum impacts, the values all fall in the same range ($1.0 \geq t_s + t_b/d \geq 1.5$). It is expected that, as debris heating increases with increasing impact velocity, less fragment damage will be found. This expectation is supported by the results of the cadmium-cadmium impacts partially described in Table X.

Table X
OBLIQUE IMPACTS SECOND SHEET DAMAGE
3.18 mm Cd Spheres – 5.08 cm Spacing

Angle of Obliquity	Shield Thickness (mm) Cd	
	0.48	1.22
30	Rear Spall	Safe
45	Rear Spall	Safe
60	Safe	Safe
3.18 mm 7075-T6 Al Second Sheets 6.13 to 6.43 km/sec		

Because of the low melting temperature of the cadmium these represent "higher velocity" impacts than the aluminum. When the thickness of the rear sheet for the 0.48-millimeter shields was increased to 6.35 millimeters the structure was "safe." Even though the cadmium projectiles are approximately three times the mass of the aluminum projectiles, the damage was due to second-sheet rear surface spall and not fragment impact. Also, the second sheets required to resist the cadmium impacts was no more than for the aluminum impacts.

From these results it is concluded that if a two-sheet structure can resist a low-velocity impact it can resist the fragment damage due to an oblique impact.

With the exception of one test, no cases of blast-loading failure were found in the tests. The one exception was a very thin backup sheet with the impact at 30^{o}. Even in this case the second sheet was perforated in several places (see Figure 74). Momentum transfer experiments were performed with aluminum-aluminum impacts as described previously. The results of these are shown in Table XI.

Table XI
3.18 mm Al SPHERES IMPACTING AT 7.6 km/sec, 5.08 cm SPACING, MAXIMUM MEASURED MOMENTUM INTENSITY

t_s/d	Angle of Impact 0^{o}	30^{o}	45^{o}	60^{o}
0.2	10,000	–	3,000	700
0.5	2,100	1,000	1,000	1000 gm cm/sec cm^2

3.18mm Al SPHERE
7.47 km/sec 30° FROM NORMAL
1.60mm 1100-0 Al SHIELD
5.08 cm SPACING
0.64mm 7075-T6 Al BACKUP

Figure 74 Perforation of Very Thin Backup Sheet

The maximum momentum intensity measured for the oblique impacts is less in both cases than for comparable normal impacts. This is expected, as the debris must travel a greater distance from the shield to the second sheet as the angle is increased. Also, as the angle is increased the amount of projectile debris which passes through the shield decreases. From the momentum intensity measurements it may be concluded that the debris which strikes the second sheet is widely dispersed in spray angle. The gross-deformation tensile failure mode is more strongly influenced by momentum intensity than total momentum. Therefore, it is concluded that any structure which can resist the gross-deformation tensile failure for a normal impact will not fail through this mechanism for an oblique impact.

NON-OPTIMUM SHIELDS

Both Maiden and McMillan[6] and Sandorff[7] designated what was termed an optimum shield. This was defined as a shield that produced a debris cloud in a particular form. The combination of the hydrodynamic CAMEO calculations coupled with the gross-deformation failure analysis and the spall calculations show that an optimum shield is rather hard to define. On the basis of the analysis and the experiments it is easily seen that if the shield is too thin a severe weight penalty is imposed. However, there is a very wide range of minimum-weight structures available (see Figure 49) where the weight can be split between the shield and backup. Because of the rapid increase in backup thickness required to prevent fracture when the t_s/d ratio becomes small, and the severe slope of the strain versus thickness for large strains, it seems advisable to keep the t_s/d ratio as large as possible and to design the backup thickness to accept low maximum strain. As was seen previously, the overriding factor in determining the spall or gross-deformation failure is the intersheet spacing and the fact that the failure thicknesses are proportional to the reciprocal of the spacing squared.

It is very likely that meteoroid impacts will occur for which the shield thickness is much greater than that shown in Figure 49, i.e., t_s/d is greater than one. Impacts of this type will result in debris clouds with fragments.

The greater-than-optimum shield situation was experimentally investigated using 3.2mm aluminum projectiles, 5.08cm spacing, a velocity of 7.5 km/sec, and various-thickness shields and backups of 7075-T6 aluminum. The damage inflicted upon 1.6mm-thick backup targets in these tests is shown in Figures 75 and 76. The results of all the tests can be conveniently summarized in the solid-line construction of Figure 77. Straight lines have been drawn between known points A, B, and C, where t_A (thickness at point A) corresponds to the thickness of the rear sheet necessary to prevent spall detachment with no shield; t_B (thickness at point B) is the total thickness of the structure to give 4% maximum strain (from Figure 35) at optimum shield thickness of $t_s/d = 0.15$; and $t_C = t_A$ is the thickness of shield necessary to prevent spall detachment and thus require no backup sheet. The experimental results indicate that, for design purposes, if the structure is designed above ABC then no perforation of the rear sheet will occur. Note that, at a given velocity, thickness $t_A = t_C$ scales approximately as particle diameter d , whereas t_B scales ad d^3.

TWO-SHEET SCALING

The results of the analysis and experiments indicate that shield thicknesses scale with projectile diameter and backup thicknesses scale with projectile mass or diameter cubed. The total structure would then scale as between the diameter to the first and third power. It is generally agreed that the failure thickness of a single-sheet structure is proportional to the projectile diameter.[8, 9, 10] These two statements would indicate that if the projectile mass were very large a single-sheet structure would be better than a two-sheet structure. However the two-sheet results are qualified as applying only to structures in which the spacing is greater than eight projectile diameters. With this restriction two sheets are better than one. For spacings less than this the projectile-shield debris is still quite dense and results, upon impact on the second sheet, in cratering of the second sheet. The analysis utilized herein does not apply to this case, but it is reasoned that a two-sheet structure is always better than one because any high-velocity impact upon a shield results in the spread of the projectile-shield debris, the loss of energy and, at most, a slight increase in the total momentum. The impact of the second sheet is then less severe than if there were no shield because the energy per unit area and momentum per unit area are less.

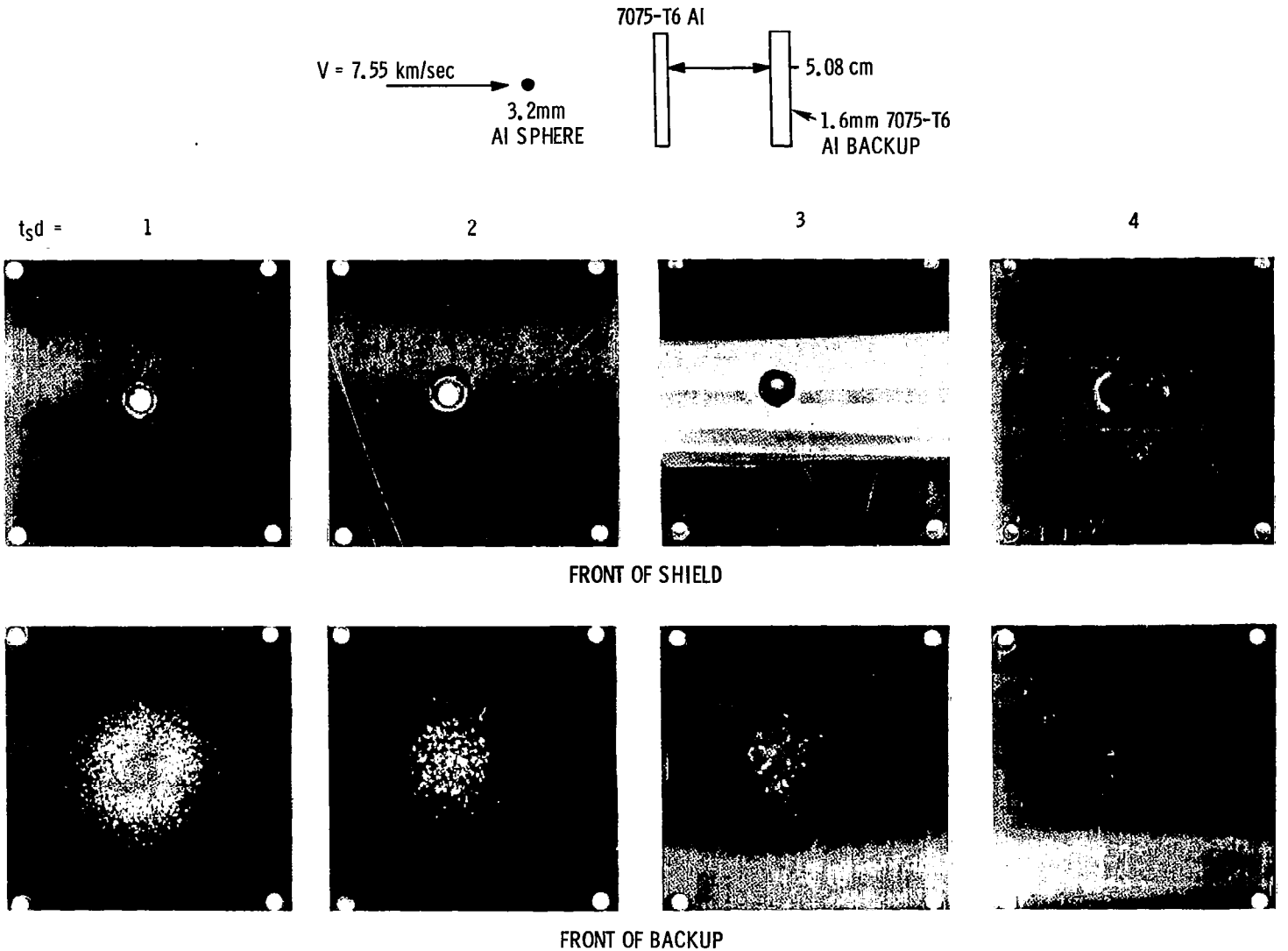

Figure 75 Targets Having Greater Than Optimum Shields (Front)

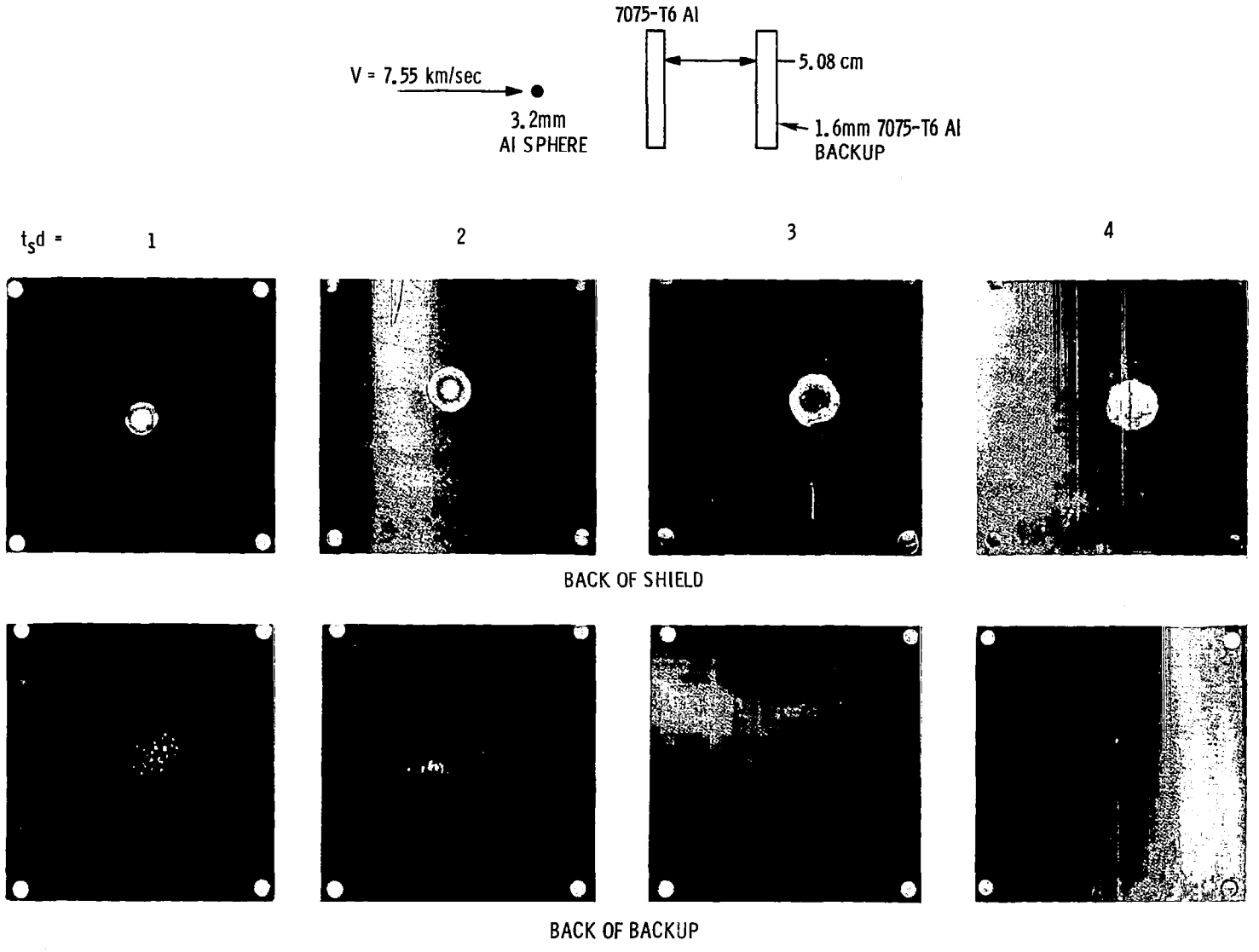

Figure 76 Targets Having Greater Than Optimum Shields (Rear)

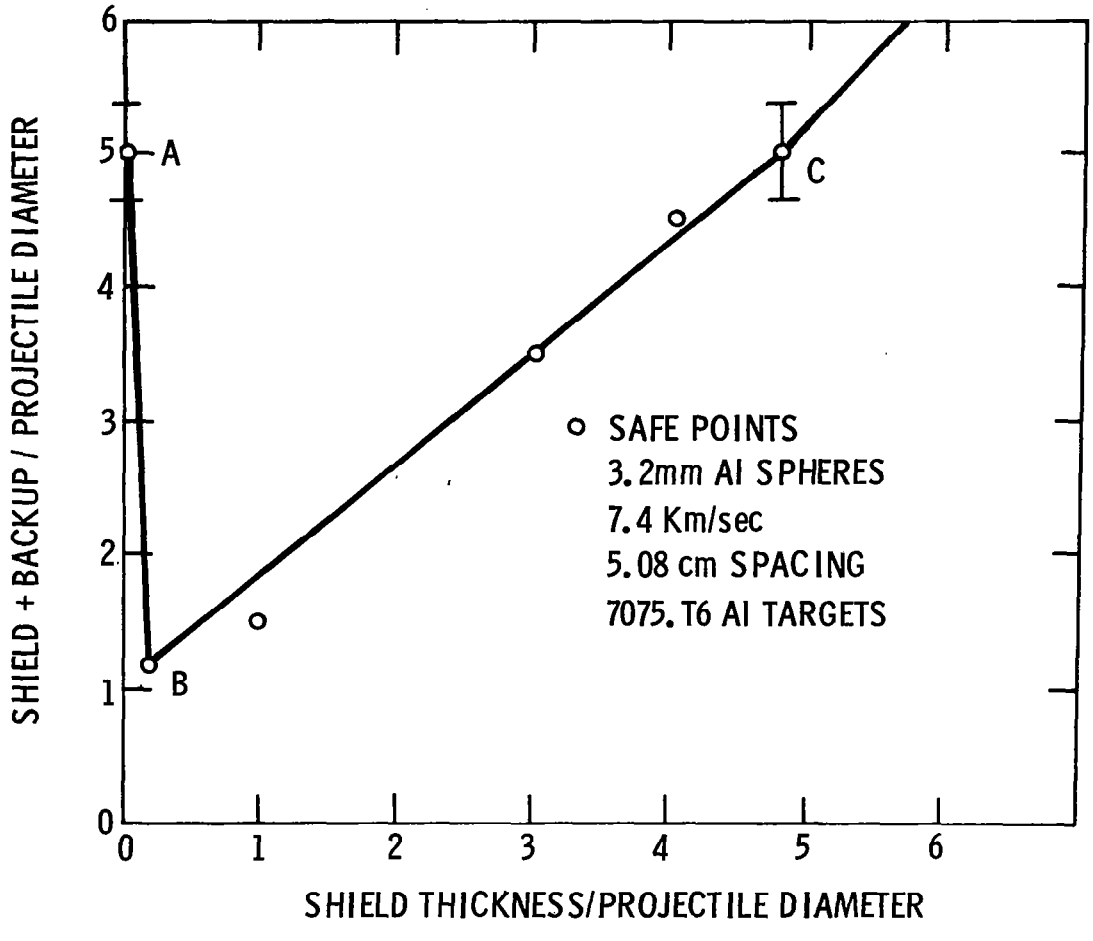

Figure 77 Safe Thickness vs Shield Thickness

This same reasoning also applies to velocity scaling; thus it is concluded that two sheets are always better than one.

EVALUATION OF TWO-SHEET STRUCTURES

The impact resistance of two sheet structures can be evaluated utilizing the information given previously. The basic two-sheet structure must be evaluated to cover the probable impact conditions. Evaluations of three structures have been performed and are presented as examples of the method.

The three structures are the Apollo Service Module Block 1 and 2 and the Lunar Excursion Module. The Service Module structure consists of two thin aluminum sheets 0.405 millimeter thick spaced 2.54 centimeters apart. The Block 1 structure has a honeycomb between the two sheets with a cell size of 6.35 millimeters and a wall thickness of 0.0254 millimeter. The Block 2 structure has a honeycomb with a 4.75-millimeter cell size and a wall thickness of 0.0178 millimeter. The Lunar Excursion Module structure consists of a 0.102-millimeter aluminum sheet spaced 5.08 centimeters from a 0.635-millimeter aluminum second sheet. All three structures were assumed to consist of 7075-T6 aluminum.

The structures are evaluated on the basis of their vulnerability to solid aluminum impacts. This is conservative, as an underdense material would cause less damage. By using Equation (6) the critical masses can be determined for impacts at 30 kilometers per second. These masses are 2.64×10^{-3} grams for the Service Module (the honeycomb has initially been ignored) and 2.1×10^{-3} grams for the Lunar Excursion Module.

Next the critical masses are determined for the honeycomb by scaling the uniform plate gross-deformation results given in Figures 34 and 35. The critical mass for the Block 1 Service Module structure is 1.78×10^{-4} grams, and is 10^{-4} grams for the Block 2 structure.

Finally the low-velocity impact critical masses are determined from the results given in Table VIII. Here the honeycomb can be ignored, as the particle does not break up upon impact. The critical masses are 3.4×10^{-4} grams for the

Service Module structure and 2.54×10^{-4} grams for the Lunar Excursion Module structure.

These critical masses can then be employed to determine fluxes and probabilities of no failure from the NASA environment.[2] For a probability of no failure of 0.99 the Service Module Block 1 structure has an area-time of exposure of 91,500 feet^2-days ignoring the honeycomb, 2,510 feet^2-days for all impacts normal and in the center of the honeycomb cell, and 5,900 feet^2-days for the low velocity impact. For the Block 2 structure the area-times are the same as for the Block 1 structure except for the honeycomb, which is 1,160 feet^2-days.

For the Lunar Excursion Module structure the area-times are 66,200 feet^2-days for normal impacts at 30 kilometers per second and 2,050 feet^2-days for low-velocity impacts. The low-velocity evaluation also provides for oblique impact fragment damage.

The exposure times given should be taken as lower bounds as all considerations have been conservative. The honeycomb analysis considers only the worst case, low-velocity (2.5 kilometers per second) impacts seem unlikely, and oblique impact fragment damage is not expected to be a problem for high-velocity impacts. The true exposure times would therefore be expected to tend toward the higher values.

CONCLUSIONS

The results of this combined theoretical-experimental investigation of thin-sheet impact can be summarized as follows:

1. High-velocity meteoroid impacts normal to the surface of two-sheet structures will cause failure of the entire structure, primarily through gross-deformation tensile failure of the second sheet.

2. For reasonably large intersheet spacings, spall of the rear surface of the second sheet is not expected because of the low density of the debris that strikes it.

3. On an equal-weight basis, two sheets provide more protection than n sheets for the same total spacing.

4. Honeycomb structure between the sheets of a two-sheet structure can cause channeling of the projectile-shield debris, and in no case is a honeycomb expected to increase the impact resistance of a two-sheet structure.

5. Impacts of underdense projectiles are expected to be less severe to two-sheet structures than normal-density projectiles because of greater dispersion of the projectile-shield debris.

6. Oblique impacts will produce fragment damage no worse than the worst low-velocity impact. A structure that will resist gross-deformation tensile failure from a normal impact will not suffer gross-deformation tensile failure from the same impact at an angle of obliquity.

REFERENCES

1. Maiden, C.J., "Meteoroid Impact," Space Exploration, McGraw-Hill Book Company, Inc., New York, 1964, pp. 236–284
2. Burbank, P.B., Cour-Palais, B.G. and McAllum, W.E., "A Meteoroid Environment for Near-Earth, Cislunar, and Near-Lunar Operations," NASA TN D-2747, Apr 1965
3. Dohnanyi, J.S., "Model Distribution of Photographic Meteors," Bellcomm, Inc., Report TR63-340-1, Mar 1966
4. Clough, N. and Lieblein, S., "Significance of Photographic Meteor Data in the Design of Meteoroid Protection for Large Space Vehicles," NASA TN D-2958, Aug 1965
5. Naumann, R., "Pegasus Satellite Measurements of Meteoroid Penetration (Feb 16–Jul 20, 1965)," NASA TMX-1192, Dec 1965
6. Maiden, C.J. and McMillan, A.R., "An Investigation of the Protection Afforded a Spacecraft by a Thin Shield," AIAA J., Vol. 2, No. 11, 1964, pp. 1992–1998
7. Sandorff, P., "A Meteoroid Bumper Design Criterion," Sixth Symposium on Hypervelocity Impact, AD-423-063, Aug 1963, Vol. III, pp. 41–67
8. Bjork, R.L., "Review of Physical Processes in Hypervelocity Impact and Penetration," Sixth Symposium on Hypervelocity Impact, AD-423-063, Vol. II, pp. 1–58, Aug 1963
9. Riney, T.D. and Heyda, J.F., "Hypervelocity Impact Calucations," Seventh Symposium on Hypervelocity Impact, AD-463-228, Vol. II, pp. 77–186, Feb 1965
10. Walsh, J.M. and Johnson, W.E., "On the Theory of Hypervelocity Impact," Seventh Symposium on Hypervelocity Impact, AD-463-228, Vol. II, pp. 1–76, Feb 1965
11. Wagner, M.H., Brooks, N.B. and Bjork, R.L., "Impact of a Porous Aluminum Projectile on Aluminum at 20 and 72 km/sec," Seventh Symposium on Hypervelocity Impact, AD-463-229, Vol. III, pp. 1–54, Feb 1965
12. Witmer, E.A., Balmer, H.A., Leech, J.W. and Pian, T.H.H., "Large Dynamic Deformation of Beams, Rings, Plates and Shells," AIAA J., Vol. 1, No. 8, pp. 1848, 1963
13. Summers, J.L., and Nysmith, C.R., "The Resistance of a Variety of Composite Space Structures to Hypervelocity Impact," Proceedings of the Fifth Structures and Materials Conference, Palm Springs, California, Sponsored by the AIAA, pp. 386–393, Apr 1964
14. Kreyenhagen, K.N., Bjorke, R.C., and Brooks, N.B., "Numerical Solution of Oblique Impacts," Seventh Symposium on Hypervelocity Impact," AD-463-229, Vol. III, pp. 55–74, Feb 1965

APPENDIX A
COMPUTER CODES USED FOR PREDICTING LARGE PLASTIC DEFORMATIONS OF STRUCTURES

In recent years, many investigators[1—4] have attempted to determine responses of various structural elements to blast or impulsive loadings. Symonds,[5] for example, has developed a "rigid-plastic" theory of deformation in which it is assumed that no elastic deformation takes place, so that all the energy imparted to the system is channeled into plastic deformation of the structure. This type of analysis has two major disadvantages:

1) The energy input to the system must be much greater than the elastic strain-energy that can be stored by the structure.
2) Only permanent deformations are obtained; i. e., no time-history of the response can be found.

The most recent technique which is not subject to these limitations was developed by Witmer, et al,[6] at the M.I.T. Aeroelastic and Structures Research Laboratory. This technique as applied to beams and plates is described briefly.

THEORY

The dynamic equilibrium equations for the structural element shown in Figure A-1 can be written

$$\begin{aligned} &\frac{\partial}{\partial s}(N\cos\theta) - \frac{\partial}{\partial s}(Q\sin\theta) + F_y - m\ddot{v} = 0 \\ &\frac{\partial}{\partial s}(N\sin\theta) + \frac{\partial}{\partial s}(Q\cos\theta) + F_z - m\ddot{w} = 0 \\ &\frac{\partial M}{\partial s} - Q = 0 \end{aligned} \qquad \text{(A-1)}$$

where m = mass per unit length of structure

θ = slope of structural element

N, Q, M = normal force, shear force, and bending moment at a given cross section

$\ddot{v}, \ddot{w}$ = accelerations in the horizontal and vertical directions

F_y, F_z = forces per unit area in the horizontal and vertical directions

In the derivation of Eqs. (A-1), the effects of shear deformation and rotatory inertia have been neglected. In the case of impulsive loading, F_y and F_z are zero, and the beam is considered to have an initial velocity. Similar equations are written for the plate.

Equation (A-1) may be phrased in finite difference form and interpreted as describing a lumped-parameter model consisting of masses connected by weightless, straight links. (These equations, as well as a complete description of the model, can be found in Reference 6.)

The beam is of rectangular cross section, and the cross-sectional area is distributed among six "flanges," as shown in Figure A-2. The mass is distributed among 62 mass points. The plate similarly has 41 mass points (see Figure A-3) and is six "flanges" thick.

Equations (A-1) and the corresponding strain-displacement equations for both the plate and beam have been programed for an IBM 7044 digital computer using Fortran IV language.[7, 8] The program describes the motion of the structure and the resulting strains in the six flanges as a function of time. This allows determination of the amount of strain, their location, and the time of occurence.

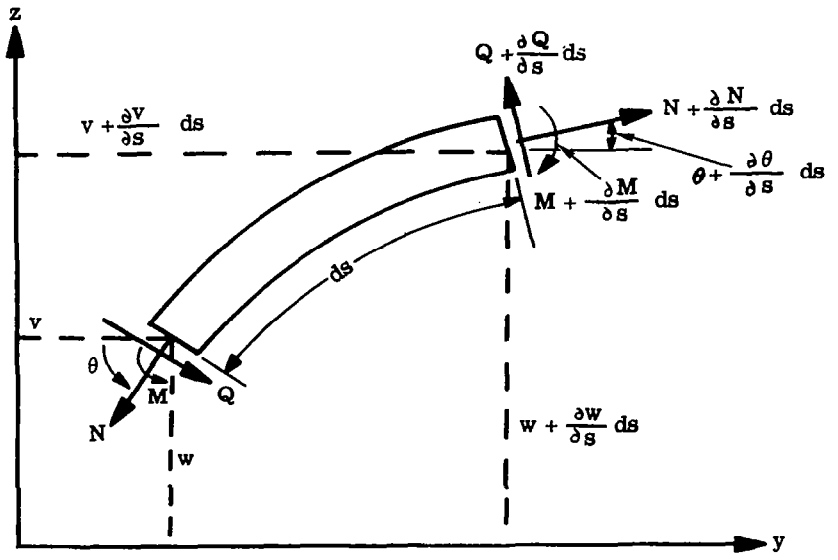

Figure A-1 Coordinate System and Internal Forces

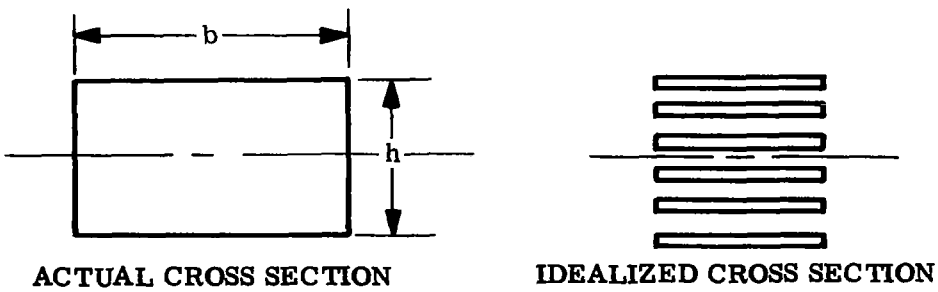

Figure A-2 Idealized Thickness Model

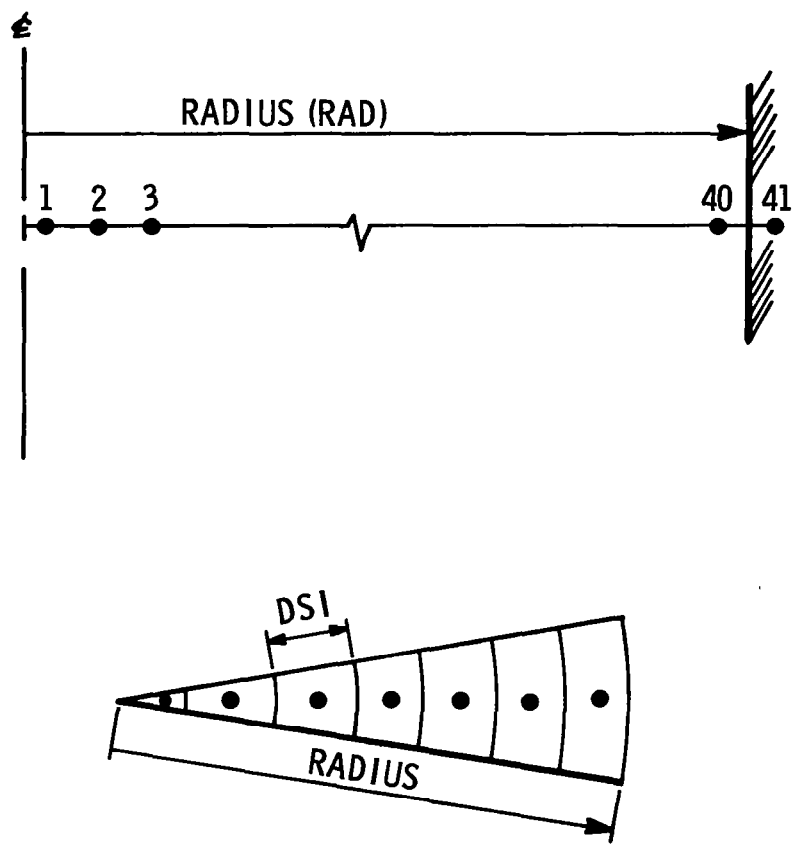

Figure A-3 Plate Idealization

REFERENCES FOR APPENDIX A

1. H.H. Bleich and M.G. Salvadori, "Impulsive Motion of Elasto-Plastic Beams," Transactions of the American Society of Civil Engineers, Sep 1953

2. M.M. Chen, P.T. Hsu, and T.H.H. Pian, "Impulsive Loading of Rigid-Plastic Curved Beams," Fourth U.S. National Congress of Applied Mechanics, 1962

3. M.F. Conroy, "The Plastic Deformation of Built-In Beams Due to Distributed Dynamic Loading" (paper presented at the Summer Conference of Applied Mechanics Division, American Society of Mechanical Engineers, June 9—11, 1964, Boulder, Colorado)

4. P.E. Duwez, D.S. Clark, and H.F. Bohnonblust, "The Behavior of Long Beams Under Impact Loading," J. Appl. Mech., Mar 1950

5. E.H. Lee, and O.S. Symonds, "Large Plastic Deformations of Beams Under Transverse Impact," J. Appl. Mech. Vol. 19, 1952

6. E.A. Witmer, H.A. Balmer, J.W. Leech, and T.H.H. Pian, "Large Dynamic Deformations of Beams, Circular Rings, Circular Plates, and Shells," AIAA J. Vol. 1, No. 8, 1963, p. 1848

7. R.E. Sennett and D.E. Skaar, "Structures I — The Response of Beams and Rings to High Intensity, Short-Duration Loading," GM Defense Research Laboratories, TR65-08, Feb 1965

8. R.E. Sennett, and D.E. Skaar, "Structures II — The Response of a Clamped Circular Plate to Impulsive Loads," GM Defense Research Laboratories, TR66-63, Oct 1966

APPENDIX B

TWO-DIMENSIONAL LAGRANGIAN CODE FOR ELASTIC-PLASTIC MEDIA

INTRODUCTION

The problem set up here is the solution, by finite difference methods, of wave propagation in compressible media in two space dimensions, of either rectangular or cylindrical geometry. Lagrangian grid representation is used. For this system the motion of the medium is described with reference to a mesh attached to the material. This results in a limitation of the method; serious difficulties arise when physical situations involve severe distortions of the original mesh.

The program, as described here, can be used with either a fluid or elastic perfectly plastic solid. Either the Mie-Gruneisen or the Tillotson[1] equation of state can be used for describing the hydrodynamic component of the stress. Other equations of state may be incorporated, as well as equations of state to describe the behavior of other media such as, for example, explosives.

Several two-dimensional time-dependent Lagrangian codes have been developed: TENSR,[2] HEMP,[3] PIPE,[4] RAVE I,[5] etc. The method used here follows that formulated earlier by Wilkins (HEMP)[3] and Herrmann (RAVE I).[5] The equations and the finite difference deviations are given in the following pages.

EQUATIONS OF MOTION

The governing equations of motion in their Lagrangian form are as follows:

(1) Conservation of Mass.

$$\dot{\rho} + \rho (\dot{e}^{xx} + \dot{e}^{yy} + \dot{e}^{zz}) = 0$$

where ρ is the medium density, e^{ij} the strain, and the dot indicates a time derivative. With the present nomenclature, x , y , z can either be rectangular

coordinates or a cylindrical coordinate system . The cylindrical coordinate system is used for the axial symmetric problem, in which case x denotes the radial coordinate and z the axial coordinate.

The strain rates are defined as follows:

$$\dot{e}^{ij} = 1/2\left(\frac{\partial u^i}{\partial x^j} + \frac{\partial u^j}{\partial x^i}\right)$$

where u^i indicates particle velocity in direction i , e.g.

$$u^x = \partial x/\partial t$$

and

$$\left[\frac{\partial u^i}{\partial x^j}\right] = \begin{bmatrix} \frac{\partial u^x}{\partial x} & 0 & \frac{\partial u^x}{\partial z} \\ 0 & (\alpha-1)\frac{u^x}{x} & 0 \\ \frac{\partial u^z}{\partial x} & 0 & \frac{\partial u^z}{\partial x} \end{bmatrix}$$

Here α is a coefficient which takes on a value of unity for motion in the x-z plane and 2 for axial symmetric motion.

(ii) Conservation of Momentum

$$\rho a^x = \frac{\partial t^{xx}}{\partial x} + \frac{\partial t^{xz}}{\partial z} + (\alpha-1)\frac{t^{xx} - t^{yy}}{x}$$

$$\rho a^z = \frac{\partial t^{xz}}{\partial x} + \frac{\partial t^{zz}}{\partial z} + (\alpha-1)\frac{t^{xz}}{x}$$

where a^i is the acceleration in direction i , and b^{ij} are the stress components.

(iii) Conservation of Energy

$$\rho \dot{e} = p \frac{\dot{\rho}}{\rho} + \rho^{\alpha} \dot{e}$$

where

$$p = -1/3 \, (t^{xx} + t^{yy} + t^{zz})$$

$$\rho \dot{e} = 2 d_t^{rr} d_{\dot{e}}^{rr} + 2 d_t^{rz} d_{\dot{e}}^{rz} + 2 d_t^{zz} d_{\dot{e}}^{zz} + d_t^{rr} d_{\dot{e}}^{zz} + d_t^{zz} d_{\dot{e}}^{rr}$$

$$d_t^{ij} = t^{ij} + p$$

$$d_{\dot{e}}^{ij} = \dot{e}^{ij} + 1/3 \frac{\dot{\rho}}{\rho} \partial^{ij}$$

$$\partial^{ij} = \begin{cases} 1 & \text{for} \quad i = j \\ 0 & \text{for} \quad i \neq j \end{cases}$$

so that

$$d_t^{xx} + d_t^{yy} + d_t^{zz} = 0$$

$$d_{\dot{e}}^{xx} + d_{\dot{e}}^{yy} + d_{\dot{e}}^{zz} = 0$$

Since during a given time step an element of the body rotates, it is necessary to correct the stress so as to refer to the fixed coordinate system. The objective stress rates are defined by

$$\overset{\nabla}{t}{}^{xx} = \dot{t}^{xx} - 2 w_{xz} t^{xz}$$

$$\overset{\nabla}{t}{}^{xz} = \dot{t}^{xz} + w_{xz} (t^{xz} - t^{zz})$$

$$\overset{\nabla}{t}{}^{zz} = \dot{t}^{zz} + 2 w_{xz} t^{xz}$$

where

$$w_{xz} = 1/2\left(\frac{\partial u^x}{\partial z} - \frac{\partial u^z}{\partial x}\right)$$

The above equations together with an equation of state are the required equations for solution of wave propagation problems. Three different equations of state are considered in the text for fluid and elastic plastic media.

For given initial and boundary conditions specific problems can be solved within the limit of the Lagrangian code described.

REFERENCES

1. J. H. Tillotson, "Metallic Equations of State for Hypervelocity Impact," General Atomic Report GA-3216, July 18, 1962

2. G. Maenchen and S. Sack, "The Tensor Code," University of California, Lawrence Radiation Laboratory, UCRL-7316, April 9, 1963.

3. M. L. Wilkins, "Calculation of Elastic-Plastic Flow," University of California, Lawrence Radiation Laboratory, UCRL-7322, April 19, 1963

4. C. S. Godfrey, D. J. Andrews, E. T. Trigg and M. Wilkins, "Prediction Calculations for Free Field Ground Motion," Air Force Weapons Laboratory Technical Documentary Report No. WL-TDR-64-27, May 1964

5. W. Herrmann and M. O'Brien, "RAVE I," Aeroelastic and Structures Research Laboratory, (Massachusetts Institute of Technology) Report No. 1021, June 1964

APPENDIX C
DATA SHEETS

SHOT NO.	PROJECTILE MATERIAL	DIAMETER (mm)	SHIELD MATERIAL	THICKNESS (mm)	SPACING (cm)	BACKUP MATERIAL	THICKNESS (mm)	VELOCITY (km/sec)	TOTAL PENETRATION (mm)	HOLE SIZE (mm)	SPRAY DIAMETER (mm)	SPRAY ANGLE	MV/mv	REMARKS
D-878	2017	3.18	1100-0	0.534	5.08	7075-76	3.18	7.68	0.96	6.1	102	90		
	AL		AL			AL								
879							1.60	7.81	HOLE	—	94	86		PISTON HIT
880							0.813	8.08	HOLE	6.1	89	82.5		
901				0.635			12.7	—	—	—	—	—		NO IMPACT
902								7.46	.89	6.6	94	86		
903								7.29	.92	6.6	97	87.5		
904								7.60	.89	6.6	94	86	1.27	
905				1.02				7.80	1.07	9.2	89	82.5		
909								7.50	1.17	8.6	89	82.5	1.34	
910								2.78	2.02	6.1	51	53.5	1.08	
911								5.43	1.48	7.2	84	79		
912							6.35	4.76	1.76	7.4	79	76	1.31	
913				0.635				4.72	1.96	5.8	81	77	1.25	
914				0.305				4.82	2.49	4.6	86	80.5	1.32	
915				1.60				4.72	1.81	8.6	94	86	1.42	
916				0.305				2.91	2.90	4.1	56	58		
917				1.60				2.85	2.06	6.9	41	44	1.07	
918				0.635				3.78	2.32	5.8	76	74		SHEAR DISK HIT
919								6.28	1.32	6.1	97	87.5		
920				0.305				6.89	1.58	4.8	102	90		
921				1.60				5.18	1.83	9.2	74	72		
947				0.305				2.91	3.03	4.1	51	53.5		
948								7.56	.78	—	97	87.5		
949				1.60				—	—	—	—	—		NO IMPACT
950				0.635				3.99	3.31	6.1	89	82.5		
951								6.40	1.35	—	97	87.5		PISTON HIT
952				0.305				3.14	—	—	76	74		SHEAR DISK HIT

SHOT NO.	PROJECTILE MATERIAL	DIAMETER (mm)	SHIELD MATERIAL	THICKNESS (mm)	SPACING (cm)	BACKUP MATERIAL	THICKNESS (mm)	VELOCITY (km/sec)	TOTAL PENETRATION (mm)	HOLE SIZE (mm)	SPRAY DIAMETER (mm)	SPRAY ANGLE	MV/mv	REMARKS
D-972	2017 AL	1.60	1100-0 AL	0.305	5.08	7075-T6 AL	0.813	7.89	0.33	3.3	99	88.5		
973							0.407	7.78	.79	3.6	97	87.5		BACKUP BENT
974							1.60	7.78	.31	—	102	90		PISTON HIT
975							0.407	7.87	.36	3.6	89	82.5		
976		3.18		0.635			6.35	4.57	2.28	6.4	84	79		
977								6.61	1.35	7.1	102	90	1.29	
978				0.305				7.56	.71	—	97	87.5		PISTON HIT
979				1.60				7.56	1.64	10.9	89	82.5	1.49	
980				0.305				7.65	.89	5.3	97	87.5	1.31	
992								3.00	3.15	4.3	84	79	1.22	
993				0.635				3.87	2.32	5.8	74	72	1.29	
994	PYREX							3.63	1.14	5.8	89	82.5		
995								6.58	1.02	6.4	97	87.5	1.36	
996	2017 AL			1.02	1.27			6.96	2.26	8.4	25	27.5	1.30	
997				0.635	5.08			3.76	1.81	5.6	76	74		
998	Cd		Cd	0.330			12.7	2.94	—	4.6	99	88.5		SHEAR DISK HIT
999								5.34	.49	5.6	99	88.5		
1000								—	—	—	—	—		NO IMPACT
1012	1100-0 AL	4.12 x 4.14 CYLINDER	1100-0 AL	0.635				4.97	2.85	7.6	109	90.5		
1013								7.22	3.38	8.1	109	90.5	1.51	
1014								5.47	2.09	7.9	109	90.5		
1018	Cd	3.18	Cd	0.330				—	—	—	—	—		NO IMPACT
1019								5.61	.46	5.3	89	82.5	1.34	
1020								—	—	—	—	—		NO IMPACT
1021								—	—	—	—	—		NO IMPACT
1022								—	—	—	—	—		NO IMPACT

SHOT NO.	PROJECTILE MATERIAL	DIAMETER (mm)	SHIELD MATERIAL	THICKNESS (mm)	SPACING (cm)	BACKUP MATERIAL	THICKNESS (mm)	VELOCITY (km/sec)	TOTAL PENETRATION (mm)	HOLE SIZE (mm)	SPRAY DIAMETER (mm)	SPRAY ANGLE	MV/mv	REMARKS
						7075-T6			BACKUP					
D-1872	Cd	3.18	Cd	1.22	5.08	Al	1.02	6.95	BENT	11.4	98	88		
								ESTIMATED						
1873				0.64			2.04	6.90		7.70	94	86		
1874							1.78	7.01		7.80	88	82		
1875				0.33			12.7	6.89	0.48	5.43	80	76		
1876				1.22				6.58	1.32	11.1	96	87		
1877		2.57		0.48				6.83	0.48	6.07	108	93		
								ESTIMATED						
1878								6.90	0.48	6.00	105	92		
								ESTIMATED	BACKUP					
1879							1.27	6.50	BENT	5.95	94	86		
1880							0.81	6.86		5.89	92	84		
1881		3.18		1.22				6.70		11.3	104	91		
1882				0.33			1.27	6.40	0.64	5.38	80	76		
1883				1.22				7.01	1.27	11.3	97	87	1.35	
1884				0.48				7.01	0.48	6.75	78	75	1.39	
1885		2.57						7.10	0.48	5.92	95	86		
1886							0.64	6.74	BACKUP	5.92	95	86		
									BENT					
1887		3.18		1.22				6.98	BACKUP	11.3	97	87		
									FRACTURED					
1888							12.7	6.89	1.22	11.4	100	89	1.52	
1889				0.33				6.83	0.33	5.61	85	80	1.42	
1890		2.57		0.48				6.89	0.48	6.07	95	86	1.39	
1891								4.91	0.58	5.61	85	80	1.31	
									BACKUP					
1892							0.46	6.50	FRACTURED	5.95	94	86		
									BACKUP					
1893					12.2		0.38	6.89	BENT	6.04	190	86		
1894		3.18		0.64			0.81	6.77		7.31	>180	>82		
1895							0.64	7.04		7.05	>160	>76		
1896					5.08		1.27	6.95		7.72	93	85		
1897							1.02	6.89		7.59	97	87		
									BACKUP					
1898							0.38	6.77	FRACTURED	7.50	94	86		

SHOT NO.	PROJECTILE MATERIAL	DIAMETER (mm)	SHIELD MATERIAL	THICKNESS (mm)	SPACING (cm)	BACKUP MATERIAL	THICKNESS (mm)	VELOCITY (km/sec)	TOTAL PENETRATION (mm)	HOLE SIZE (mm)	SPRAY DIAMETER (mm)	SPRAY ANGLE	MV/mv	REMARKS
D-1044	Cd	3.18	Cd	0.635	5.08	7075-T6	12.7	5.48	0.66	7.6	97	87°		
1045								6.40	.69	7.6	99	89	1.42	
1046								3.18	.86	7.0	91	83	1.21	
1047							6.35	6.49	.76	7.6	97	87		
1048		4.0		.762				3.44	.81	7.9	127	103		
1049		3.18		.635				6.46	.71	—	99	86		PISTON HIT
1050	Ti	2.62	1100-0	1.02				—	—	—	—	—		NO IMPACT
1051	Cu	2.08						4.17	3.30	5.1	86	81		
1052	Ti	2.62						3.49	2.92	5.1	76	74		
1053								7.25	2.03	—	89	83		PISTON HIT
1054	Cu	2.08						7.10	2.06	6.4	83	79		
1055	Al	3.05						7.16	1.04	9.4	93	86		
1056								3.62	1.40	7.1	66	66		
C-722		3.18		.635				7.93	.71	4.8	95	86		
723							4.75	7.41	.89	4.8	—	—		
725				1.02			.813	7.02	—	—	—	—		PISTON HIT
726								5.43	∞	7.9	—	—		
D-1114	NYLON	4.19					6.35	2.92	1.19	7.9	53	56		
1115								6.10	1.17	9.7	102	90		
1116								6.80	1.27	10.9	108	94		
1117	Al	3.18		.635			12.7	3.26	2.49	5.1	56	58		
1118								3.11	2.90	5.1	56	58		
1119								3.29	1.57	5.1	61	62		
1120								3.38	2.16	5.1	61	62		
1121								5.61	1.73	6.4	86	81		
1122								5.64	1.73	6.4	84	79		
1123								5.61	1.65	6.4	85	80		

SHOT NO.	PROJECTILE MATERIAL	DIAMETER (mm)	SHIELD MATERIAL	THICKNESS (mm)	SPACING (cm)	BACKUP MATERIAL	THICKNESS (mm)	VELOCITY (km/sec)	TOTAL PENETRATION (mm)	HOLE SIZE (mm)	SPRAY DIAMETER (mm)	SPRAY ANGLE	MV/mv	REMARKS
D-1124	Al	3.18	1100-0	0.635	5.08	7075-T6	12.7	5.78	0.81	—	81	77°		PISTON HIT
1125								7.50	.84	6.6	76	74		
1126								—	—	—	—	—		NO IMPACT
1127								7.32	1.02	—	89	83		PISTON HIT
1128								7.29	.74	6.6	89	83		

SHOT NO.	PROJECTILE MATERIAL	DIAMETER (mm)	SHIELD MATERIAL	THICKNESS (mm)	SPACING (cm)	BACKUP MATERIAL	THICKNESS (mm)	VELOCITY (km/sec)	TOTAL PENETRATION (mm)	HOLE SIZE (mm)	SPRAY DIAMETER (mm)	SPRAY ANGLE	MV/mv	REMARKS
						7075-T6								
D-1153	Cd	2.56	Cd	0.635	5.08	Al	1.60	3.84	0.76	6.1	102	90		
1154		3.18		330			12.7	3.69	.69	4.8	89	82		
1155				.635				5.12	.89	5.2	89	82		
1156				.330				3.87	.74	4.8	76	74		
			1100-0											
1157	Al		Al	1.02			6.35	6.89	1.19	8.1	102	90	1.34	
1222	Cd		Cd	.330				3.55	1.04	4.85	86	81		
1223				.635				5.12	.81	7.22	89	82		
			1100-0											
1224	PYREX		Al				6.35	4.92	1.65	5.68	89	82	1.23	
1225	Al			1.02	2.54		12.7	5.88	1.65	7.87	43	81	1.42	
1226			Cd	.330	1.27			6.10	1.09	5.89	36	109	1.40	
1227	Cd				5.08			—	—	—	—	—		NO LAUNCH
1228								—	—	—	—	—		NO LAUNCH
	1100-0	4.12 x 4.14	1100-0											
1229	Al	CYLINDER	Al	635				5.61	2.13	7.97	109	94	1.28	
1230	Cd	3.18	Cd	.330				3.60	.66	4.62	99	89	1.26	
			1100-0											
1231	Al	1.59	Al	.305				4.36	1.04	2.8	61	62		
1232							3.18	6.16	.43	3.2	91	84		PISTON HIT
1233				.152				4.69	1.02	2.5	61	62		
1234								6.59	.89	—	84	79		PISTON HIT
1235				.305				6.50	.46	3.0	99	89	1.18	
1236		3.18		.635			12.7	6.61	1.19	6.50	99	89	1.25	
1237								7.10	1.14	6.63	98	87		SABOT HIT
1238								7.19	.97	6.60	99	89		
1239								7.19	1.14	6.65	98	87	1.32	
1240								—	—	—	—	—		NO LAUNCH
1241								7.38	1.25	6.63	94	86		SABOT HIT
1242								7.26	.89	6.63	94	86		PISTON HIT

SHOT NO.	PROJECTILE MATERIAL	DIAMETER (mm)	SHIELD MATERIAL	THICKNESS (mm)	SPACING (cm)	BACKUP MATERIAL	THICKNESS (mm)	VELOCITY (km/sec)	TOTAL PENETRATION (mm)	HOLE SIZE (mm)	SPRAY DIAMETER (mm)	SPRAY ANGLE	MV/mv	REMARKS
			1100-0			7075-T6								
D-1307	Al	1.59	Al	0.81	5.08	Al	0.40	—	—	—	—	—		NO LAUNCH
1308								—	—	—	—	—		NO LAUNCH
1314		3.18		9.52			6.35	7.59	9.52	14.5	—	—	1.27	
1315				3.18				—	—	—	—	—		NO LAUNCH
1316				12.7				6.88	11.0	16.1	—	—		
1317				3.18				7.47	1.27	14.3	—	—		PISTON HIT
1318	Inlyte	6.35		1.02			12.7	7.26	3.02	11.2	140	108		PISTON HIT
1319	Al	3.18		9.52			1.59	7.38	9.52	14.4	—	—		
1320				3.18				7.41	+	14.5	63	64		PISTON HIT
1321				6.35			6.35	7.50	6.40	15.9	76	74		PISTON HIT
1323							1.59	7.47	+	15.8	76	74		PISTON HIT
1324	Cd		Cd	0.635			12.7	5.38	0.635	7.35	76	74	1.41	
1325								5.70	0.630	7.37	76	74		
1326								5.70	0.762	7.67	76	74		PISTON HIT
1327								5.76	0.630		76	74	1.38	
			7075-T6											
1328	Al		Al	3.18			1.59	7.50	+	11.7	76	74		PISTON HIT
1329				6.35				7.38	+	10.5	—	—		
1330				12.7				7.44	7.02	11.7	—	—		
1331				9.52				7.50	9.52	7.37	—	—		
1332				12.7				7.47	6.83	11.2	—	—		
1333			1100-0 Al	0.635	1.27		12.7	7.47	2.72	6.78	32	102		
1334					2.54			7.47	1.35		54	90		PISTON HIT
1335								7.32	1.55	6.78	76	74		PISTON HIT
1336					1.27			7.29	2.74	6.76	20	83		
1337	50% FOAM Ni	2.62		1.02	5.08		6.35	3.48	3.18	4.93	63	64		
1338	Al	3.18		0.635			9.52	7.53	1.19	6.48	102	98		
1344	50% FOAM Cu	2.62		1.02			12.7	3.29	0.238	4.59	51	53	1.46	

+ BACKUP BENT

SHOT NO.	PROJECTILE MATERIAL	DIAMETER (mm)	SHIELD MATERIAL	THICKNESS (mm)	SPACING (cm)	BACKUP MATERIAL	THICKNESS (mm)	VELOCITY (km/sec)	TOTAL PENETRATION (mm)	HOLE SIZE (mm)	SPRAY DIAMETER (mm)	SPRAY ANGLE	MV/mv	REMARKS
	50%		1100 - 0			7075 -T6								
D-1345	FOAM Cu	2.62	Al	1.02	5.08	Al	12.7	5.15	2.34	5.82	76	74°	1.25	
	50%													
1346	FOAM Ni							5.03	2.49	5.94	76	74	1.35	
1347								6.70	2.18	—	—	—		PISTON HIT
1348	Cu	2.08						7.10	2.01	6.58	—	—		PISTON HIT

SHOT NO.	PROJECTILE MATERIAL	DIAMETER (mm)	SHIELD MATERIAL	THICKNESS (mm)	SPACING (cm)	BACKUP MATERIAL	THICKNESS (mm)	VELOCITY (km/sec)	TOTAL PENETRATION (mm)	HOLE SIZE (mm)	SPRAY DIAMETER (mm)	SPRAY ANGLE	MV/mv	REMARKS
			1100-0			7075-T6								
D-1349	NYLON	4.19	Al	1.02	5.08	Al	12.7	6.31	1.32	9.38	98	87°	1.55	
1350	Al	3.18			2.54			7.38	1.63	8.64	36	70		
1351					1.27			7.47	2.67	8.34	20	77	1.33	
1352				0.635				7.07	2.54	6.60	19	72	1.35	
			7075-T6											
1353			Al	19.6				7.56	6.53	11.7				
1366				15.7				7.53	6.45	13.7				
1367				6.35	5.08		3.18	—	—	—	—	—		NO LAUNCH
1368								7.65	6.78	10.8				
			1100-0											
1369	Cu	2.08	Al	1.02			12.7	—	—	—	—	—		NO LAUNCH
1371	NYLON	4.19						7.13	1.30	9.65	114	96	1.51	
1384	Al	3.18		.635			0.635	7.77	—	—	—	—		PISTON HIT
1385				1.02			12.7	—	—	—	—	—		NO LAUNCH
1386				.635				7.43	—	—	—	—		PISTON HIT
1387							0.635	—	—	—	—	—		NO LAUNCH
1388							12.7	—	—	—	—	—		NO LAUNCH
1389								5.18	2.77	6.20	102	90	1.33	
1390						1100-0 Al		7.68	1.12	6.79	102	90		PISTON HIT
						7075-T6								
1391	INLYTE	4.90				Al	6.35	4.69	1.12	7.32	112	95	1.20	
1392								7.89	1.70	7.80	—	—		PISTON HIT
1393				.305				4.68	0.74	6.04	89	82	1.25	
1394				.635				7.91	1.60	7.90	142	109	1.24	
1395				.305				—	—	—	—	—		NO LAUNCH
						1100-0								
1396	Al	3.18		.635		Al	12.7	7.56	1.30	6.76	114	96	1.24	
						7075-T6								
1397				1.59		Al		7.62	2.13	10.9	89	82	1.50	
1398								5.21	2.34	9.37	71	70	1.41	
1399	INLYTE	4.90		305			6.35	7.86	—	—	—	—		PISTON HIT
1400	Al	3.18		.635			0.635	7.49	PERFORATION	6.71	102	90		

SHOT NO.	PROJECTILE MATERIAL	DIAMETER (mm)	SHIELD MATERIAL	THICKNESS (mm)	SPACING (cm)	BACKUP MATERIAL	THICKNESS (mm)	VELOCITY (km/sec)	TOTAL PENETRATION (mm)	HOLE SIZE (mm)	SPRAY DIAMETER (mm)	SPRAY ANGLE	MV/mv	REMARKS
			1100-0			7075-T6								
D-1401	Al	3.18	Al	0.635	5.08	Al	12.7	7.32	—	—	—	—		SABOT HIT
1402									—	—	—	—		NO LAUNCH
1403									—	—	—	—		NO LAUNCH
1404								7.56	1.30	6.78	99	88		0.0312 GRAM/CM^3 STYROFOAM BACK OF SHIELD
1405		1.59					0.406	7.78	—	—	—	—		PISTON HIT
1406								—	—	—	—	—		NO LAUNCH
1407	Cd	3.18	Cd				12.7	—	—	—	—	—		NO LAUNCH
1408								—	—	—	—	—		NO LAUNCH
1409								—	—	—	—	—		NO LAUNCH
1410								5.00	—	—	—	—		NO IMPACT
1411								—	—	—	—	—		NO LAUNCH

SHOT NO.	PROJECTILE MATERIAL	DIAMETER (mm)	SHIELD MATERIAL	THICKNESS (mm)	SPACING (cm)	BACKUP MATERIAL	THICKNESS (mm)	VELOCITY (km/sec)	TOTAL PENETRATION (mm)	HOLE SIZE (mm)	SPRAY DIAMETER (mm)	SPRAY ANGLE	MV/mv	REMARKS
	2017		1100-0			7075-T6			FIRST					2 - 0.635 mm BACKUPS
D-1449	Al	3.18	Al	0.635	5.08	Al	0.635	8.14	SHEET	6.81	102	90		SPACED 5.08 cm
									SECOND					3 - 0.407 mm BACKUPS
1450							0.407	7.90	SHEET	6.93	102	90		SPACED 5.08 cm
1452	Cd		Cd	0.350			12.7	—	—	—	—	—		NO LAUNCH
1453								5.18	.508	5.41	102	90	1.28	
1454				0.635				6.40	.635	7.92	102	90	1.39	
1455								6.53	.635	8.03	102	90		
1456		2.56			15.2		1.59	4.27	.635	6.32	254	80		
1457		3.18			5.08		12.7	6.53	.635	7.59	102	90		
	2024-T3	3.18X 9.53	2024-T3			2024-T3								
1458	Al	ROD	Al	1.59	10.2	Al	25.4	4.63	6.84	7.65	178	82	1.43	
		2.49X14.9												
1459		ROD						4.74	8.74	—	184	84		
		4.55X4.55												
1460		ROD						4.94	1.53	10.2	193	87	1.32	
1461		5.23						4.91	1.45	10.3	189	84	1.37	
		6.61X2.21												
1462		DISC						4.79	2.18	12.5	172	81	1.25	
	2017		1100-0			7075-T6								
1463	Al	3.18	Al	0.635	5.08	Al	0.635	7.59	—	—	—	—		SABOT HIT
1464								—	—	—	—	—		NO LAUNCH
1465								—	—	—	—	—		NO LAUNCH
1466							1.02	7.74	—	—	—	—		PISTON HIT
1467								—	—	—	—	—		NO LAUNCH
1468							0.635	7.56	*	6.76	—	—		SPACING FILLED WITH 0.03 GRAM/CM³ STYROFOAM
	2024-T3	3.63x 7.27	2024-T3			2024-T3								
1473	Al	ROD	Al	1.59	10.2	Al	25.4	3.87	4.25	7.90	152	74		
1474								5.40	5.03	8.79	184	84	1.43	
1475								2.93	3.18	7.27	133	67	1.20	
1476								6.10	4.55	9.48	184	84	1.39	
		2.11x21.1												
1477		ROD						4.45	17.2	5.8	152	74		

* SHIELD AND BACKUP BENT

SHOT NO.	PROJECTILE MATERIAL	DIAMETER (mm)	SHIELD MATERIAL	THICKNESS (mm)	SPACING (cm)	BACKUP MATERIAL	THICKNESS (mm)	VELOCITY (km/sec)	TOTAL PENETRATION (mm)	HOLE SIZE (mm)	SPRAY DIAMETER (mm)	SPRAY ANGLE	MV/mv	REMARKS
	2017		1100-0			7075-T6								
E 1	Al	3.18	Al	0.305	5.08	Al	6.35	1.15	1.12	3.33				
2				.635				1.09	1.17	3.61				
3				1.02				1.10	1.17	4.04				
4				1.59				1.10	1.59	4.37				
5				.305				0.72	0.46	3.30				
9							12.7	1.89	1.83	3.74				
10				.635				1.94	1.73	4.65				
11				1.02			6.35	1.87	1.85	4.95				
12				1.59				1.92	2.26	5.82				
13				.305			12.7	2.68	2.64	4.19				
14				.635				2.07	1.83	4.63				
15				1.02			6.35	2.72	2.06	6.05				
16				1.59				2.75	2.16	6.96				
39				.635			2.54	2.56	3.18	4.88				PERFORATED
40							3.18	2.46	3.81	4.86				PERFORATED
41							3.81	2.40	3.58	4.68				
42							4.45	2.52	2.92	4.91				
43				1.02			1.90	2.43	2.92	5.69				PERFORATED
44							2.54	2.65	3.56	5.89				PERFORATED
45							3.18	2.59	2.62	5.87				
46							3.81	2.47	2.57	5.79				
47				1.59			0.81	2.08	2.41	6.02				PERFORATED
48							1.59	2.14	3.20	6.08				PERFORATED
49							2.54	2.12	2.36	6.05				
50							3.18	2.14	1.78	6.05				
51				.635			2.54	1.99	3.18	4.50				PERFORATED
52							3.18	1.90	3.20	4.44				

SHOT NO.	PROJECTILE MATERIAL	DIAMETER (mm)	SHIELD MATERIAL	THICKNESS (mm)	SPACING (cm)	BACKUP MATERIAL	THICKNESS (mm)	VELOCITY (km/sec)	TOTAL PENETRATION (mm)	HOLE SIZE (mm)	SPRAY DIAMETER (mm)	SPRAY ANGLE	MV/mv	REMARKS
	2017		1100-0			7075-T6								
E-53	Al	3.18	Al	0.635	5.08	Al	3.81	1.90	2.44	4.50				
54							4.45	1.90	2.16	—				SABOT HIT

SHOT NO.	PROJECTILE MATERIAL	DIAMETER (mm)	SHIELD MATERIAL	THICKNESS (mm)	SPACING (cm)	BACKUP MATERIAL	THICKNESS (mm)	VELOCITY (km/sec)	TOTAL PENETRATION (mm)	HOLE SIZE (mm)	SPRAY DIAMETER (mm)	SPRAY ANGLE	MV/mv	REMARKS
			1100-0			7075-T6			BACKUP					2.54 cm STYROFOAM
D-1537	Al	3.18	Al	0.64	5.08	Al	1.02	7.47	BENT	6.60	—	—		AGAINST BACKUP
1539								7.47		6.68	30	34		2.54 cm STYROFOAM AGAINST SHIELD
1540								7.59		6.78	18	20		2.54 cm STYROFOAM CENTERED BETWEEN SHEETS
1541				2.54			12.7	7.50	1.45	6.65	43	80		
1542							6.35	7.59	1.50	6.73	43	80		
1543							3.18	7.56	1.85	6.68	43	80		
1544					1.27		12.7	7.44	2.72	6.71	33	105		
1545							6.35	7.44	3.12	6.71	24	87		
1546					10.2		0.64	7.41	1.19	6.71	> 153	> 45		
1547							1.60	7.50	HOLE	6.73	> 153	> 45		
1548					2.54		2 0.64	7.44	HOLE	6.65	—	—		ALL PLATES PERFORATED
1550					1.69		3 0.41	7.44	HOLE	6.68	—	—		ALL PLATES PERFORATED
1552					10.2		0.41	7.41	SMALL HOLES	6.70	> 153	> 45		
1553					3.81 1.27		2 0.64	7.44	HOLE	PISTON HIT	—	—		
1554			STYROFOAM 1100-0	5.08	0 2.54		1.27 0.64	7.50	HOLE	PISTON HIT	—	—		
1555			Al	.64	10.2		0.64	7.47	BACKUP BENT	6.78	—	—		
1556					2.54		12.7	7.32	1.42	6.73	46	84		
1557					1.27			7.35	2.59	6.73	23	84		
1558					5.08		0.64	4.04	HOLE	5.79	—	—		5.08cm STYROFOAM BETWEEN SHEETS
1559					2.54		6.35	5.55	2.11	6.22	46	84		
1560					1.27		12.7	5.86	3.00	6.43	20	76		
1561	NYLON	4.19			5.08		6.35	7.50	1.17	7.95	102	90		
1562	Al	3.18			3.81 1.27		2 0.64	7.42	HOLE	—	—	—		PISTON HIT
1563			STYROFOAM 1100-0	5.08	0 5.08		1.27 0.64	7.59	~ 1.3	—	76	74		
1564			Al	.64	5.08		6.35	5.43	2.03	6.17	43	46		
1566							1.27	4.33	1.35	5.84	—	—		5.08cm STYROFOAM BETWEEN SHEETS
1567					1.69		2 0.64	4.36	HOLE	6.05	—	—		ALL PLATES PERFORATED

SHOT NO.	PROJECTILE MATERIAL	DIAMETER (mm)	SHIELD MATERIAL	THICKNESS (mm)	SPACING (cm)	BACKUP MATERIAL	THICKNESS (mm)	VELOCITY (km/sec)	TOTAL PENETRATION (mm)	HOLE SIZE (mm)	SPRAY DIAMETER (mm)	SPRAY ANGLE	MV/mV	REMARKS
			1100-0			7075-T6	2			PISTON				ALL PLATES
D-1568	Al	3.18	Al	0.64	5.08	Al	0.64	7.47	HOLE	HIT	—	—		PERFORATED
1570								4.39	HOLE	5.84	—	—		ALL PLATES PERFORATED 10.2 cm STYROFOAM
1571					10.2		0.41	7.38	0.64	6.68	—	—		BETWEEN SHEETS 5.08 cm STYROFOAM
1572					5.08		0.64	7.44	BACKUP BENT	6.73	—	—		BETWEEN SHEETS 5.08 cm STYROFOAM
1573							1.27	4.41	1.40	5.84	—	—		BETWEE SHEETS
1574	NYLON	4.19					0.64	5.06	HOLE	7.55	102	90		
1575							6.35	4.11	1.22	7.32	102	90		
1576	Cd	3.18	Cd		2.54		3.18 (2)	5.40	~3.8	7.50	—	—		
1577					1.69		1.60 (3)	5.85	~3.8	7.50	—	—		
1578					5.08		4.83	6.22	~0.64	7.85	58	59		
1579					10.2		1.27	6.22	BACKUP BENT	7.67	>153	>45		
1580				1.22	5.08		12.7	3.69	1.98	9.83	96	80		
1581								5.18	1.22	10.7	61	62		
1582								6.34	1.22	11.2	57	59		
1583		2.56		0.64			1.60	6.43	0.64	7.11	95	86		
			1100-0							6.91				
1584	Al	3.18	Al					7.26	2.16	7.75	102	—		30°
1585								7.53	HOLE	7.82 8.69	105	—		45°
1586								7.50	2.23	7.32 12.7	105	—		60°
1587				1.02				7.59	1.98	8.79 9.30	102	—		30°
1588								7.38	HOLE	8.94 10.2	89	—		45°
1589								7.50	HOLE	8.64 10.9	102	—		60°
1590				1.60				7.44	HOLE	10.9 11.3	95	—		30°
1591							0.64	7.47	HOLE	10.9	102	—		30°
1602							1.60	7.29	HOLE	10.7 11.5	89	—		45°
1603								7.41	HOLE	10.7 13.1	76	—		60°
1604	Cd		Cd	0.48			3.18	6.13	2.08	6.53 7.65	64	—		30°
1605								6.16	2.54	6.78 8.34	76	—		45°

OBLIQUE ANGLES MEASURED FROM VERTICLE

SHOT NO.	PROJECTILE MATERIAL	DIAMETER (mm)	SHIELD MATERIAL	THICKNESS (mm)	SPACING (cm)	BACKUP MATERIAL	THICKNESS (mm)	VELOCITY (km/sec)	TOTAL PENETRATION (mm)	HOLE SIZE (mm)	SPRAY DIAMETER (mm)	SPRAY ANGLE	MV/mv	REMARKS
						7075-T6				6.55				
D-1606	Cd	3.18	Cd	0.48	5.08	Al	3.18	6.13	1.55	10.9	76	—		60°
			1100-0							6.93				
1607	Al		Al	0.64				7.50	1.14	8.15	108	—		30°
										7.26				
1608								7.54	3.12	8.81	105	—		45°
										7.36				
1609								7.65	2.24	10.7	111	—		60°
1610				1.02				—	—	—	—	—		45°-NO IMPACT
										8.91				
1611								7.65	2.36	9.95	105	—		45°
									BACKUP					5.08cm STYROFOAM
1612				0.64			0.64	7.47	BENT	6.63	—	—		BETWEEN SHEETS
														2.54 cm STYROFOAM
1613							1.02	7.56		6.63	—	—		AGAINST SHIELD
														2.54 cm STYROFOAM
1614								7.47		6.73	—	—		AGAINST BACKUP

SHOT NO.	PROJECTILE MATERIAL	DIAMETER (mm)	SHIELD MATERIAL	THICKNESS (mm)	SPACING (cm)	BACKUP MATERIAL	THICKNESS (mm)	VELOCITY (km/sec)	TOTAL PENETRATION (mm)	HOLE SIZE (mm)	SPRAY DIAMETER (mm)	SPRAY ANGLE (DEGREES)	MV/mv	REMARKS
D1622	Cd	3.18	Cd	.50	2.54	7075-T6AL	1.60	6.0	2.08	6.96	50.8	53		
D1623	"	"	"	"	1.27	"	.81	"	2.92	6.58	82.6	78		5 PLATES; 1-Cd 4-7075-T6AL, 1.27cm SPACING
D1624	"	"	"	"	7.62	"	"	5.93	.48	6.26	108	53		
D1625	"	"	"	"	5.08	"	3.35	5.97	2.21	6.75 6.68	79.3	76		
D1626	"	"	"	"	.64	"	4.23	6.06	2.92	6.94	76.2	74		8 PLATES 7075-T6 AL 4.06mm, .64cm SP.
D1639	AL	"	1100-0AL	.64	2.54	"	2.54	7.65	4.55	6.55 6.68	70	38		3 PLATES 7075-T6AL LAST 2:, 64mm THK
D1640	"	"	"	"	"	"	4.57	7.70	1.52	6.65	6.48	16		5.08cm SPACING
D1641	"	"	"	"	3.81	"	.64 1.13	7.65	1.75	6.70	114	96		"
D1642	"	"	"	"	1.27 3.81	"	.64 1.60	7.66	2.22	6.45	63.5	64		"
D1643	"	"	"	"	1.27 5.08	"	.64 "	7.71	.64	6.58	76.2	74		" 5.08cm UR. FOAM BETW. SHIELD + BACKUP
D1644	"	"	"	"	7.62	"	.41	7.66	"	6.65	108	90		5.08cm STYROFOAM AGAINST SHIELD
D1645	"	"	"	"	5.08 10.2	"	.64 .41	7.62	"	6.68	82.6	44		7.62cm STYROFOAM AGAINST SHIELD
D1646	"	"	"	"	5.08 "	"	6.35 "	7.60	1.07	7.12	95.3			TARGET TILTED BACK 30° FROM VERTICAL
D1647	"	"	"	"	"	"	"	7.65	1.30	7.95 7.40	101.6			45°
D1648	"	"	"	"	"	"	"	7.62	2.15	8.66 7.37	95.4			" 60°
D1649	"	"	"	1.02	"	"	12.7	6.80	1.32	10.3 7.08	79.3	76		"
D1650	Ni 50%	2.56	"	.64	"	"	"	6.50	5.20	6.80 5.16	76.3	74		
D1651	"	"	"	1.02	"	"	1.60	6.59	2.62	6.53	82.6	44		
D1652	Cu (50%)	"	"	"	"	"	.64 12.7	6.61	2.39	6.40	101.6	90		
D1653	"	"	"	.64	"	"	"	5.99	3.35	4.73	79.3	76		
D1654	"	"	"	1.02	"	"	1.60	6.17	4.83	6.70	79.3	74		
D1655	AL	3.18	"	.64	"	"	.64 "	7.63	.64	6.69				5.08cm UR. FOAM BETW. SHIELD + BACKUP
D1656	"	"	"	"	"	"	"	7.56	.64	6.62	28.4	31		2.54cm UR. FOAM AGAINST SHIELD
D1657	"	"	"	"	"	"	1.02 .64	7.62	"	6.73	35.0	38		2.54cm UR. FOAM AGAINST BACKUP
D1662	"	"	"	"	3.81	"	1.12	7.53	2.39	7.95	89.0			TARGET TILTED BACK 30° FROM VERTICAL
D1663	"	"	"	"	1.27 3.81	"	.64 1.12	7.46	1.86	7.09 9.79	228 31.8			60°
					1.27	"	.64			7.52				"

SHOT NO.	PROJECTILE MATERIAL	DIAMETER (mm)	SHIELD MATERIAL	THICKNESS (mm)	SPACING (cm)	BACKUP MATERIAL	THICKNESS (mm)	VELOCITY (km/sec)	TOTAL PENETRATION (mm)	HOLE SIZE (mm)	SPRAY DIAMETER (mm)	SPRAY ANGLE (DEGREES)	MV/mv	REMARKS
D1664	Al	3.18	1100-0Al	.64	5.08	7075-T6Al	3.18	3.76	3.81	6.59	76.2			TARGET TILTED BACK 30° FROM VERT.
D1665	"	"	"	"	"	"	4.96	4.15	5.59	7.52	95.2			TARGET TILTED BACK 45° FROM VERT.
D1666	"	"	"	"	"	"	3.18	"	1.37	6.27 9.27	82.5			TARGET TILTED BACK 60° FROM VERT.
D1667	"	"	"	"	"	"	"	7.68	.64	6.35 6.91	121 28.5	31		2.54cm FOAM AGAINST SHIELD
D1668	"	"	"	"	"	"	.64 "	7.65	"	6.77	22.1	24		2.54cm FOAM AGAINST BACKUP
D1669	"	"	"	"	"	"	2.29	7.56	1.25	6.75	102	90		
D1670	"	"	"	1.60	"	"	.64 2.29	7.52	1.60	11.0	98.3	88		
D1671	"	"	"	.64	"	1100-0Al	.64 3.18	7.50	3.40	6.75	105	92		
D1672	"	"	"	"	"	"	.64 1.60	7.54	2.24	6.68	25.4	28		
D1673	"	"	"	"	"	7075-T6Al	.64 6.35	3.82	2.69	6.63	82.6			TARGET TILTED BACK 30° FROM VERT.
D1674	"	"	"	"	"	"	"	3.64	2.64	5.90 6.00	82.6			TARGET TILTED BACK 4-5° FROM VERT.
D1675	"	"	"	"	"	"	3.18	3.77	3.96	7.55 5.61	79.4	76		
D1676	"	"	"	"	"	"	.64 6.35	7.46	.64	6.73	31.8	35		2.54cm FOAM AGAINST BACKUP
D1682	"	"	"	"	2.54	"	2.54	7.41	3.18	6.60				LAST 2 PL.: 1100-0Al .635mm THK, 5.08cm SP.
D1683	"	"	"	"	"	"	.64 1.27	7.52	4.55	6.65	31.8	35		LAST 2 PL.: 1100-0Al 5.08cm SPACING
D1684	"	"	"	"	"	"	"	"	1.91	6.67	38.1	41		"
D1685	"	"	"	"	"	"	2.54 3.81	7.55	2.31	"	127	102		"
D1686	"	"	"	"	3.81	"	.64 1.12	7.35	4.11	6.70	44.4	47		LAST 2 PL.: 7075-T6Al .64mm THK, 5.08cm SP.
D1687	"	"	"	"	1.27 3.81	"	.64 1.12	7.47	3.94	6.66	31.8	35		"
D1689	"	"	"	"	1.27 3.81	"	.81 .64	7.35	3.07	6.04	47.4	50		(.81mm + .64mm THK) "
D1690	"	"	7075-T6Al	"	1.27 3.81	1100-0Al	1.27 .64	6.98	1.27	5.75	41.2	44		(1.27mm + .64mm THK) LAST 2 PL.: 7075-T6Al 5.08cm SPACING
D1691	"	"	1100-0Al	"	1.27 3.81	7075-T6Al	2.54 1.60	7.38	>1.93	6.55	35.0	38		"
D1693	Cd	"	Cd	.48	1.27 5.08	"	.64 6.35	4.18	2.03	7.67	114			(.64mm THK) TARGET TILTED BACK 45° FROM VERTICAL
D1694	"	"	"	"	"	"	"	5.94	1.68	6.45 8.38	152 127			"
D1695	"	"	"	"	"	"	"	3.86	1.12	6.80 6.93	152 121			" 30°
D1696	"	"	"	"	"	"	"	6.16	.711	5.91 6.60	140 102			" "
										7.52	152		"

SHOT NO.	PROJECTILE MATERIAL	DIAMETER (mm)	SHIELD MATERIAL	THICKNESS (mm)	SPACING (cm)	BACKUP MATERIAL	THICKNESS (mm)	VELOCITY (km/sec)	TOTAL PENETRATION (mm)	HOLE SIZE (mm)	SPRAY DIAMETER (mm)	SPRAY ANGLE (DEGREES)	MV/mv	REMARKS
D1697	Cd	3.18	Cd	.48	5.08	7075-T6Al	6.35	3.80	1.93	9.38	102			TARGET TILTED BACK 60° FROM VERTICAL
										6.50	153			
D1698	"	"	"	"	"	"	"	6.40	1.63	9.75	108			"
										6.70	114			"
D1699	"	"	"	"	"	"	3.18	6.28	4.34	5.38	88.9	83		
D1700	"	"	"	1.22	"	"	"	6.31	1.63	11.2	"	"		
D1701	Al	"	1100-0Al	.64	"	"	6.35	7.46	.64	16.7	35.0	38		1 IN. FOAM AGAINST SHIELD
										13.2				
D1702	"	"	"	"	"	"	"	"	"	6.63	31.8	35		1 IN. FOAM AGAINST BACKUP
D1703	"	"	"	"	"	"	"	7.40	"	6.56	"	"		

SHOT NO.	PROJECTILE MATERIAL	DIAMETER (mm)	SHIELD MATERIAL	THICKNESS (mm)	SPACING (cm)	BACKUP MATERIAL	THICKNESS (mm)	VELOCITY (km/sec)	TOTAL PENETRATION (mm)	HOLE SIZE (mm)	SPRAY DIAMETER (mm)	SPRAY ANGLE	MV/mv	REMARKS
	2017		1100-0			7075-T6								2.54 cm POLYURETHANE
D-1704	Al	3.18	Al	0.64	5.08	Al	6.35	7.35	0.64	6.55	—			FOAM AGAINST BACKUP
1711	Cd		Cd	0.33			3.18	6.40	0.66	5.38	102	90		
1712				1.22				6.40	1.22	11.1	152	113		
1713				0.33			4.75	6.49	1.27	5.61	84	80		
1714				1.22			2.28	6.37	—	11.2	84	80		BACKUP BENT
1715							3.18	—	—	—	—			NO LAUNCH
										10.7	92			
1716								6.34	1.88	11.6	119			45°
										10.6	99			
1717								6.43	2.31	12.5	119			60°
										11.2	86			
1718							3.18	6.43	1.65	11.5	104			30°
	2017		1100-0								127			
1719	Al		Al	0.64	10.2			7.50	1.02	—	197			30° PISTON HIT
											145			
1720								7.50	3.10	—	208			45° PISTON HIT
										6.94	152			
1721								7.04	1.65	9.57	226			60°
										11.0	152			
1722				1.60			1.60	7.41	2.11	11.3	196			30°
										10.0	140			
1723								7.47	PERF.	12.2	191			60°
1724			STEEL	0.13	5.08		6.35	7.59	1.02	—	102	90		PISTON HIT
1725				0.025				7.56	PERF.	—	46	49		PISTON HIT
			1100-0		2.54		1.27							
1731			Al	0.64	2.54		1.27	7.47	PERF.	—				3 PLATES, 2.54cm
					3.81		0.64		PERF. 2nd					APART - PISTON HIT
1732					1.27		1.27	7.78	SHEET	—				3 PLATES - PISTON HIT
					3.81		1.12							
1733					1.27		0.64	7.32	PERF.	—				3 PLATES - PISTON HIT
					3.81		1.60							
1734					1.27		0.64	7.71	PERF.	6.58				3 PLATES
					3.81		1.12							
1735					1.27		0.64	7.80	PERF.	6.76				3 PLATES
					2.54		1.27	ESTIMATED						
1736					2.54		1.02	7.67	PERF.	6.60				3 PLATES
					3.81		0.64							
1737					1.27		1.02	7.65	PERF	6.66				3 PLATES

ANGLES MEASURED FROM VERTICAL

SHOT NO.	PROJECTILE MATERIAL	DIAMETER (mm)	SHIELD MATERIAL	THICKNESS (mm)	SPACING (cm)	BACKUP MATERIAL	THICKNESS (mm)	VELOCITY (km/sec)	TOTAL PENETRATION (mm)	HOLE SIZE (mm)	SPRAY DIAMETER (mm)	SPRAY ANGLE	MV/mv	REMARKS
	2017		1100-0			7075-T6				7.32	97			
D-1751	Al	2.39	Al	1.02	5.08	Al	1.27	7.10	PERF.	8.13	99			45°
										7.42	102			
1752							2.54	7.59	1.96	8.38	102			45°
										7.03	76			
1753							1.27	7.56	PERF.	8.64	112			60°
			7075-T6							20.4				
1766		4.76	Al	19.1	——	——	——	7.44	10.5	21.4	——			
			1100-0			7075-T6								
1767			Al	1.02	2.54	Al	19.1	7.35	3.26	10.5	43	80		
	1100-0	3.56x3.56												
1768	Al	CYLINDER		0.81	5.08		3.18	7.20	PERF.	8.46	102	90		
1769							12.7	7.20	2.24	9.41	102	90		
1770							3.18	7.25	3.61	8.48	104	91		
	2017									8.92	97			
1771	Al	3.18		1.02				7.62	1.96	11.1	114			60°
										10.8	91			
1772				1.60				7.56	2.74	11.9	97			45°
										10.2	84			
1773								7.53	3.84	12.5	109			60°
										7.67	56			
1774								3.38	2.31	9.40	58			60°
										7.57	71			
1775				1.02			6.35	4.48	1.98	9.02	86			45°
										8.41	89			
1776								6.03	2.92	9.71	97			45°
										7.19	66			
1777								3.87	2.77	9.15	86			45°

SHOT NO.	PROJECTILE MATERIAL	DIAMETER (mm)	SHIELD MATERIAL	THICKNESS (mm)	SPACING (cm)	BACKUP MATERIAL	THICKNESS (mm)	VELOCITY (km/sec)	TOTAL PENETRATION (mm)	HOLE SIZE (mm)	SPRAY DIAMETER (mm)	SPRAY ANGLE	MV/mv	REMARKS
			1100-0			7075-T6								
D-1788	Al	2.38	Al	0.46	5.08	Al	0.64	7.68	PERF	5.08	102	90		
1789		4.76		1.02			3.18	7.62	2.67	10.5	114	97		
1790		6.35		1.27			6.35	7.34	3.64	13.6	127	103		
1791		2.38		0.46			0.46	7.50	PERF	4.83	102	90		
1792		4.76		1.02			4.19	7.62	2.08	10.6	114	97		
1793		6.35		1.27			7.55	7.47	3.66	13.9	84	79		
1802		3.18		0.64			1.60	7.86						30° MOMENTUM TRANSFER TARGETS
1803								7.86						
1804								7.90						45°
1805								7.13						60°
1806				1.60				7.62						30°
1807								7.50						45°
1808								7.62						60°
1809	Cd		Cd	0.33				7.31						
1810								7.01						
1811				0.64				7.13						
1812				1.22				—	—	—	—	—		NO LAUNCH
1813								7.13						
1814				0.33			2.28	6.94	0.33	5.89	76	73		
1815				0.64				7.01	0.64	7.88	51	53		
1816				1.22			1.60	6.94	—	—	—	—		SABOT HIT
1817	Pb		Pb	0.88			12.7	5.48	—	—	—	—		SABOT HIT
1818								4.51	—	—	—	—		SABOT HIT
1819				1.78				4.85	2.39	15.9	76	73	1.48	
1820								4.51	2.14	15.3	89	82	1.43	
1821				0.88				4.36	2.04	10.15	89	82	1.24	
1822								4.18	1.14	10.10	95	86	1.24	

SHOT NO.	PROJECTILE MATERIAL	DIAMETER (mm)	SHIELD MATERIAL	THICKNESS (mm)	SPACING (cm)	BACKUP MATERIAL	THICKNESS (mm)	VELOCITY (km/sec)	TOTAL PENETRATION (mm)	HOLE SIZE (mm)	SPRAY DIAMETER (mm)	SPRAY ANGLE	MV/mv	REMARKS
						7075-T6								
D-1823	Cd	3.18	Cd	1.22	5.08	Al	1.60	—	—	—	—			SABOT HIT
1824				0.64				—	—	—	—			NO LAUNCH
1825								6.64	0.64	8.05	76	73		
1826				0.33			2.28	6.79	PERF	5.79	64	65		
1827				1.22			1.60	6.67	1.22	11.5	83	78		
1828				0.33			2.54	6.92	PERF	5.85	51	53		
1829				1.22			1.27	6.79	1.22	11.7	76	73		
1830				0.33			3.18	6.79	CRACK	5.82	44	47		FRACTURED THICKNESS
1850	Al		1100-0 Al	0.64	1.27		12.7	7.47	2.82	6.60	23	84	1.29	
1851				1.02	2.54			7.62	1.60	8.72	41	78	1.39	
1852				0.64				5.82	2.04	6.25	43	81	1.36	
1853				1.60				7.86	2.21	11.0	41	78	1.45	
1854								5.64	2.16	9.67	41	78	1.32	
1855					5.08		6.35	—	—	—	—	—		PISTON HIT
1856				0.64			12.7	5.30	2.90	6.12	108	93	1.39	
1857				6.30			6.35	7.77	2.31	4.90	102	90	1.32	

SHOT NO.	PROJECTILE MATERIAL	DIAMETER (mm)	SHIELD MATERIAL	THICKNESS (mm)	SPACING (cm)	BACKUP MATERIAL	THICKNESS (mm)	VELOCITY (km/sec)	TOTAL PENETRATION (mm)	HOLE SIZE (mm)	SPRAY DIAMETER (mm)	SPRAY ANGLE (degrees)	SPACING (cm)	BACKUP MATERIAL	THICKNESS (mm)	TOTAL PENETRATION (mm)	REMARKS (Dimensions in mm)
D-1899	Cd	3.18	Cd	0.33	11.2	7075-T6	1.60	6.89	Bubble	5.59	76	90	5.08	7075-T6Al	0.812	none	
1900	"	"	"	"	"	"	1.27	6.78	"	5.59	94	50	"	"	"	"	
1901	Pb	"	Pb	1.68	5.08	"	"	5.04	"	13.7	14.7	90	"	"	"	"	
1902	"	"	"	"	"	"	0.64	4.51	Fracture	16.3 14.7	—		"	"	"	"	
1903	"	"	"	"	"	"	0.812	4.63	"	15.7	86	80	"	"	"	"	
1904	"	"	"	"	"	"	1.02	4.34	"	14.2	76	75	"	"	"	"	
1905	Cd	"	Cd	1.22	"	"	"	6.95	"	11.2	127	100	"	"	"	Penetration	14.6 OD 13.8 ID Tube
1906	"	"	"	"	"	"	"	6.93	15.7mm Hole	11.7 11.2	104	90	"	"	"	"	14.6 OD 13.8 ID Tube
1907	"	"	"	"	"	"	"	6.85	"	11.7 11.2	152	110	"	"	"	"	14.2 OD 13.2 ID Tube
1908	"	"	"	0.33	"	"	3.18	6.92	16.0mm Hole	11.4 5.89	18	15	"	"	"	"	14.4 OD 13.6 ID Tube
1909	"	"	"	"	"	"	"	6.99	14.3mm Hole	6.10 6.10	22	20	"	"	"	"	13.7 OD 13.6 ID Tube
1910	"	"	"	1.22	"	"	2.54	6.81	15.2mm Hole	11.2	18	15	"	"	"	"	14.5 OD 14.1 ID Tube
1911	"	"	"	0.48	"	"	"	6.84	Bubble	11.7 6.86	64	60	"	"	"	none	direct hit no Tube
1912	"	"	"	"	"	"	"	6.84	16.0mm Hole	6.86	30	30	"	"	"	Penetration	14.5 OD 14.1 ID Tube
1913	"	"	"	"	"	"	"	6.85	17.0mm Hole	6.86	20	20	"	"	"	"	direct hit 14.4 OD 14.2 ID Tube
1914	"	"	"	"	"	"	"	6.80	Bubble	7.11 7.11	140	105	"	"	"	none	direct hit 14.5 OD 14.1 ID Tube
1915	Al	"	1100-0	1.60	"	"	"	7.25	" + Crack	8.89 10.7	89	80	"	"	"	"	45° from Vertical 14.3 OD 14.2 ID Tube
1916	Intte	6.85	Cd	0.64	"	"	1.60	7.48	Penetration	10.7 10.4	152	110	"	"	"	—	no Tube
1917	Al	3.18	1100-0	"	"	"	2.54	7.60	"	10.9 6.60	152	110	"	"	"	—	14.5 OD .556 ID Tube
1918	"	"	"	"	"	"	"	6.89	"	—	—	—	"	"	"	Penetration	14.4 OD 14.2 ID Tube
1919	Cd	"	Cd	0.48	"	"	"	6.64	"	7.11 8.64	127	100	"	"	"	Bubble	14.4 OD 14.2 ID Tube 45° from Vertical
1920	"	"	Cd	"	"	"	"	6.89	Bubble	6.60 8.64	127	100	"	"	"	none	14.3 OD 14.1 ID Tube 45° from Vertical
1921	"	"	Cd	"	"	"	4.83	6.82	12.7mm Hole	6.86 7.11	19	15	"	"	"	Bubble	14.5 OD 14.1 ID Tube
1922	"	"	"	"	"	"	6.35	6.95	Bubble	6.86 7.11	19	15	"	"	"	"	"
1923	"	"	"	0.33	11.2	"	0.82	6.87	"	5.38 5.84	38	20	"	"	"	"	no Tube
1924	"	"	"	1.22	"	"	0.25	6.52	Fracture	11.2 11.7	—	—	"	"	"	"	"
1925	"	2.56	"	0.48	"	"	"	—	"	6.10	—	—	"	"	"	"	"

SHOT NO.	PROJECTILE MATERIAL	DIAMETER (mm)	SHIELD MATERIAL	THICKNESS (mm)	SPACING (cm)	BACKUP MATERIAL	THICKNESS (mm)	VELOCITY (km/sec)	TOTAL PENETRATION (mm)	HOLE SIZE (mm)	SPRAY DIAMETER (mm)	SPRAY ANGLE	SPACING (cm)	BACKUP MATERIAL	THICKNESS (mm)	TOTAL PENETRATION (mm)	REMARKS (Dimensions in mm)
1926	Pb	3.18	Pb	1.75	11.2	7075-T6 Al	0.38	4.87	Bubble	16.3	—	—	5.08	7075-T6 Al	0.812	none	No Tube
1927	"	"	"	"	"	"	0.812	4.84	Fracture	15.5	—	—	"	"	"	"	"
1928	"	"	Cd	1.22	"	"	0.38	6.92	—	16.8 11.4	—	—	"	"	"	"	"
1929	"	"	"	0.33	"	"	0.64	6.92	Bubble	11.9 5.33	—	—	"	"	"	"	"
1930	"	"	"	1.22	2.54	"	3.18	—	—	5.59 —	—	—	"	"	"	—	"
1931	"	"	"	"	"	"	2.87	6.77	Penetration	11.7	60	90	"	"	"	—	"
1932	"	"	"	1.65	5.08	"	0.82	6.85	Bubble	11.7 13.7	81	50	"	"	"	none	"
1933	"	"	"	"	"	"	0.64	6.88	Fracture	14.0 13.7	74	70	"	"	"	"	"
1934	"	"	"	"	"	"	0.30	7.00	Small spall	14.0 13.7	152	110	"	"	"	Penetration	"
1935	Al	"	1100-0	0.64	"	"	2.54	7.05	Spall	14.2 6.60	30	30	"	"	"	none	25.4 OD 0.127 to 0.356 wall Thickness
1936	"	"	"	"	"	"	"	7.73	Penetration	6.86 6.86	33	60	"	"	"	"	Same as above 60° from Vertical
1937	"	"	"	"	"	"	1.60	7.62	Split	7.62 6.60	91	80	"	"	"	Penetration	No Tube
1938	"	"	"	1.60	"	"	"	7.82	"	10.9	81	75	"	"	"	—	"
1939	"	"	"	0.64	11.2	"	"	7.76	"	6.60	152	75	"	"	"	none	"
1940	"	"	"	1.60	"	"	"	7.63	"	10.9 11.2	152	75	"	"	"	"	"
1941	Cd	"	Cd	"	5.08	"	"	6.95	"	13.7 14.0	76	75	"	"	"	"	"
1942	"	"	"	"	11.2	"	"	6.85	"	13.2 14.2	152	75	"	"	"	"	"
1943	"	"	"	0.019	5.08	"	2.54	6.67	Sub. Pent.	7.11 7.62	15	15	"	"	"	"	15.9 Tube at 15° to 30° from Vertical
1944	"	"	"	"	"	"	"	6.78	Penetration	7.11 7.87	76	75	"	"	"	—	16.0 Tube 6.78 @ 60° from Vertical
1945	"	"	"	"	"	"	"	5.85	—	—	25	25	"	"	"	—	25.4 Tube @ 27.4 @ 30° from Vertical
1946	"	"	"	"	"	"	"	6.36	Penetration	6.60	51	50	"	"	"	—	25.4 Tube as above Vertical
1947	"	"	"	"	"	"	"	6.36	"	7.11 8.12	60	55	"	"	"	—	9.65 Tube 0.82 Thick
1948	"	"	"	1.22	"	"	"	6.72	"	11.2 11.4	152	110	"	"	"	—	"
1949	"	"	"	1.60	"	"	"	—	—	11.2 11.4	152	110	"	"	"	—	"
1950	"	"	"	"	"	"	"	6.67	Penetration	12.9	102	90	"	"	"	—	16.0 Tube @ 60°
1951	"	"	"	1.22	2.54	"	3.18	6.57	"	11.2 11.4	51	90	"	"	"	Penetration	No Tube
1952	"	"	"	0.48	8.64	"	12.7	—	—	—	—	—	"	"	"	—	"

Appendix C

SHOT NO.	PROJECTILE MATERIAL	DIAMETER (mm)	SHIELD MATERIAL	THICKNESS (mm)	SPACING (cm)	BACKUP MATERIAL	THICKNESS (mm)	VELOCITY (km/sec)	TOTAL PENETRATION (mm)	HOLE SIZE (mm)	SPRAY DIAMETER (mm)	SPRAY ANGLE	SPACING (cm)	BACKUP MATERIAL	THICKNESS (mm)	TOTAL PENETRATION (mm)	REMARKS (Dimensions in mm)
1953	Cd	3.18	Cd	0.48	0.64	7075-T6 Al	6.35	6.64	Spall	—	33	—	5.08	7075-T6 Al	0.812	Penetrated	no Tube
1954	"	"	"	0.33	11.2	"	0.25	6.79	Fracture	6.59	152	75	"	"	1.02	bubble	"
1955	"	"	"	1.60	2.54	"	2.54	6.78	Penetration	5.84 13.7	51	90	"	"	0.812	"	"
1956	"	"	"	"	"	"	3.18	6.73	Spall	14.2 13.2	51	90	"	"	"	none	"
1957	"	"	"	0.33	5.08	"	2.29	6.73	Bubble	13.7 5.84	127	10	"	"	"	"	"
1958	"	"	"	0.48	"	"	2.54	6.85	Penetration	6.10 4.86	25	25	"	"	1.02	Penetration	25.4 Tube 0.127 t 30° from Vertical
1959	"	"	"	0.23	11.2	"	0.71	6.73	Fracture	7.62 5.59	152	75	"	"	0.812	bubble	no Tube from #1958 on.
1960	"	"	"	0.64	5.08	"	0.81	6.62	Bubble	5.84 7.62	38	40	"	"	"	none	
1961	"	"	"	"	11.2	"	0.25	——	Fracture	7.87 7.62	152	75	"	"	"	"	
1962	"	"	"	0.33	5.08	"	2.29	6.76	Bubble	5.59	56	55	"	"	"	"	
1963	"	"	"	"	"	"	3.18	6.25	"	5.33	51	50	"	"	"	"	
1964	"	"	"	"	"	"	4.83	6.82	"	5.59 5.59	38	40	"	"	"	"	
1965	"	"	"	"	11.2	"	0.71	6.78	Fracture	5.84 6.57	152	75	"	"	"	"	
1966	"	"	"	0.64	5.08	"	0.64	6.57	"	5.84 7.87	152	110	"	"	"	bubbled	
1967	"	"	"	"	1.27	"	12.7	6.86	Spall	8.89	30	90	"	"	"	none	
1968	Al	"	1100-0	"	"	"	"	7.79	Bubble	6.60	25	85	"	"	"	"	
1969	"	"	"	"	"	"	6.36	7.83	Spall	—	25	85	"	"	"	"	
1970	"	"	250	1.60	"	"	"	——	——	——	——	—	"	"	"	——	
1971	"	"	"	"	"	"	"	7.18	Bubble	10.4	28	55	"	"	"	none	
1972	Cd	"	1100-0	0.64	"	"	4.83	6.85	penetration	6.60	25	50	"	"	"	——	
1973	"	"	"	"	0.64	"	6.35	6.80	"	—	25	—	"	"	1.02	partial	
1974	"	"	Cd	"	"	"	"	6.82	"	8.13	25	—	"	"	"	fracture	
1975	"	"	"	"	2.54	"	0.64	6.80	Partial	4.38 7.87	—	—	2.54	"	0.635	partial	102 7075-T6 Backup
1976	"	"	"	0.48	5.08	"	1.02	6.85	"	6.86	—	—	5.08	"	1.02	none	5.1cm space perforated as above, no damage
1977	"	"	"	0.64	2.54	"	0.64	7.06	"	7.11 8.64	—	—	2.54	"	"	partial	as above, dimpled
1978	"	"	"	"	"	"	1.02	7.02	"	7.87	—	—	"	"	"	"	
1979	"	"	"	0.64	0.64	"	12.7	6.93	Spall	8.12 8.38	36	—	5.08	"	1.60	none	

SHOT NO.	PROJECTILE MATERIAL	DIAMETER (mm)	SHIELD MATERIAL	THICKNESS (mm)	SPACING (cm)	BACKUP MATERIAL	THICKNESS (mm)	VELOCITY (km/sec)	TOTAL PENETRATION (mm)	HOLE SIZE (mm)	SPRAY DIAMETER (mm)	SPRAY ANGLE	SPACING (cm)	BACKUP MATERIAL	THICKNESS (mm)	TOTAL PENETRATION (mm)	REMARKS (Dimensions in mm)
1980	Cd	3.18	Cd	0.48	5.08	7075-T6Al	1.27	6.90	Bubble	6.96	51	50	5.08	7075-T6Al	1.60	none	
1981	"	"	7075-T6	12.7	11.2	"	1.60	6.93	Penetration	7.11 12.2	127	65	"	"	"	"	
1982	"	"	Cd	0.64	2.54	"	1.02	6.85	Pen&Fract.	7.87	76	110	2.54	"	"	Pen&Fract	
1983	"	"	"	0.33	5.08	"	2.29	7.03	Fracture	5.57	45	50	5.08	"	2.29	none	
1984	"	"	"	0.64	2.54	"	1.02	7.05	Pen&Fract.	5.84 7.62	—	—	2.54	"	"	Pen&Fract	
1985	"	"	"	"	"	"	"	7.03	"	7.87	—	—	5.08	"	1.02	"	
1986	"	"	"	"	"	"	0.64	—	"	7.87	—	—	2.54	"	"	"	1.02 7075-T6 backup ringed as above, dimpled
1987	"	"	"	"	"	"	"	7.02	"	7.62 7.87	—	—	5.08	"	"	"	
1988	"	"	"	0.48	0.32	"	12.7	6.97	Penetration	—	28	—	"	"	1.60	bulge	
1989	"	"	"	0.64	5.08	"	10.2	6.94	Fracture	7.62 7.87	—	—	"	"	1.02	none	
1990	"	"	"	"	2.54	"	0.64	7.02	Pen&Fract.	7.62 7.87	—	—	2.54	"	1.60	Pen&Fract	1.60 7075-T6 backup slight scatter
1991	"	"	"	0.64	0.64	"	"	6.36	Bulge plate Perf. 1st 6 plates	7.62	7 plates worse, 635 mm spaced, (same as no. 2 plate)		—	—	—	—	